TUNING OF MULTIFUNCTIONAL PROPERTIES OF UNDOPED AND DOPED $BiFeO_3$

by

Héctor Almanzor Chinchay Espino

A thesis submitted in partial fulfillment of the requirements for the degree of

MASTER OF SCIENCE
in
Physics

UNIVERSITY OF PUERTO RICO
MAYAGÜEZ CAMPUS
2018

Approved by:

_____	_____
Oscar Perales-Pérez, Ph.D. President, Graduate Committee	Date
_____	_____
Félix Fernández, Ph.D. Member, Graduate Committee	Date
_____	_____
Sergiy Lysenko, Ph.D. Member, Graduate Committee	Date
_____	_____
Alexandra Gregory Crespo, Ph.D. Representative of Graduate Studies	Date
_____	_____
Rafael A. Ramos, Ph.D. Chairperson of the Department	Date

ABSTRACT

This work studied the effect of the incorporation of Co^{2+} and Mn^{2+} species on the structural and magnetic properties of nanocrystalline powders of $BiFeO_3$ (BFO) synthesized by the sol-gel and thermal treatment method at 700°C for 15, 30 and 45 mins. X-ray diffraction (XRD) measurements showed diffraction patterns that belong to the rhombohedral perovskite structure of $BiFeO_3$ for all undoped samples. Minimum presence of impurities was obtained for samples thermally annealed for 30 minutes. The measurements of magnetic hysteresis loops indicated that undoped BFO samples exhibited antiferromagnetic ordering, with a maximum magnetization obtained at 30 minutes of annealing time. XRD measurements verified the rhombohedral perovskite structure for Co-BFO samples. However, a secondary phase of Ferrite Cobalt (CFO) was detected for 9, 10 and 15% Co; the formation of CFO inhibited the growth of the impurity phases. Magnetic hysteresis measurements evidenced a ferromagnetic behavior for all Co-$BiFeO_3$ samples due the presence of CFO. A saturation magnetization of 4.13 emu/g and a coercivity of 1083.4 Oe were achieved at 15 % of Co. On the other hand, XRD measurements showed that the Mn-doped BFO samples exhibited a rhombohedral perovskite structure only for 3% Mn. Samples at 5% and 7% Mn reported the tetragonal structure, which was attributed to the incorporation of Mn(II) species in Bi sites. The relative amount of impurity phases increased with time owing decomposition of BFO. These paramagnetic impurity phases affected the corresponding magnetic properties. Magnetic characterization revealed a ferrimagnetic behavior in the 7% Mn-BFO powder, whereas a paramagnetic trend was observed for other compositions. The optimal doping condition was reached at 7% Mn with a ferrimagnetic order and a maximum magnetization of ~ 0.68 emu/g.

RESUMEN

Este trabajo estudió el efecto de la incorporación de especies de Co^{2+} y Mn^{2+} sobre las propiedades estructurales y magnéticas de polvos nanocristalinos de $BiFeO_3$ (BFO) sintetizados por el método de sol-gel y tratamiento térmico a 700°C durante 15, 30 and 45 minutos. Mediciones de difracción de rayos X (XRD) mostraron patrones de difracción que pertenecen a la estructura perovskita rombohedral de la BFO para todas las muestras sin dopar. Presencia mínima de impurezas fue obtenida en muestras tratadas térmicamente durante 30 minutos. Las mediciones de curvas de histéresis magnética indicaron que las muestras de BFO no dopadas exhiben un ordenamiento antiferromagnético, con una magnetización máxima obtenida a 30 minutos de tiempo de recocido. Mediciones de XRD verificaron la estructura perovskita rombohedral para muestras de Co-BFO. Sin embargo, una fase secundaria de Ferrita de Cobalto (CFO) fue detectada para 9, 10 y 15% de Co; la formación de CFO inhibió el crecimiento de las fases de impureza. Mediciones de histéresis magnética evidenciaron un comportamiento ferromagnético para todas las muestras Co-BFO debido a la presencia de CFO. Una magnetización de saturación de 4.13 emu/g y una coercividad de 1083.4 Oe fue alcanzada a 15% de Co. Por otro lado, mediciones de XRD mostraron que las muestras de Mn-BFO exhibieron una estructura perovskita rombohedral sólo para 3% Mn. Muestras a 5% y 7% Mn reportaron la estructura tetragonal, lo cual fue atribuido a la incorporación de Mn(II) especies en los sitios del Bi. Las cantidades relativas de fases de impureza incrementaron con el tiempo debido a la descomposición de BFO. Estas fases de impurezas paramagnéticas afectaron las correspondientes propiedades magnéticas. Caracterización magnética reveló un comportamiento ferrimagnético in los polvos a 7% Mn-BFO, mientras que una tendencia paramagnética fue observada para otras composiciones. Las condiciones óptimas de dopaje fueron alcanzadas a 7% Mn con un orden ferrimagnético y una magnetización máxima de 0.68 emu/g.

DEDICATORY

To God, for his unconditional love

To my family, in special for my grandmother Chayo, my parents Héctor, Charo y Juan, my brothers Briam, Paula, Jordy y Juancito, and my uncles Chachi and Lucho for their support and love.

ACKNOWLEDGMENTS

Many people helped me to finish this work, I would like to express my gratitude to everyone.

- My advisor Dr. Oscar Perales for his excellent scientific advice, support and friendship.
- My co-advisor Dr. Felix Fernandez for his support in the review of my thesis.
- Dr. Sergiy Lysenko for his support in the review of my thesis.
- Dr. Boris Renteria for his support and advice in the measurements at the Nano materials Processing Laboratory at UPRM.
- Dr. Segundo Jáuregui for his support and friendship.
- To my "Comuna" Gina Montes and Abdiel Oquendo for their unconditional scientific advice, support and friendship.
- To my undergraduate students Christian Villa and Carlex Morales for their excellent work and support in this research, and for their friendship.
- To my partners of the Nano materials Processing Laboratory at UPRM, Myrna, Raquel, Olga, Ana, Angélica, Rebeca, Miguel, Milton and Santiago, for their support and friendship.
- All graduate students of Physics Department, for their friendship and constant support.
- To Myriam Padilla and Adelaida Rivera administrative staff of CREST.
- To IFN Program, CREST Program and PR NASA Summer Internship Program

Table of Contents

Table List

Figure List

CHAPTER I: INTRODUCTION

1.1 Motivation

Nanomaterials have attracted attention due novel properties that these materials present in comparison with bulk. Structures as nanoparticles, thin films, nanorods, etc. are synthesized to achieve tuning and control of the matter at these dimensions. At nanometric scale (1 to 100nm) materials may exhibit remarkable size-dependent structural, optical, mechanical, electrical and magnetic properties. This size-dependent behavior has opened the possibility of applications of nanomaterials in several fields of investigation; in biomedicine for example, magnetic nanoparticles are used for drug delivery, hyperthermia, removal of pathogens, etc., whereas, electronic devices like optical sensors and data storage devices can also be further developed. Besides, some nanostructures can exhibit multifunctionality, i.e. more than two functional properties in the same structure; multiferroic materials are a good alternative since they can combine magnetic and electric properties [1].

Multiferroics materials present spontaneous and tunable ordering of two or more properties like ferromagnetism, ferroelectricity and ferroelasticity. Researchers commonly assign the term "multiferroic" for materials with only ferroelectric and ferromagnetic (or other kind of magnetic order) features [1]–[3]. Alignment of spins in ferromagnetism can be switched applying a magnetic field, and electric dipole moment is altered by an electric field, but multiferroics exhibit magnetoelectric effect, therefore it is possible tune spin arrangements with an electric field, and a magnetic field can change electric polarization [4]. Among the multiferroics, bismuth ferrite is the only one that shows electric and magnetic behavior at room temperature [1], [5].

Bismuth ferrite (BFO) exhibits a perovskite structure and an antiferromagnetic character with Neel temperature of ~643K, and ferroelectricity with a Curie temperature of ~1100K [1], [6]. These properties make BFO an excellent candidate for applications in data storage, spintronic, electronic devices, and solar energy devices [7].

There are a lot of methods for synthesis of $BiFeO_3$ in powders and thin films, including hydrothermal [8], sol-gel [9], solid state [10], pulsed laser deposition (PLD) [11], spin-coating [12], among others. Sol-Gel is the most used method for synthesis of BFO, since it is easy, cheap, fast and highly reproducible, besides allows appropriate control of crystallite size and chemical composition [13]. The principal challenge in synthesis of BFO is to avoid formation of impurity phases that could affect the properties of the material. The weak magnetic behavior of BFO, due its antiferromagnetic order, and reported leakage current are other challenges of current importance. Doping is an alternative procedure to improve magnetic and electric properties, and could handle the control of impurities and electric leakage [14], [15].

Incorporation of dopant species in the host BFO induces distortion in the crystal structure, this can promote a spin rearrangement and consequently a transition of magnetic character, similarly cell distortion could give rise to non-centro symmetricity between positive and negative charges what will produce an electrical polarization [1]. Additionally, guest features can contribute in the properties, for example doping with magnetic transition metals (like Co^{2+}, Mn^{2+} or Ni^{2+}). Intermediate oxides (impurities) normally emerge in the annealing process of precursor samples, suitable time and temperature parameters are needed to minimize these phases, but some dopant elements can suppress impurities as well [16]. Co^{2+} and Mn^{2+} are good candidates to replace diamagnetic bismuth species in BFO since they would improve magnetic properties by two ways,

magnetic features of the dopants, and distortion in crystal lattice induced by their differences in ionic radii with respect to Bi^{3+} (the ionic radii of Bi^{3+} (1.20 Å) is larger than that Co^{2+} (0.78 Å) and Mn^{2+} (0.80 Å)). Doping of $BiFeO_3$ with Co species can also promote the development of ferromagnetic Cobalt Ferrite as a dispersed phase within the BFO matrix, which would provide magnetic properties to the host material [17]. In turn, doping of $BiFeO_3$ with Mn species could allow the formation of Manganese Ferrite secondary phases along with the primary BFO host, but this has not been previously reported. Also, incorporation of Mn species in the BFO host system can produce a phase transition from rhombohedral to tetragonal crystal structure in Mn-doped BFO systems, what could induce a change in the magnetic order of BFO [18].

Incorporation of cobalt or manganese species in bismuth places can enhance magnetic properties but might reduce electrical polarization, due bismuth displacement cause the electric dipole moment. On the other hand, ferroelectrics need to be strong insulators, and most of magnetic species used for doping are conductors [1]. In general, conditions to improve any property either electric o magnetic, will cancel a part of the other property indirectly, hence is necessary find optimal parameters of synthesis and suitable doping conditions to have an equilibrium between the multiferroic properties of $BiFeO_3$.

On the above basis, the next work presents the synthesis and characterization of undoped and Co-doped $BiFeO_3$ and Mn-doped $BiFeO_3$ nanocrystalline powders synthesized by the Sol-Gel method. The effect of annealing temperature, time and composition on the corresponding structural and magnetic properties of the powders were investigated, with the aim of minimizing the presence of impurity phases and determine the mechanisms related to the variation in the material properties.

1.2 Aim of study

1.2.1 Main objective

Determine the role of the dopant type and amount on the structural and magnetic properties in Bismuth Ferrite-based powders.

1.2.2 Specific objectives

- Determine optimum processing conditions to produce impurities-free undoped and doped-BFO powders.
- Determine the corresponding structural and magnetic properties for undoped and doped BFO as a function of crystallite size and composition.
- Propose mechanisms involved with the size and composition-dependence of magnetic properties in undoped and doped Bismuth Ferrite.

1.3 Chapters contents

Chapter II will present theoretical concepts about multiferroics, crystal structure of Bismuth Ferrite and mechanisms of their electric and magnetic properties. Theory for magnetoelectric coupling and finally some applications of multiferroics. Chapter III actualized previous works of Co-Doped $BiFeO_3$ and Mn-Doped $BiFeO_3$ systems will be shown. Chapter IV will explain synthesis methods for powders and thin films of bismuth ferrite, and characterization techniques used for the study of structural and magnetics properties of bismuth ferrite. Results and their interpretation will be discussed in Chapter V whereas the main conclusions will be presented in Chapter VI.

CHAPTER II: THEORICAL BACKGROUND

2.1 Multiferroics

The term “ferroic” is used for the study of materials that have ferromagnetic, ferroelectric or ferroelastic order, materials with two or more of this behaviors in a same phase are called “multiferroics” [1]. Stress fields **σ** can change strain **ε**, magnetization **M** is exhibit in response to magnetic field **H**, and an electric field **E** induces electric polarization **P**, interaction between these fields can tune different ferroic properties at a same structure (Figure 2.1). Usually the term “multiferroic” is applied when coexist only spontaneous ferroelectric and ferromagnetic order. Additionally, electromagnetic coupling allows control of magnetic order applying an electric field and not only through magnetic fields, likewise, magnetic field induces changes in electric dipoles by the same effect [19], [20].

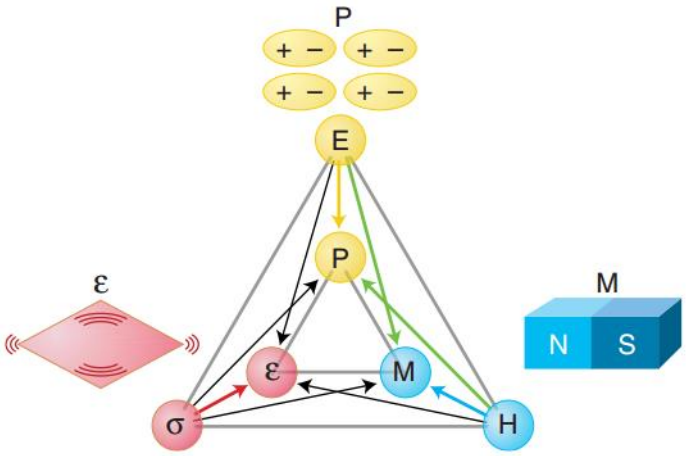

Figure 2.1 Coupling between ferroic properties in multiferroic materials [21].

There are two types of multiferroics, the type-I have order electric and magnetic that originate independently each other due that the orders are distributed on different sublattices of the material,

besides, their natural behaviors arise from mechanisms that work separately, therefore have a weak electromagnetic coupling. Probably the most known structure within this group are the perovskite multiferroics ABO_3, where the cation in site-A gives the character ferroelectric to material, and cation in B-site controls magnetism, for example: $BiFeO_3$, $YMnO_3$, etc [22]. In multiferroics type-II ferroelectricity is induce for the spin arrangement of the structure, hence have a strong magnetoelectric coupling, examples of this materials are rare earth manganites [23]. For all these properties, multiferroics are studied for application in spintronic, electronic devices, memories, sensor, etc. [22], [24].

2.2 Ferromagnetism

Magnetization is produced from two sources, the motion of electrons in their orbits (similar to electric current induces magnetic fields) and the intrinsic spin moment of electrons [25]. According the spin ordering and paired or unpaired electrons in a crystal, the material can respond in diverse ways to an external magnetic field and therefore exist distinct magnetic orders. In Figure 2.2 are showed the ordering of the magnetic moments in magnetic materials, in diamagnetic order the net magnetic moment is zero, all electrons are paired, when a magnetic field is applied in these materials, magnetic moments are aligned in opposite direction to the magnetic field applied. Paramagnetic materials have unpaired electrons, but they are in disordered positions, if a magnetic field is applied, the magnetic moments are aligned in the same direction of the field. In ferromagnetic order exist regions call magnetic domains where the individual magnetic moments point in a same direction inside each region, due these domains, such materials have a better magnetic behavior, when a magnetic is applied, magnetic domains aligned to the magnetic field.

Magnetic moments can be aligned in antiparallel form, and therefore have a net magnetic moment zero, these materials are called antiferromagnetics and when a magnetic field is applied, then, magnetic moments are aligned to field, but they stand in antiparallel form to compensate one to another. These materials have not exactly a net magnetic moment zero, they can have a magnetic moment different to zero but small, due to spin canting or defects according the crystal structure of the material. There is other magnetic order with magnetic moments aligned in antiparallel form like antiferromagnetic behavior, but the magnetic moments are of different intensity of magnitude, hence they have a resultant magnetic moment and do not cancel mutually, these materials are called ferrimagnetics [26].

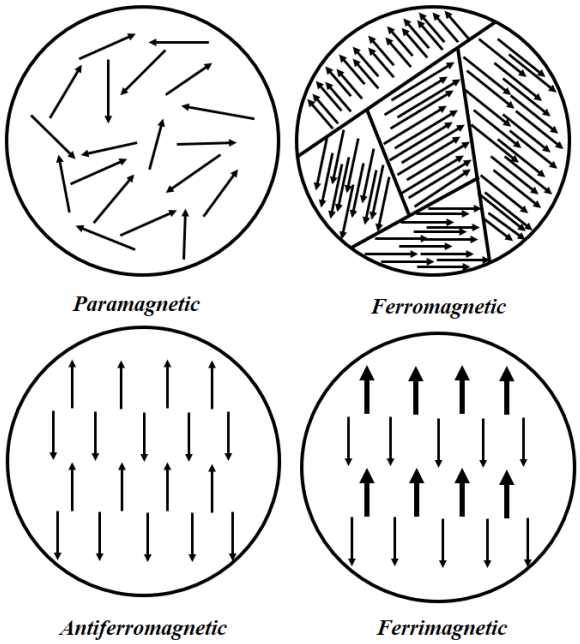

Figure 2.2 Magnetic ordering of the different magnetic materials [26].

When a magnetic field is applied in a material, it is magnetized, this magnetization is the contribution of the magnetic moments for unit of volume of the material according this equation:

$$\boldsymbol{M} = \frac{\boldsymbol{dm}}{\boldsymbol{dV}} \tag{2.1}$$

Normally, in small volumes like crystals, magnetization can be given in units of Bohr magnetons $\boldsymbol{\mu_B}$, 1 $\boldsymbol{\mu_B}$= 9.27x 10^{-21} erg/Oe [26], [27].

When plotted magnetization $\boldsymbol{M}$ versus applied magnetic field $\boldsymbol{H}$ a magnetic hysteresis loop is obtained for ferromagnetic and ferrimagnetic materials (Figure 2.3). Furthermore, as the intensity of the external magnetic field increases, the magnetic moments are aligned in direction of field until the saturation magnetization $\boldsymbol{M_S}$ is reached. If the magnetic field is removed and the material retains certain magnetization, it is called remanence magnetization $\boldsymbol{M_R}$. In order to demagnetize the material a coercive field $\boldsymbol{H_C}$ is applied causing the remanence magnetization to be reduced a zero. A magnetic field in opposite direction is applied for complete the magnetic hysteresis loop [26]. If the material is considered for applications in data storage and non-volatile memories, all these magnetics properties mentioned above have to be investigated.

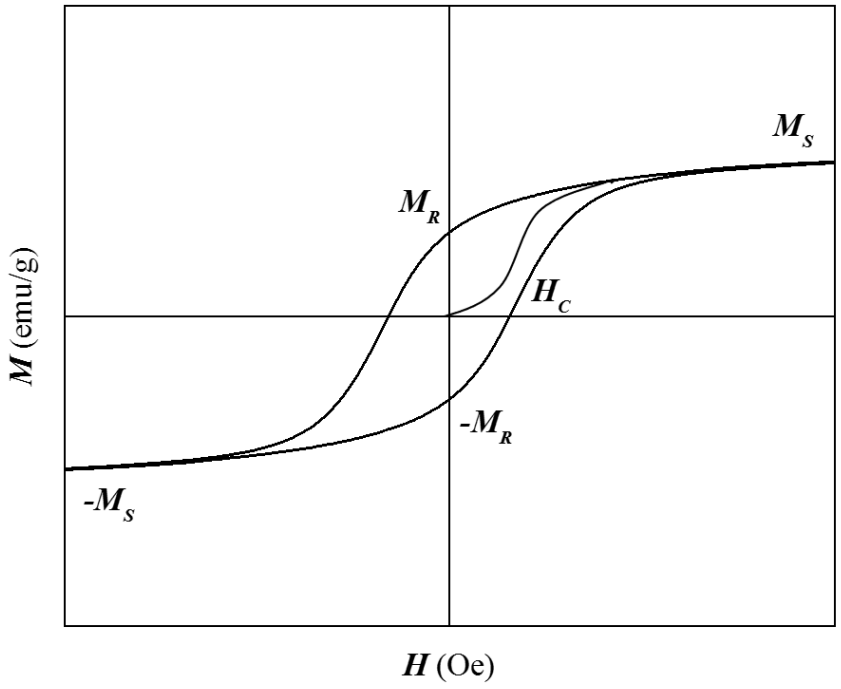

Figure 2.3 Magnetic Hysteresis Loop.

2.3 Ferroelectricity

Electric properties of the materials come from a phenomenon call electric polarization, where ions or their electrons (or other mobile charge carriers) experience a relative displacement induced for an external electric field, or electric dipoles are oriented towards electric field direction [28]. Polarization is defined as the contribution of all electric dipoles for unit of volume, and there are five types of electric polarization explained below [29].

Electronic Polarization

This kind of polarization is presented in atoms or molecules in most materials, it shows a displacement of outer electron cloud respect to atomic nucleus, therefore depends of atomic number and number of electrons present in the outermost shell.

Atomic or Ionic Polarization

Materials with two or more kind of atoms form ions due they share electrons, displacement of these anions and cations produce ionic polarization.

Oriental Polarization (Dipolar Polarization)

Some molecules with asymmetrical structures present permanent electric dipoles oriented in random directions in absence of external electric fields; when a field is applied, dipoles are oriented towards field direction and a net polarization is obtained and, when the field is removed, dipoles return original position due thermal agitation.

Space Charge Polarization

It is produced for the movement of charge carrier (electrons, holes and ions). They are trapped and cannot discharge at an electrode.

Spontaneous Polarization

Paraelectric and Ferroelectric materials have electric order (like magnetic order) in their crystal structures, that's mean that electric dipoles have a preferential orientation, and therefore such materials show spontaneous polarization and net polarization in absence of an external electric field. Paraelectric materials show polarization different to zero in presence of an electric field, when the field is removed, polarization returns zero, by other hand, ferroelectric materials show a spontaneous and switchable electric polarization, and they have electric domains just like in ferromagnetic materials, when an electric field is applied, electric domains are aligned in the field direction. These materials display this behavior only up to a critical temperature called Curie temperature, above which a material goes through a phase transition. Such materials are characterized through measurement of electrical polarization versus electric field, resulting in a ferroelectric hysteresis loop (Figure 2.4).

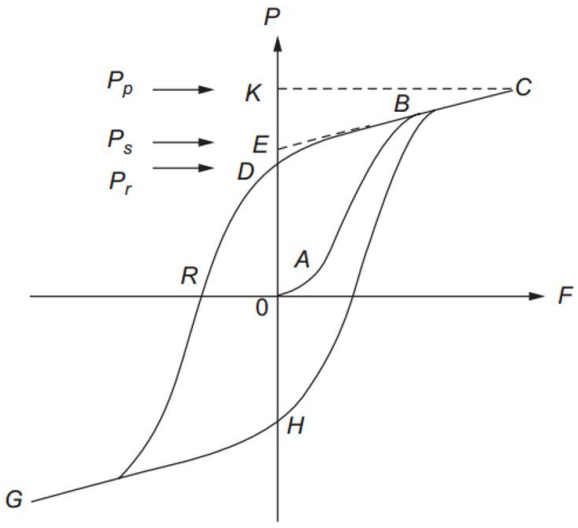

Figure 2.4 Ferroelectric Hysteresis Loop [29].

According to Figure 2.4 when apply a low electric field ***F***, electric polarization ***P*** change linearly with field (section *0A*), but when field is increased, polarization does not change linearly,

and dipoles get aligned parallel to the applied field up to reach a saturation state (section *BC*) where the point *K* shows the value of saturation polarization $\boldsymbol{P_p}$. If section *BC* is tangentially prolonged to intersect the polarization axis, a spontaneous polarization $\boldsymbol{P_s}$ (point *E*) is reached. If the field is removed, a remanent polarization $\boldsymbol{P_r}$ is achieved (point *D*). Furthermore, a coercive field is necessary to back this remanent polarization to zero (point *R*). Finally, the hysteresis loop is completed when a field in reversal direction is applied.

2.4 Bismuth Ferrite Properties

Bismuth Ferrite (BFO) is the most known multiferroic material that exhibits ferroelectric and antiferromagnetic ordering at room temperature. Additionally, it possesses good optical and photovoltaics properties, therefore these features make it an excellent candidate in applications like sensors, data storage, non-volatile memories, RAM memories and photovoltaics devices. $BiFeO_3$ has a perovskite structure type ABO_3, with cation Bi^{3+} in A-site and cation Fe^{3+} in B-site, handling and control of this structure allow the possibility of an electromagnetic coupling, this mechanism opens chances for applications in other kind of devices.

2.4.1 Crystalline Structure of $BiFeO_3$

Bismuth Ferrite has rhombohedral distorted perovskite crystal structure with space group R3c, it has a lattice parameter a_{rh} = 3.965Å and rhombohedral angle α_{rh} : 89.3-89.4° [6], rhombohedral structure is obtained from cubic perovskite unit cell (Figure 2.5 (a)), where in cube corners are the bismuth ions, and inside cube there is a FeO_6 octahedra, two pseudocubic cells have joined to form rhombohedral structure (Figure 2.5 (c)), and its octahedra tilting angle is about

11°. Additionally, a highly distorted tetragonal-like phase of BFO can be reached (Figure 2.5 (d)) with large *c*/*a* ratio, where *a* and *c* are the lattice parameters in tetragonal phase.

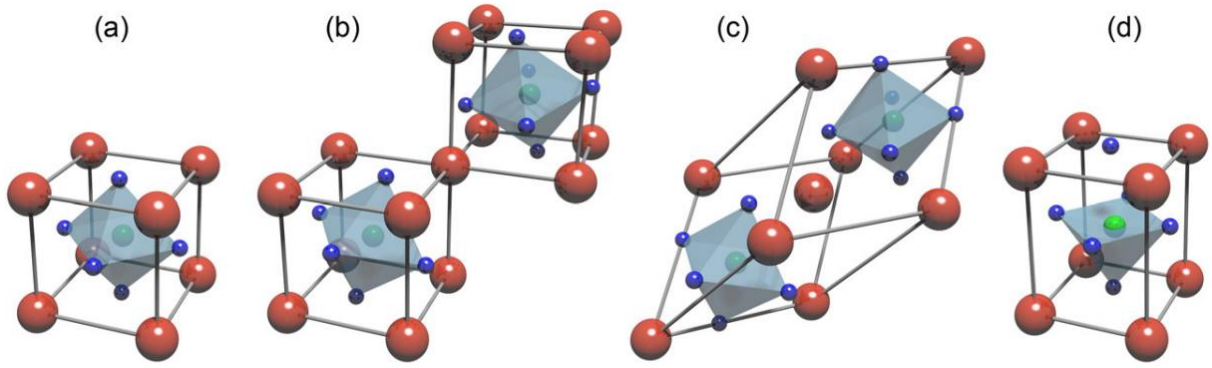

Figure 2.5 Pseudocubic structure of BFO (a), two pseudocubic joined (b) to form rhombohedral structure of BFO (c), tetragonal phase of BFO (d) [30].

On the other hand, there is a hexagonal representation of space group R3c, i.e. unit cell is depicted in a hexagonal frame of reference (Figure 2.6), where the hexagonal c-axis with [001] direction is parallel to the diagonal of the perovskite cube with [111] direction. Lattice parameters of BFO in hexagonal setting are a_{hex} = 5.58Å and c_{hex} = 13.90Å [6], most of researchers use this setting rather rhombohedral structure for estimate structural parameters [31]–[34].

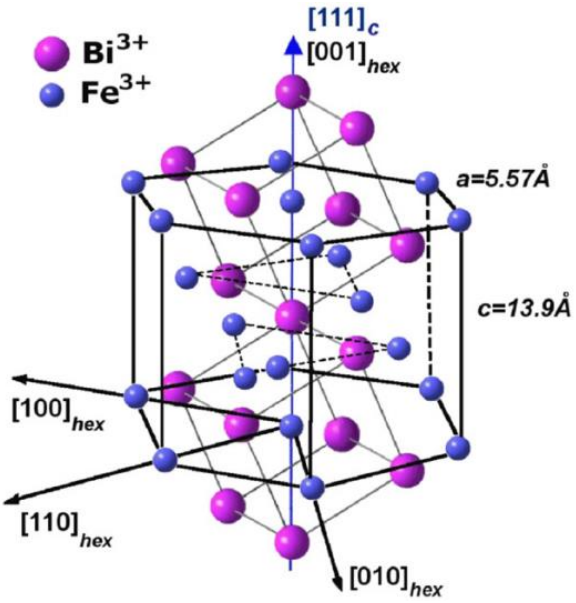

Figure 2.6 Crystal structure of Bismuth Ferrite in hexagonal unit cell and rhombohedral representation [3].

2.4.2 Magnetic Properties

Bismuth Ferrite has a G-type antiferromagnetic order with a Neel temperature of ~ 673 K [35], each Fe^{3+} spin is surrounded for 6 antiparallel spin of the nearest Fe^{3+} neighbors (Figure 2.7).

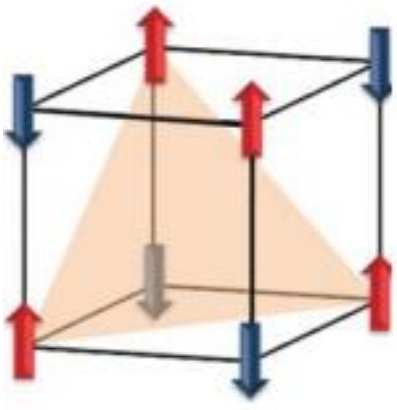

Figure 2.7 G-type antiferromagnetic order of Bismuth Ferrite [36].

Superexchange interaction

Antiferromagnetic ordering is produced by a quantum mechanical effect called superexchange. Commonly, exchange interaction occurs between two neighboring atoms when the coupling of their orbits results in a direct exchange of electrons between the atoms. The exchange gives rise a rearrangement of the electron spins. This process is carried out in agreement with Pauli's principle and Hund's rule.

Superexchange interaction is an indirect exchange of electrons between two atoms through of a non-magnetic ion mediator. The O^{2-} anion is the mediator in the Fe-O-Fe bond that allow the superexchange in $BiFeO_3$. The only way that the interaction between the 2p orbital from O^{2-} and the 3d orbitals from Fe^{3+} takes place is that O^{2-} anion donate their electrons to the Fe ions. Figure 2.8 shows a schematic illustration of the superexchange effect. Assuming that the five electrons in the 3d orbital for the left Fe-ion have up-spin states, the electron donated from the oxygen must have a down-spin state to satisfy Pauli'principle. Also, the remaining electron in oxygen will have an up-spin state and, using the same argument, when this electron is donated to the right Fe-ion, the five electrons of this ion should have down-spin states. Hence, antiparallel spin alignment is promoted between the Fe-ions [37].

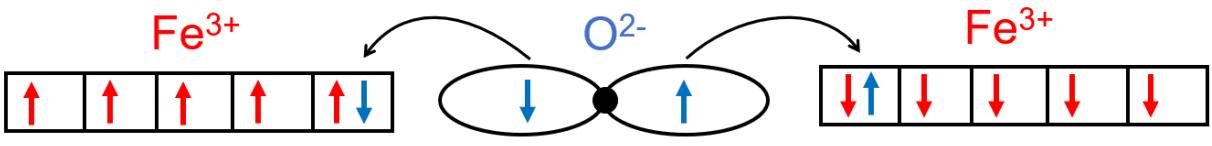

Figure 2.8 Superexchange interaction effect in $BiFeO_3$ [26].

According to Goodenough-Kanamori rules when the Fe-O-Fe bond angle is between 120°-180° the exchange is strong and induces an antiferromagnetic order. On the other hand, if the Fe-O-Fe bond angle is ~90° the exchange induces a weak ferromagnetic order [25].

Dzyaloshinski-Moriya interaction and Spiral Spin Structure

In materials with R3c symmetry the spins are not totally antiparallel due to Dzyaloshinski-Moriya interactions on which the spins display a weak canting moment, and this produce a weak ferromagnetism in $BiFeO_3$. Additionally, the ordering of the spins in BFO have a spiral spin configuration with a periodicity of 62 nm. This spiral spin structure induce net ferromagnetism equals to zero [6], [38].

2.4.3 Ferroelectric Properties

Structure noncentrosymmetric of bismuth ferrite is due to ferroelectricity induce for stereochemical active $6s^2$ lone electrons pair of Bi^{2+} cations, these electrons lead displacement of cations Bi^{2+} with respect the oxygen octahedral cage (Figure 2.9). BFO has a ferroelectric transition at Curie temperature of ~ 1103 K, and the ferroelectric polarization is along diagonal of the perovskite unit cell in [111] direction [6].

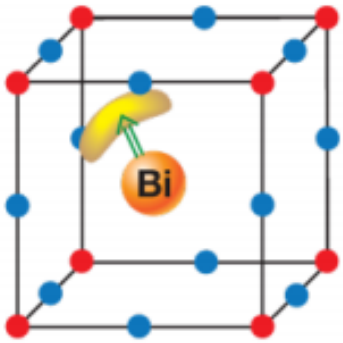

Figure 2.9 Electric polarization of BFO induced for stereochemical active lone electrons (yellow lobes). (Fe ions: red, O ions: blue) [39].

2.5 Magnetoelectric Coupling

An interesting characteristic of multiferroics is that they present ferroelectric and ferromagnetic orders in a same phase, but if magnetic properties can be switched with electric field as well as magnetic field, and the same behavior happens with electric properties, it opens a lot of possibilities of applications, this phenomenon is known as magnetoelectric coupling.

Magnetoelectric effect can be described for free energy G, if expand it in terms of the magnetic field M and electric field E [28]:

$$G(E, H) = G_0 + P_i E_i + M_i H_i + \frac{1}{2}\varepsilon_{ij} E_i E_j + \frac{1}{2}\mu_{ij} H_i H_j + \alpha_{ij} E_i H_j + \frac{1}{2}\beta_{ijk} E_i H_i H_k + \frac{1}{2}\gamma_{ijk} H_i E_j E_k + \ldots \quad (2.2)$$

Where M_i and P_i are the spontaneous magnetization and electric polarization, respectively; μ is the magnetic permeability; ε is the dielectric permittivity; α correspond to the linear magnetoelectric susceptibility tensor; and β and γ are the bilinear magnetoelectric susceptibility tensors. In a particular case, $BiFeO_3$ exhibit quadratic magnetoelectric effect in undoped phase, doping BFO destroy spiral spin structure and linear (firs order) magnetoelectric effect is showed [33].

CHAPTER III: LITERATURE REVIEW

3.1 Undoped $BiFeO_3$

Bismuth Ferrite is a known multiferroic that exhibit antiferromagnetic and ferroelectric properties at room temperature, but it presents some problems to its development in electronic devices due weak magnetism and leakage current, specimens free-impurities is other principal challenge. Different methods of synthesis to undoped phase of BFO in powders and thin films have been used to overcome these issues through control of particle size and changes in synthesis parameters of undoped BFO.

M. Hasan *et al.* [40] synthesized Bismuth Ferrite nanoparticles using a modified Pechini sol-gel method, the precursor powders were annealed at 400-600°C for 2 hours in air. Finally, samples were washed with acetic acid to removal of impurities. Washing minimized impurities for all the temperatures. They found that while annealing temperature is reduced, particle size decrease too, additionally, magnetization was increased with decrease size particle, 40 nm particles obtained a value of 1.4 emu/g in contrast with 21 nm particles with 7.5 emu/g. A change from antiferromagnetic to ferromagnetic order is evident in the M-H loops, researchers suggest as possible reasons for an enhancement in magnetization to size confinement effect, surface spin disorder and a distortion in spin cycloid magnetic structure. Spin cycloid magnetic structure is given in single phase bismuth ferrite, with an antiferromagnetic order G-type [41].

By other hand, M. Sakar *et al.* [42] reported the synthesis of BFO nanostructures by a wet chemical hydro-evaporation method, and analyzed effect of annealing temperature (450°C, 550°C

and 650°C) in structural and magnetic properties of the samples, XRD patterns showed impurity phases only in specimens annealed at 450°C, maybe due kinetic formation of BFO at this lower temperature. Grain sizes were calculated using Scherrer's equation showing a decrease as well as annealing temperature reduced. Bismuth Ferrite annealed at 450°C and 650°C exhibited an antiferromagnetic behavior, while BFO annealed at 550°C showed a weak ferromagnetism. According to the authors, oxygen vacancies in the material would induce an improvement in magnetic properties, FTIR analysis for samples annealed at 550°C verified a shift of the bending vibration of Fe-O bond towards higher frequency indicating presence of oxygen vacancies.

L. Wang *et al.* [10] prepared bismuth ferrite nanoparticles through low-heating temperature solid-state method, precursors were calcined between 425-600°C for 2 hours, the resultant specimens were leached with HNO_3 to remove secondary phases. A marked increase in magnetization for samples calcined at 600°C was found, authors attribute this behavior to secondary phases of γ-Fe_2O_3 reported in other research where presence of maghemite do not appear in XRD, but it was detected for other techniques [43].

Measurement of electrical properties in powders require convert them in pellets, some problems like porosity and compaction can appear in its preparation. S. Godara *et al.* [44] produced bismuth ferrite nanoparticles by auto-combustion route, powders were processed into pellets and annealed at 500°C for 2 hours. The particle size of the BFO nanoparticles was 50nm and they reported a week ferromagnetic order in M-H hysteresis loop measured at room temperature. Ferroelectric hysteresis (P-E) loop showed that the sample was able to bear an electric field as high

as 85kV/cm without breaking down which was attributed to very low leakage current of the order of $\mu A/cm^2$. The remanent polarization was obtained to be 0.4 $\mu C/cm^2$. Unlike powders, synthesis of BFO thin films exhibit large remnant polarization.

Z. Lin *et al.* [45] prepared bismuth ferrite thin films by sol-gel spin coated method and analyzed effects of annealing temperature on microstructure and ferroelectric properties. Acetic acid was used as solvent and thin films were deposited on the quartz glass and Pt/(100nm)/Ti(30nm)/SiO_2(500nm)/Si(500µm) substrates, samples were annealed at 550°C, 600°C and 650°C for 10 min in oxygen atmosphere. XRD showed an increase in impurities phases ($Bi_2Fe_4O_9$: mullite) with rise of annealing temperature. These secondary phases are attributed to volatilization of some reactants like bismuth nitrate and decomposition phases at high temperatures. The grains size in the films were calculated using Scherrer's equation obtaining values of 20nm, 22nm and 29nm for 550°C, 600°C and 650°C respectively. P-E hysteresis loop was measured at 200 Hz, the remanent polarization decreased with rise in annealing temperature, authors suggest two reasons: $Bi_2Fe_4O_9$ present in samples annealed at 650°C have a Curie temperature in -23°C, therefore exhibit paralectric order at room temperature and reduce the remnant polarization in the sample. By other hand, oxygen vacancies are others motives for change in remanent polarization, besides they enhance leakage current that is harmful for electric properties. An increase in coercive electric field was observed when the annealing temperature raised.

Y. Wang *et al.* [46] observed small saturation polarization but high saturation magnetization in thin films synthesized via sol-gel spin coating method, with control of thickness of the films by the number of layers spin coated. Samples were annealed at 630°C in air for 300-400 sec. Remnant polarization and saturated polarization were 0.36 and 0.88 μC/cm^2 and 0.69 and 1.87 μC/cm^2 for the films of 100 and 130nm in thickness, respectively, electric properties were measured at 1kHz. Films with 130nm of thickness displayed ferromagnetic behavior with a saturation magnetization of 95 emu/cm^3.

Epitaxial $BiFeO_3$ thin films heterostructures were grown in phase pure by J. Wang *et al.* [47] via pulsed laser deposition (PLD) onto single crystal $SrTiO_3$ (100) substrates. Hysteresis P-E loop was measured at 15kHz for film with a 200 nm of thickness, and a remnant polarization of 50 to 60 μC/cm^2 was observed, an order of magnitude higher than the highest reported value of 6.1 μC/cm^2 from bulk bismuth ferrite. A thickness dependence of the magnetization was reported, for the thinnest film (70nm) the saturation magnetization was ~ 150 emu/cm^3, as film thickness increases to 400 nm, magnetization decreases to ~ 5 emu/cm^3.

One of the main challenges in Bismuth Ferrite processing is the synthesis of pure $BiFeO_3$, i.e. nanocrystalline BFO powders and thin films, without presence of impurity phases [48]. This work seeks to tackle this challenge by investigating suitable annealing conditions (temperature and time) that prevent the formation of secondary phases and enhance structural and magnetic properties of the material.

Multiferroic properties of undoped $BiFeO_3$ can be enhanced through doping, replacing different ions either in A-site or B-site (perovskite structure has this form ABO_3, in bismuth ferrite A-site and B-site correspond to Bi and Fe respectively) [49]. In this work, non-magnetic Bi species were replaced by magnetic species like Co and Mn for improve magnetic properties. An exhaustive revision in Co-doped BFO and Mn-doped BFO, in powders and films has been done, consequential effects in properties of the material have been reported.

3.2 The Co-doped $BiFeO_3$ System

G. Montes *et al.* [50] produced nanocrystalline undoped and Co doped $BiFeO_3$ (Co: 5 at.% and 10 at.%) particles replacing Co^{2+} ions in Fe-site, powders were synthesized in polyol medium and annealed for 1 hour at temperatures from 500°C to 800°C. Impurities phases like $Bi_2Fe_4O_9$ and $Bi_{25}FeO_{39}$ were evidenced for peaks between 25°-30° 2θ range coexisting with $BiFeO_3$ phase in XRD spectra. But a decrease in secondary phases at high temperatures was observed in undoped and doped samples, by other hand, average crystal size was increased with high annealing temperature.

Impurities peaks lowered when Co concentration was increased at 10 at.% and presence of Cobalt Ferrite ($CoFe_2O_4$) phase in very less amount was detected. Saturation magnetization at 10 at.% Co doped BFO was 4.2 emu/g much higher than undoped BFO of 0.3 emu/g, similarly coercivity increased of 109.5 Oe in undoped BFO up to 988 Oe in 10 at.% Co doped BFO Enhancement in saturation magnetization and coercivity could be attributed to Cobalt Ferrite phase according authors. They suggest the formation of multifunctional $CoFe_2O_4$-$BiFeO_3$ materials and control of magnetic properties as magnetization and coercivity at room temperature. The same authors doped

Co^{2+} in Bi-site too, and using the same method of synthesis added Bi excess to improve a better crystallization of the material, samples were annealed for 1 hour at 700°C. Doping with Co ions improved magnetic properties again for the presence of Ferrite Cobalt detected in short amounts for XRD analysis, and incorporation of Co inhibited the apparition of secondary phases [17].

Recently, P. *Tang et al*. [51] found also secondary phases of Cobalt Ferrite in Co-doped $BiFeO_3$ nanoparticles prepared by sol-gel method, samples were synthesized with excess 3% Bi and calcinated at 600°C for 2 h. BFO was doped with Co ions to replace Fe species, with Co at 5%, 10%, 15%, 20% and 25%. Impurities like $Bi_{25}FeO_{40}$ increased with higher doping concentrations of Co, and a small amount of $CoFe_2O_4$ was detected in XRD spectra for 20% and 25% of Co doping. M-H loops showed an antiferromagnetic behavior in undoped BFO nanoparticles, and an evident change to ferromagnetic order in samples doped with Co. Enhancement in magnetic properties when Co concentrations were increased could be attribute to destruction of spiral spin structure or magnetic features of Co^{2+}; however, samples 20% Co-doped and 25% Co-doped exhibited a high increase in saturation magnetization compared with other concentrations, presence of Cobalt Ferrite phase could be the principal reason for this marked improvement. Contribution of $Bi_{25}FeO_{40}$ in magnetic properties was discarded because it is paramagnetic at room temperature. A decrease in crystal size was evidenced when Co concentrations were increased, possibly for a difference in ionic radii in the substitution of Fe ions for Co ions, which would have induced crystal distortion and consequently a change in the multiferroic properties.

U. Khan *et al.* [38] synthesized nanocrystalline cobalt-doped bismuth ferrite by solution evaporation method. Nanoparticles with the $BiFe_{1-\delta}Co_{\delta}O_3$ stoichiometry were doped at $\delta = 0.025$, 0.05, 0.075, and 0.1 and annealed in air at 600 °C for 1 hour. XRD showed powders highly crystalline and there was no presence of impurities phases for any doping condition. An increase of crystallite size was observed with increase in Co doping, lattice parameters were calculated using hexagonal structural frame of reference, these parameters and cell volume showed a trend to decrease when increased Co concentration. Substitution of Co ions with a smaller ionic radii about Fe ions, induces a contraction of unit cell volume. Magnetic properties were studied using a vibrating sample magnetometer (VSM), M-H loops measured at room temperature showed an increment in saturation magnetization with Co doping, and an increase in coercivity up to δ=0.075. Authors attributed this enhancement in magnetic properties to the exchange interactions between Co and Fe ions and a larger magnetic moment of Co about Fe species.

K. Chakrabarti *et al* [34] studied magnetic and dielectric behavior in Co doped $BiFeO_3$ nanoparticles prepared using sol-method and sintered at 550°C for 4 hours in air. No traces of impurities phases show in XRD spectra, ensuring incorporation of Co ions in Fe sites. Reduction in volume with increase of Co doping was observed due a difference in ionic radius between Co and Fe ions. Besides a change in morphology from spherical to cubic nanostructures was observed with Co doping. Same as other researches, magnetic properties like saturation magnetization and coercivity enhanced when Co doping was increased. Powders were compacted in pellets for dielectric measurements, increase in dielectric constant and decrease in dielectric loss was found

with Co doping. Improvement in dielectric and magnetic properties make Co doped BFO a potential material in multifunctional devices.

I. Kamal *et al.* [52] obtained an enhancement in magnetic properties in Co-doped $BiFeO_3$ synthesized by sol-gel method and calcination in air for 1 hour at 600°C. Impurities phases were detected in undoped and 10%Co doped $BiFeO_3$. Increasing in unit cell volume was observed only up to 5% Co concentration, for 10% Co cell volume decreased, it could indicate that a saturation level of forming solid has been reached in 5% Co concentration. P-E loops measured at room temperature did not shown saturation due leakage current present in the samples. Authors suggested that oxygen vacancies induced increase of dielectric constant and ac conductivity, and also a decrease of loss tangent in Co doped samples compared with undoped BFO.

L. Peng *et al.* [53] prepared $BiFe_{1-x}Co_xO_3$ thin films with x= 0, 0.03, 0.05 and 0.1, using sol-gel method, reagents were dissolved in ethylene glycol and acetic acid. Solutions were deposited on quartz substrates and spin coated at 4000 rpm for 20 secs, finally precursors films were annealed at 600 °C for 300s. XRD confirmed distorted rhombohedral perovskite structure, a slight impurity peak of $Bi_2Fe_4O_9$ was observed in samples with 5% Co and 10% Co but impurity phases of Co oxides were not detected. Saturation magnetization, remanent magnetization and coercivity were increased with Co doping; authors attributed enhancement in magnetization to structure distortion due ion substitution. Ferroelectric properties were not studied.

In turn, I. Coondoo *et al.* [54] synthesized BFO and 5% Co doped BFO by chemical solution deposition method, films were coated on Pt(111)/TiO_2/SiO_2/Si(100) substrates at 2500 rpm for 30 sec and then dried, process was repeated 15 times and thin films obtained a thickness ~300 nm. Films were annealed at 550°C for 1h in N_2 atmosphere. Patterns of rhombohedrally distorted $BiFeO_3$ perovskite without impurity phases were observed in XRD, a decrease in lattice constants of Co-doped BFO in comparison with undoped BFO samples confirms substitution of Co in Fe sites. Magnetization was enhanced with Co doping, this result suggests a suppression of spiral spin structure due incorporation of Co ion in Fe sites. P-E hysteresis loop of undoped Bismuth Ferrite evidenced current leakage due to the generation of rounded shape loop. Co doped BFO film showed a better loop, possibly by a reduction in leakage current, but a smaller electric polarization and non- saturation.

Unlike previous researchers D. Barrionuevo *et al.* [55], synthesized Co doped Bismuth Ferrite thin films with compositions less than 3% Co by solution route. The films were deposited on platinum substrates with spin coating method at 5000 rpm for 30 secs and annealed at 530°C for 1h in air atmosphere. Major peaks of rhombohedral distorted perovskite structure were identified in all samples, and a peak of $Bi_2Fe_4O_9$ impurity was observed at 3% Co. Magnetic measurements showed an increase in magnetization with Co doping, enhancement could be attributed to the elimination of oxygen vacancies and structural distortion by incorporation of Co ions in Fe sites. Ferroelectric properties were measured at 10kHz with an applied electric field of 170 kV/cm, saturation was not observed in P-E hysteresis loop, but remanent polarization was enhanced from 0.08 $\mu C/cm^2$ for pure BFO to 0.4 $\mu C/cm^2$ for 2% Co doped BFO.

3.3 The Mn-doped $BiFeO_3$ System

V. Srinivas *et al.* [56] prepared nanocrystalline $Bi_{1-x}Mn_xFeO_3$ (x=0, 0.1, 0.2 and 0.3) by sol-gel method, samples were heat treated at 600 °C. Impurity phases were observed in the XRD patterns in the 2θ range between 25° and 30°, samples with Mn doping at x<0.2 exhibited rhombohedral structure, but in x=0.2 crystal structure changed to tetragonal phase and it was evidenced for a splitting of a peak at 46° in two peaks (002) and (200) that belong to tetragonal space group. Magnetic hysteresis evidenced unsaturated magnetization, although an enhancement in magnetization was manifested when Mn doping increased, a fact that was attributed to Jahn-Teller distortion effect.

Similarly, G. Arya *et al.* [57] studied ferroelectric and magnetic properties of $BiFe_{1-x}Mn_xO_3$ (Mn compositions 0%, 2.5%, 5% and 7.5%) nanoparticles synthesized by sol-gel method, powders were sintered at 820°C for 450s in air atmosphere. XRD showed presence of impurity phases for pure and Mn doped BFO samples at 2.5% Mn concentration, but in 5%Mn secondary phases were suppressed. Magnetization increased with Mn doping and the maximum value of magnetization was 0.02 emu/g for 5% Mn doped BFO, possibly because elimination of impurities in this samples. Electric measurements were done at frequency of 50Hz at room temperature, polarization-electric field (P-E) hysteresis loop with rounded shape were observed due leakage current present in all pellet samples. An improvement in the remnant polarization was evidenced with Mn doping.

F. Yan *et al*. [58] fabricated undoped and Mn-doped BFO (%Mn at 0.5% and 2%) powders using conventional solid state method. Diffraction patterns showed in XRD were identified as a

rhombohedral phase for all samples, additionally, low quantities of Mn-related impurity phases were observed. P-E hysteresis loop was measured at 1kHz and at room temperature, an increment in ferroelectric polarization was verified in Mn-doped BFO samples, a possible explanation is that Mn substitution induce a chemical strain, and it could change polarization. Leakage current increased with Mn concentration. Magnetic hysteresis showed an improvement in magnetization when Mn doping is increased.

Kuk Kim *et al.* [59] reported undoped and Mn-doped $BiFeO_3$ thin films synthesized by chemical solution deposition on $Pt(200)/TiO_2/SiO_2/Si(100)$ substrates, precursor films were deposited with spin coating method at 3500 rpm for 25 secs and annealed in the temperature range of 450-550 °C for 30 min in N_2 atmosphere. Samples showed perovskite phase in XRD analysis, and impurities were not detected. Authors suggest that Mn doping minimize oxygen vacancies and consequently leakage current is reduced, and it was reflexed in P-E hysteresis well-saturated.

W. Cai *et al.* [60] deposited Mn-doped BFO on Pt using sol-gel spin coating method, samples were annealed at 550°C for 10 min in oxygen atmosphere. XRD patterns were identified as rhombohedral distortion perovskite structure and impurity phases were not detected, that suggest total incorporation of Mn in the crystal structure. Ferroelectric hysteresis loop measured at 1 kHz did not show saturation in any samples, but an increase in remnant polarization and coercive electric field was observed when Mn doping increased.

J. Li *et al.* [61] prepared undoped and Mn-doped BFO thin films via sol-gel method, precursor films were deposited on indium tin oxide/glass substrates by spin coating method at 3000rpm for 20s. XRD analysis for undoped BFO samples showed rhombohedral perovskite structure, but in Mn-doped BFO samples a tetragonal structure was detected with a change in grain orientation growth of the films. Reducing in leakage current was observed only in small quantity of Mn concentration (Mn: 2.5%, 5% and 7.5%). Saturation magnetization was increased in the same doping contents of Mn. Authors mention two mechanisms as plausible explanations for enhancement in magnetization, incorporation of Mn could destroy spin cycloid ordering, and Jahn-Teller effect can induce a distortion in the films and therefore incite a spin rearrangement.

For Co and Mn doped BFO systems, the principal challenge is to achieve the incorporation of Co^{2+} and Mn^{2+} species in host BFO to enhance structural properties and minimize impurity levels. On the other hand, substitution of diamagnetic species of Bi for magnetically active transition metals like Co and Mn should improve magnetic properties in BFO [62]. Besides of their magnetic properties, Co and Mn species could also contribute to the formation of secondary phases such as Cobalt Ferrite and Manganese Ferrite, respectively. These ferrites have attractive magnetic properties [63], [64].

Based on the above considerations, the present work investigated the appropriate conditions of annealing time and temperature, and doping type and level, to obtain undoped and doped BFO with suitable purity, structurally and magnetic features.

CHAPTER IV: EXPERIMENTAL

4.1 Synthesis of undoped and doped powders of Bismuth Ferrite

i. Materials

All reagents were of analytical grade and used without any further purification. Bismuth Nitrate [$Bi(NO_3)_3.5H_2O$, 99.9% Alfa Aesar], Iron Nitrate [$Fe(NO_3)_3.9H_2O$, 99.9% Alfa Aesar] were used as the precursor salts, Cobalt(II) Acetate [$(CH_3CO_2)_2Co{\cdot}4H_2O$] and Manganese(II) chloride tetrahydrate [$MnCl_2{\cdot}4H_2O$, 99%, Alfa Aesar] were used as the precursor dopant elements whereas Ethylene glycol [EG, $HOCH_2CH_2OH$, 99% Alfa Aesar] was the solvent.

ii. Materials Synthesis

Well-crystallized $BiFeO_3$ nanocrystalline powders were synthesized by a modified sol-gel method proposed in our earlier works [65]. Suitable weights of $Bi_{(1-x)}Co_xFeO_3$ and $Bi_{(1-x)}Mn_xFeO_3$ salts are used to achieve the desired atomic fractions, 'x' (0, 0.03, 0.05 and 0.07, or 0, 3, 5 and 7 at.% Mn; and 0-0.10 and 0.15 or 0-10 and 15 at.%). Precursor salts were dissolved in ethylene glycol medium at 150°C under mechanical stirring for 1 hour in homogenization stage, followed by drying at 350°C for about 2 hours and milling of the precursor samples. The obtained solid precursor was then annealed in air atmosphere for 15, 30 and 45 minutes at 700°C (heating rate was 5°C/min in all the samples) to develop the desired crystalline structure. Finally, samples are in optimal conditions for characterization. Figure 4.1 shows flow diagram of the modified sol-gel synthesis of powders and Figure 4.2 shows the setup of the synthesis process.

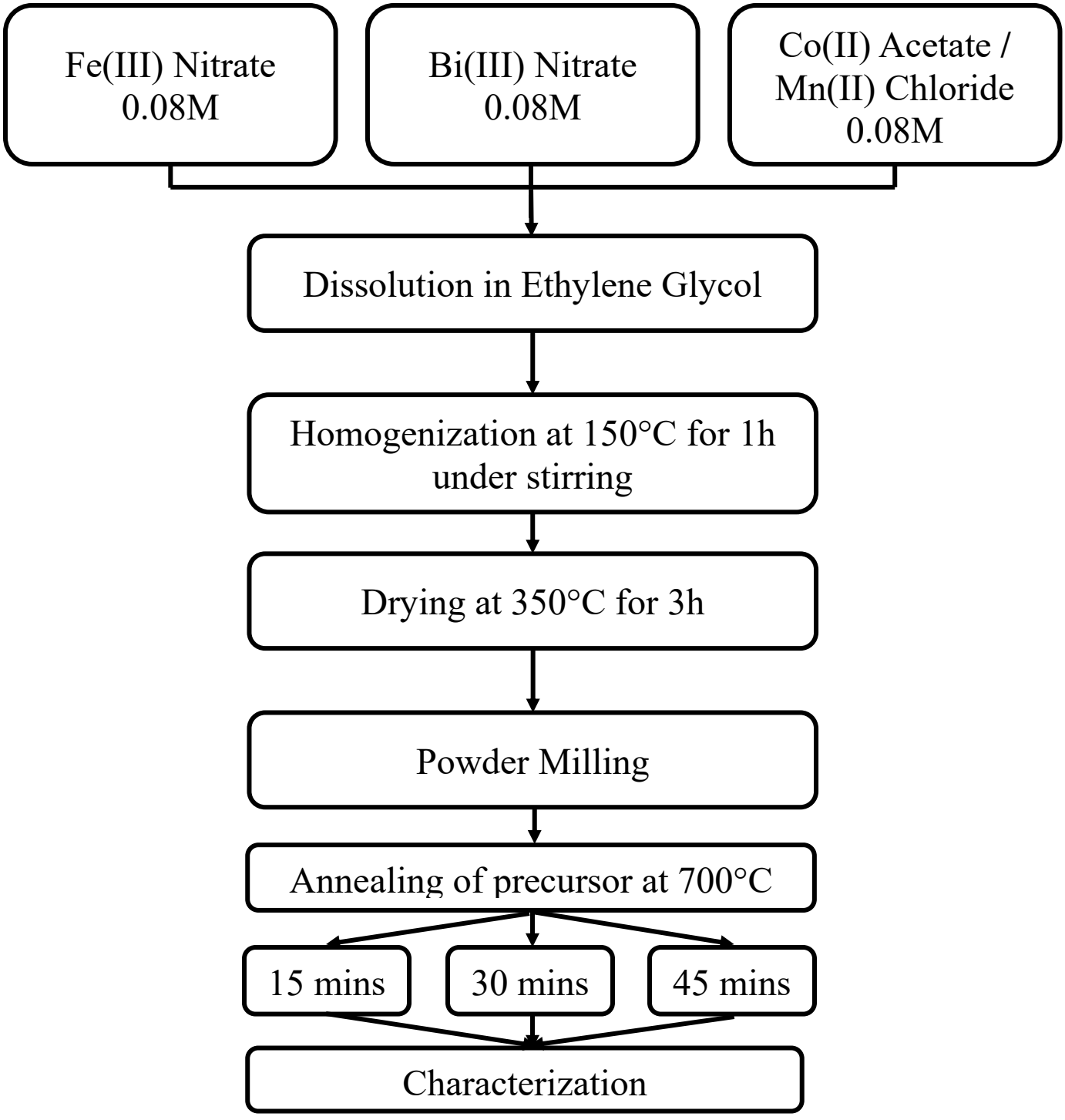

Figure 4.1 Flow diagram of the modified sol-gel method for synthesis of $Bi_{(1-x)}Co_xFeO_3$ and $Bi_{(1-x)}Mn_xFeO_3$ nanocrystalline powders.

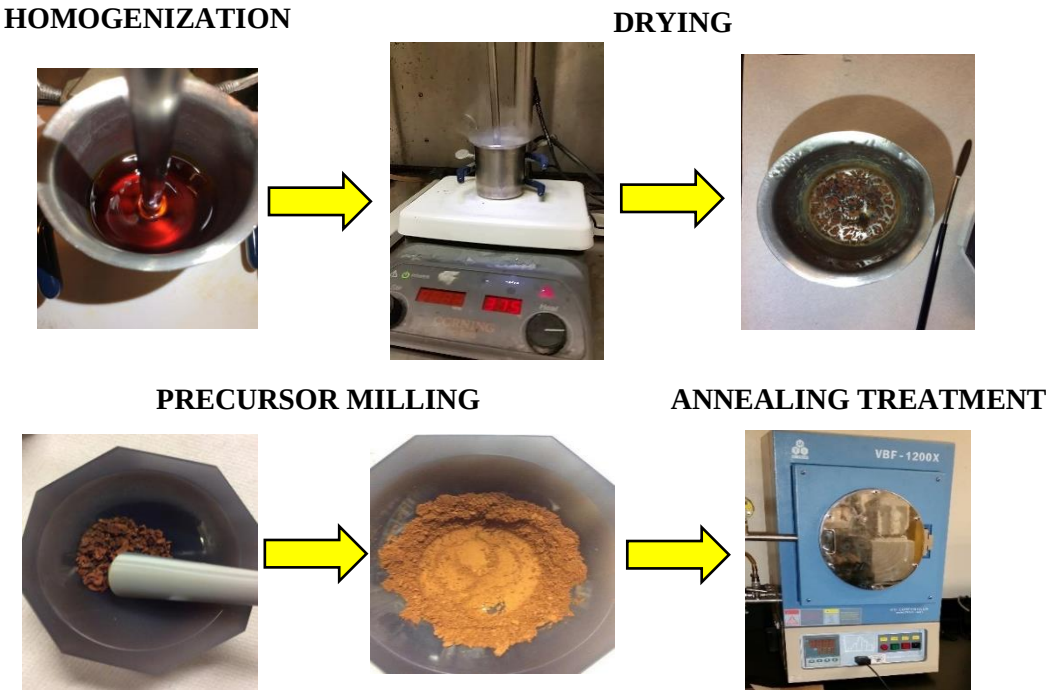

Figure 4.2 Setup for the modified sol-gel method in synthesis of $Bi_{(1-x)}Co_xFeO_3$ and $Bi_{(1-x)}Mn_xFeO_3$ nanocrystalline powders.

4.2 Synthesis of undoped and doped Thin Films of Bismuth Ferrite

i. Materials

All reagents were of analytical grade and used without any further purification. Bismuth Nitrate [$Bi(NO_3)_3.5H_2O$, 99.9% Alfa Aesar], Iron Nitrate [$Fe(NO_3)_3.9H_2O$, 99.9% Alfa Aesar] were used as the precursor salts, Cobalt(II) Acetate [$(CH_3CO_2)_2Co{\cdot}4H_2O$] was used as the precursor dopant element whereas Glacial Acetic Acid [CH_3COOH, Ricca Chemical Company] was the solvent and glycol as the viscosity-controlling additive. Silicon substrates, purchased from Addison Engineering Inc., were thoroughly cleaned before spin-coating.

ii. Materials Synthesis

Thin films were synthesized using spin coating method. The synthesis started by dissolving the above mentioned precursor salts in acetic acid. The resulting solution was stirred by convection at 255°C for 1hour. Next 5ml of glycol was added to the solution to control its viscosity and was stirred for additional 10 minutes at the same temperature (Figure 4.3 a)). A clear solution homogenous was resulted to later be added drop-wise onto a clean Si (100) substrate and spin-coated at 2800 rpm for 12 secs. After each coating cycle, produced films are pre-dried for 5 minutes at two different temperatures (80ºC and 250ºC) to remove organic residuals. These spin-coating/drying cycles were repeated for fifteen times to thick the films (Figure 4.3 b)). The precursor film was then annealed in air atmosphere for 1hour at 600°C (heating rate was 5°C/min in all the samples). Finally, samples are in optimal conditions for characterization. Figure 4.4 shows flow diagram of spin coating method for synthesis of thin films.

Figure 4.3 Setup for spin coating method employed for the synthesis of $Bi_{(1-x)}Co_xFeO_3$ thin films. a) Synthesis of initial solution. b) Spin coater and hot plates for coating/drying process of films.

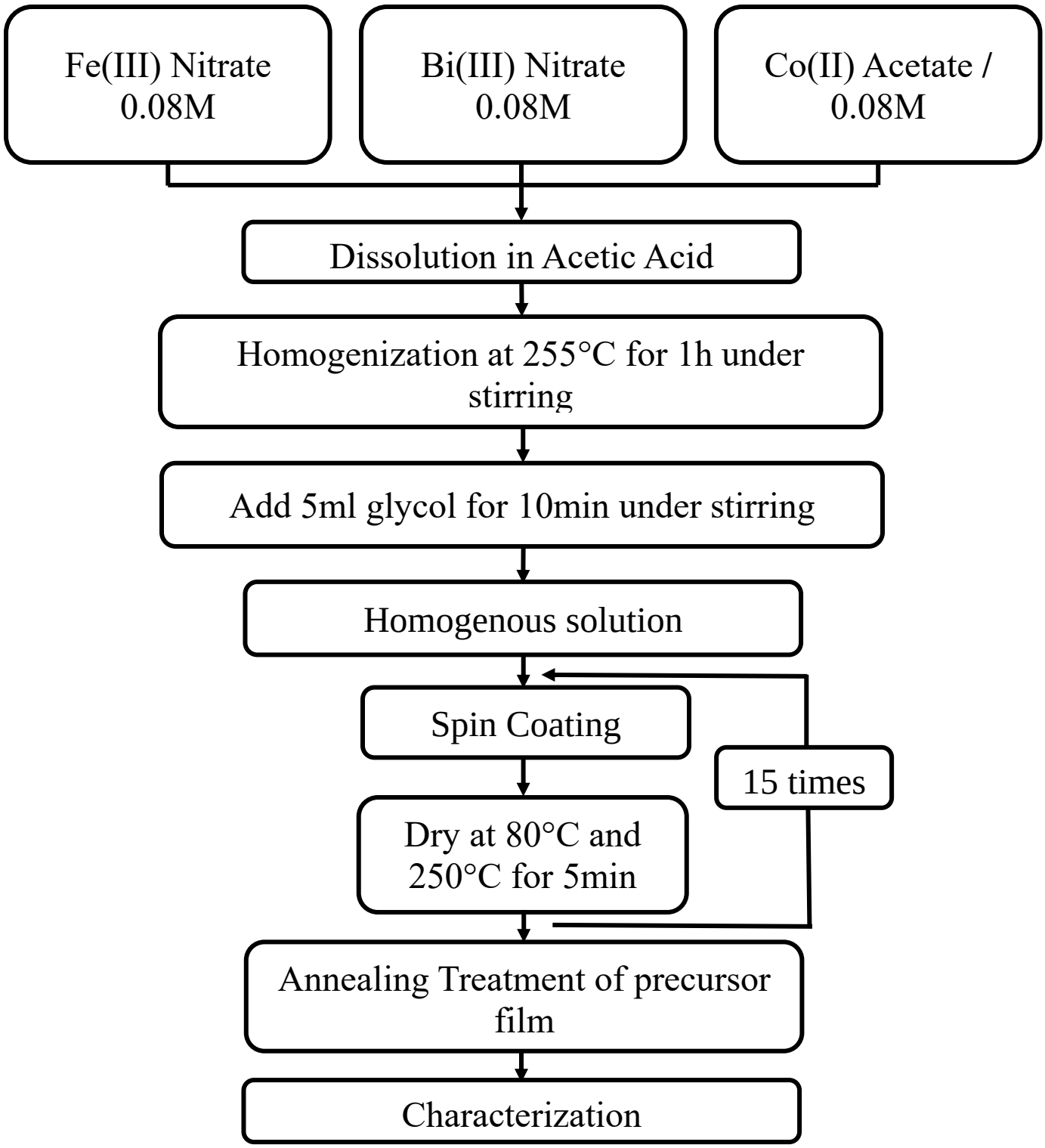

Figure 4.4 Flow diagram of spin coating method for synthesis of $Bi_{(1-x)}Co_xFeO_3$ thin films.

4.3 Characterization of the samples

The structure in the annealed samples was determined by X-ray diffractometry (XRD) using a SIEMENS D 500 diffractometer with a Cu-Kα radiation, the range of 2θ angle was setting from 20° to 65°, with a scanning step of 0.02° and 1 sec of sampling time. Fourier Transformed Infrared (FTIR) Spectroscopy confirmed the presence of perovskite structure in samples using a Shimadzu IR-Affinity spectrometer in transmittance mode. The morphology and size of the particles and were analyzed in a JEOL scanning electron microscope. Magnetic properties were measured at room temperature in a Lake Shore 7410 vibrating sample magnetometer (VSM).

4.3.1 X-Ray Diffraction (XRD)

X-Ray Diffraction is a non-destructive characterization method used to identify structural properties of the materials, we can verify the existence of crystalline (i.e. with a good atomic arrangement) or amorphous structures in the analyzed samples, determine composition of samples, lattice parameter and grain size. X-rays diffract in the crystallographic planes following Bragg's Law (Figure 4.5) [66]:

$$n\lambda = 2d\sin\theta \tag{4.1}$$

where n is an integer number indicating order of reflection, λ is the monochromatic wavelength of the x-ray beam, d is the interplanar distance of the crystallographic planes in the crystal, and θ is the incident and diffracted angle (Bragg's angle).

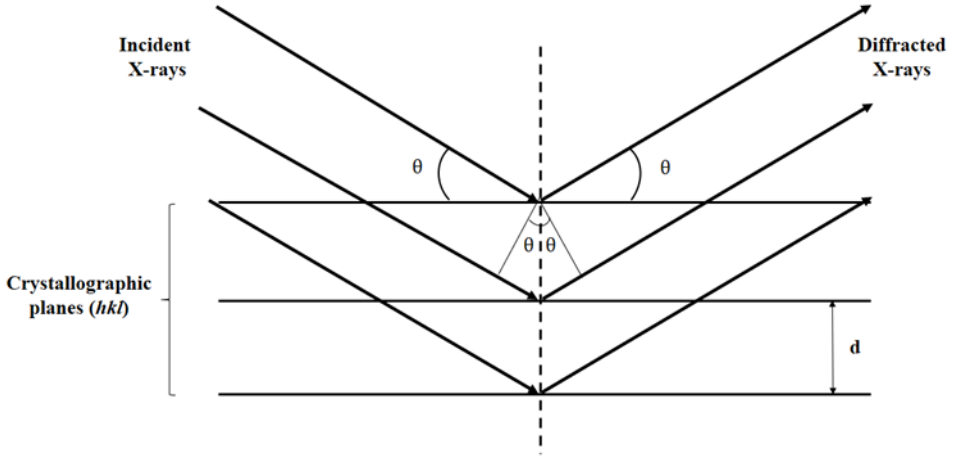

Figure 4.5 X-rays diffracting in the crystallographic planes of the crystal.

Lattice parameters can be calculated using interplanar distance ***d*** and the Miller's indexes **(*hkl*)** relating to these planes. There are different relations according to the crystal structure of the material. For this work the relation for hexagonal structure was used:

$$\frac{1}{\boldsymbol{d^2_{hkl}}} = \frac{4}{3}\left(\frac{\boldsymbol{h^2+hk+k^2}}{\boldsymbol{a^2}}\right) + \frac{\boldsymbol{l^2}}{\boldsymbol{c^2}} \tag{4.2}$$

Using Scherrer's Equation, average crystallite size can be determined if we now full width at the half high maximum (FWHM) and the diffraction angle θ [66]:

$$\boldsymbol{D} = \frac{0.9\boldsymbol{\lambda}}{\boldsymbol{B}cos\boldsymbol{\theta}} \tag{4.3}$$

B is the full width at the half high maximum (FWHM), **λ** is the wavelength of the x-rays and **θ** is the Bragg's angle. According equation (4.3) when the diffraction peaks are broader (***B*** increase), the size particle decrease. This equation has a good approximation only in the nanometric range. Phases present in the material were identified using Match Software.

4.3.2 Fourier Transform Infrared Spectroscopy (FTIR)

FTIR spectroscopy is a non-destructive technique used to identify functional groups, molecular bonds and presence of crystallographic defects qualitatively. Molecular Bonds vibrate in certain frequencies characteristic of their structure, bonds absorb infrared radiation only in these frequencies (resonant frequencies). Infrared spectrum shows bands of absorption or transmission of these frequencies to permit identification of the samples.

Crystallographic defects like vacancies can be detect qualitatively with FTIR spectroscopy, a shift in bands frequency will verify a change in the bonds vibration associated these defects, such shifts are predicted by simple harmonic oscillator model according equation (4.4) [67]:

$$\bar{\nu} = \frac{1}{2\pi c}\sqrt{\frac{k}{\mu}}\ , \quad \mu = \frac{m_1 m_2}{m_1 + m_2} \tag{4.4}$$

Where:

$\bar{\nu}$ is the wave number

c: is the velocity of light

k: is the constant force between two atoms

μ: is the reduced mass of bonding atoms m_1 y m_2

4.3.3 Scanning Electronic Microscopy (SEM)

SEM provide information about morphology and particle size, it allows observe surface features of the samples and show very detailed perception in 3 dimensional of the micrographs. Micrographs can be taking at different magnifications to determine particle size. Surface must be electrically conductive, if not, samples need a metallic coating, after that, they cannot be recovered.

4.3.4 Vibrating Sample Magnetometry (VSM)

VSM is an instrument that measures magnetic properties of bulk, powders, liquids or thin films samples. Magnetometer works on Faraday's Induction Law which says that a changing magnetic field will produce an induced voltage, this voltage can be measured and gives information about changing magnetic field in the sample. Specimen is placed in an external uniform magnetic field to magnetize it, sample is physically vibrated sinusoidally along z-axis. If the sample is magnetic, spins will alignment with the external magnetic field produced by an electromagnet. The magnetic dipole moment of the sample creates a field around the sample, as sample is moved up and down, magnetic field is changing in time and induce a voltage that is measured by magnetometer through pickup coils (Figure 4.6).

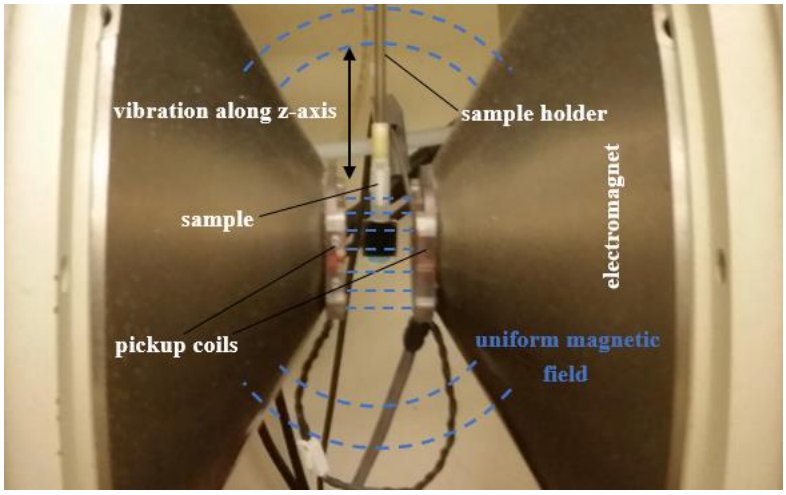

Figure 4.6 Measurement mechanism in VSM.

This instrument converts magnetic dipole moment of the samples in an ac electrical signal. Hysteresis loop or magnetization curve are obtained in this way, coercivity, saturation magnetization and remanent magnetization are found directly from magnetic hysteresis.

All graphs presented below were made in the OriginPro 9.0 software.

CHAPTER V: RESULTS AND DISCUSSION

5.1 Nanocrystalline $BiFeO_3$ powders

5.1.1 Effect of annealing time

X-Ray Diffraction (XRD) Measurements

Figure 5.1 shows the XRD patterns of undoped $BiFeO_3$ (BFO) powders synthesized by sol-gel method after an annealing treatment at 700°C for 0, 15, 30 and 45 minutes. The annealing temperature was determined according previous work within our research group [68]. The XRD patterns for the sample to 0 min correspond to the precursor material, when the samples are thermal treated, the BFO is formed. Match Software was used to verify that all main peaks fit with the rhombohedral perovskite structure of Bismuth Ferrite for all samples. As observed, less amount of impurities was observed in the samples annealed for 30 mins. Prolonging the annealing time, instead, favored the increase of the impurities. Diffraction peaks corresponding to impurity phases present in BFO, although in very low proportion, were located at 25°-30° 2θ range, and can be attributed to the presence of $Bi_2Fe_4O_9$ (mullite) or $Bi_{25}FeO_{39}$ (sillenite) [40]; such oxides can be produced for incomplete transition of precursor phases into BFO or for thermal decomposition at too high annealing temperatures and prolonged annealing times. Additionally, others reports suggest that high volatilization of Bi ions lead to generation of these secondary phases [69]–[71]. Lattice volumes were calculated considering a hexagonal frame of reference and were 365.14 $Å^3$, 367.29 $Å^3$ and 368.33 $Å^3$ for 15, 30 and 45 minutes of annealing, respectively. These values agree with others reported for undoped Bismuth Ferrite powders synthesized by different routes [14],

[72]. Average crystallite size was not determined because it exceeded the applicability limit for the Scherrer's equation.

Lattice volume increased with annealing time, but extended annealing time promoted the formation of impurity phases in undoped $BiFeO_3$. The optimum annealing time condition was at 30 mins because the formation of impurity phases was minimized. After annealing for 30 mins, the thermal energy was enough to complete the transition of intermediate phases into BFO. These impurities remained in the 15mins-annealed samples that may suggest the insufficient time to promote the recrystallization of precursors or intermediate oxide phases into the desired BFO one. In turn, prolonging the annealing to 45 minutes would have promoted the thermal decomposition of the BFO structure, which would explain the presence of impurity oxide phases in the corresponding XRD pattern.

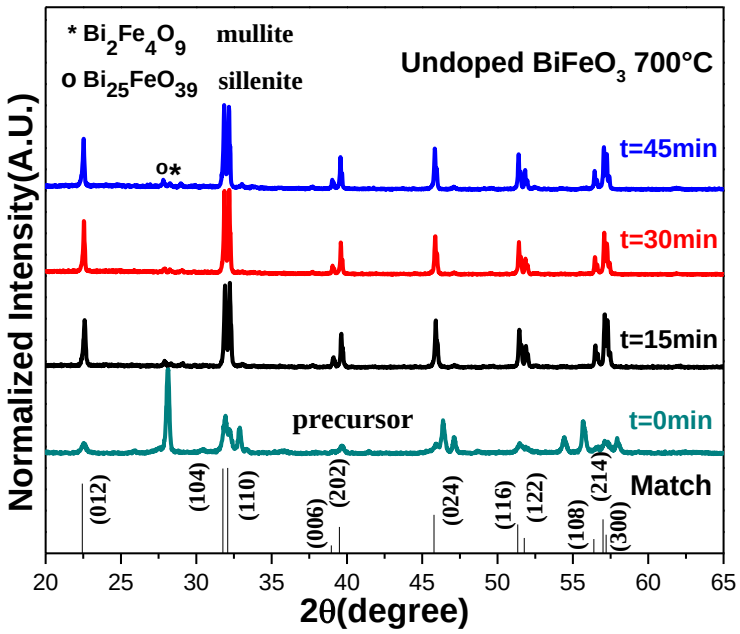

Figure 5.1 XRD patterns for undoped BFO thermal annealed at 700°C for 0, 15, 30 and 45mins.

Fourier Transform Infrared Spectroscopy Measurements (FTIR)

FTIR spectra of undoped BFO powders samples thermal annealed at 700°C for 15, 30 and 45 mins are shown in Figure 5.2. Two main bands around 813 cm^{-1} and between 537 and 539 cm^{-1} were clearly observed for all samples and are attributed to Fe-O stretching and bending vibration, respectively. The presence of bands of metal-oxygen bonds (Fe-O) verified the formation of perovskite structure in undoped bismuth ferrite samples, this is in agreement with other reports [73]. The bands in the 1383-1470 cm^{-1} range could be due to the presence of trapped nitrates that were not removed completely after thermal annealing [74]. Broad bands present between 3000-3600 cm^{-1} are assigned to antisymmetric and symmetric stretching of H_2O and OH^- bond groups, whereas the band at 2350 cm^{-1} (more pronounced for samples annealed for 15mins) would correspond to atmospheric CO_2 [40]. The annealing time did not affect the formation of the perovskite structure in undoped BFO samples.

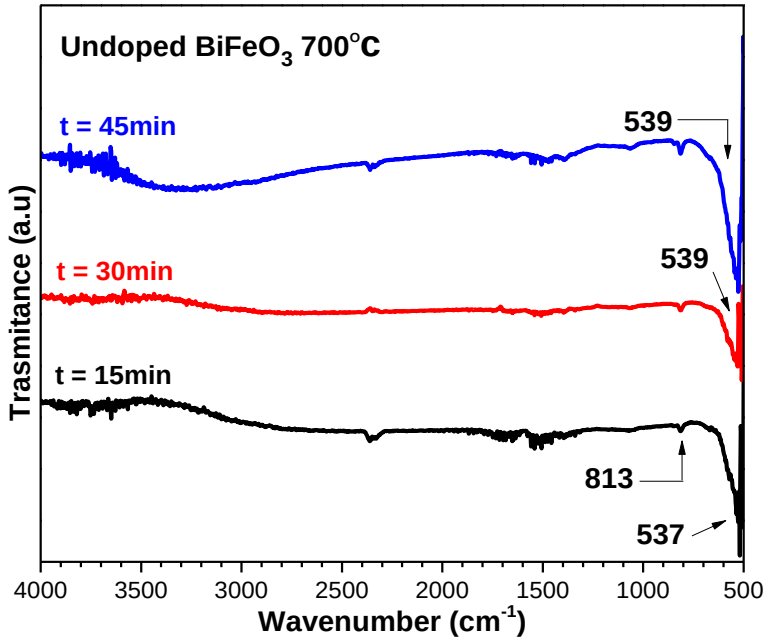

Figure 5.2 FTIR spectra for undoped BFO thermal annealed at 700°C for 15, 30 and 45mins.

Scanning Electronic Microscopy Measurements (SEM)

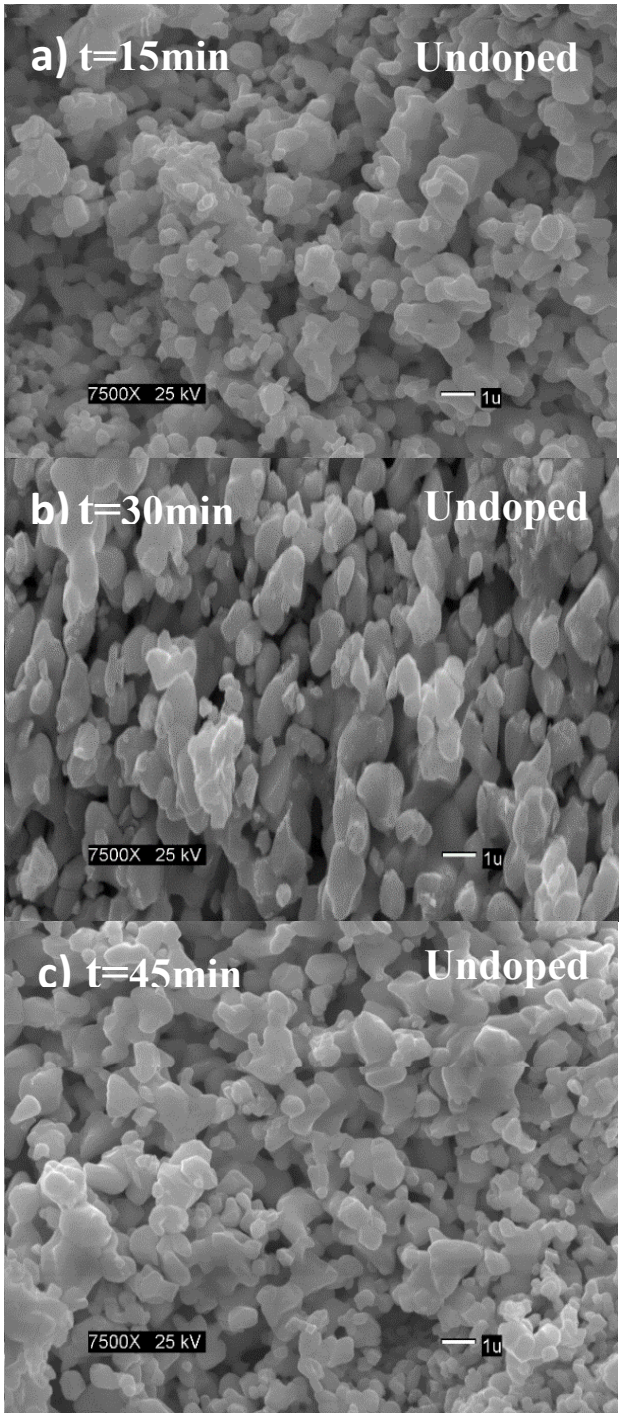

Figure 5.3 SEM micrographs for undoped BFO thermal annealed at 700°C for 15, 30 and 45mins.

Figure 5.3 shows micrographs of undoped BFO prepared by sol-gel method. Particles with random morphology and highly agglomerated micron and sub-micron individuals are observed in all samples. Generally speaking, the particles can be considered as polydisperse, i.e. particles with non-uniform sizes. The average particle size for undoped BFO annealed for 15 and 45 mins was about 0.5μm and increased up to 1.2μm in the 30 mins-annealed sample, as estimated by using ImageJ software (Table 5.1). The apparent increase in size for the particles annealed for 30 mins could be explained because the software is recognizing very agglomerated particles as one; on the other hand, if the detail of the individual particles is analyzed, the real size is in the submicrometric range. These values are somehow in agreement with the reports available in the literature [75].

Table 5.1 Average particle size for undoped BFO thermal annealed at different annealing times using ImageJ software.

Annealing time	**15min**	**30min**	**45min**
Average particle size (nm)	523.4 ± 216.3	1202.9 ± 596.4	519.7 ± 178.3

MH Measurements

M-H curves of undoped $BiFeO_3$ powders synthesized at different annealing times were measured in a magnetic field ranging from -20 kOe up to 20 kOe, (Figure 5.4). A linear relationship between magnetization and applied magnetic field was observed for all samples and verified the antiferromagnetic order with spiral spin structure of undoped BFO reported previously [70], [76], [77]. The antiferromagnetic ordering observed in undoped BFO samples can be explained for the quantum effect called superexchange interaction, where O^{-2} donate electrons to Fe^{3+} ions in the Fe-O-Fe bond, and the spin of electrons donated to Fe^{3+} ions are placed in way to promote collective antiparallel spin alignment of neighbor Fe-ions [58].

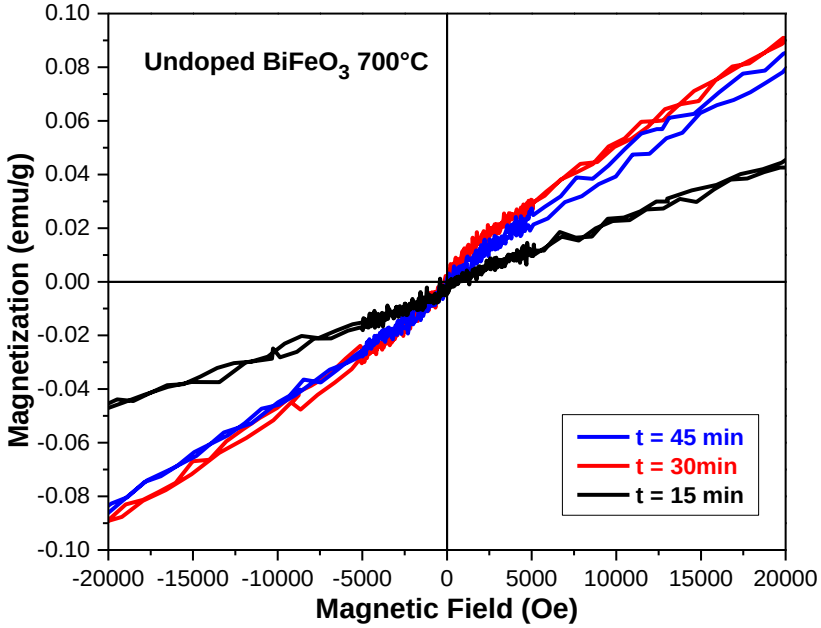

Figure 5.4 M-H curves for undoped BFO thermal annealed for 15, 30 and 45 mins.

Table 5.2 shows that maximum magnetization values which increased to double in samples annealed at 30 and 45 mins, when compared to the sample annealed for 15mins. Increase in the slope in the M-H measurements for prolongated annealing times suggest a preferential alignment of the spins in these conditions, accordingly an increase in maximum magnetization was observed.

The higher maximum magnetization value was of ~0.1 emu/g for undoped BFO obtained at 30 mins. Coercivity do not display a trend with annealing time, and their values are not as precise due to the antiferromagnetic character of the sample. Remanent magnetization values can be ignored because are within the experimental error [78].

Table 5.2 Magnetic parameters for undoped BFO thermal annealed at different annealing times.

Annealing times	***Coercivity (Oe)***	***Maximum Magnetization (emu/g)***
15min	16.0	0.05
30min	14.1	0.1
45min	107.8	0.09

5.2 Nanocrystalline Co-doped $BiFeO_3$ powders

5.2.1 Effect of annealing time

X-Ray Diffraction Measurements (XRD)

Figure 5.5 shows XRD patterns of 5% Co-doped $BiFeO_3$ nanocrystalline powders annealed at 700°C for 15, 30 and 45 minutes. A rhombohedral perovskite structure was confirmed by XRD measurements in 5% Co-doped $BiFeO_3$ powders for all annealing times. Samples annealed for 15 mins exhibited impurities phases, and when annealing time was increased to 30 and 45mins no change was observed in the impurity phases.

Volatilization of bismuth species would have made unstable the BFO and promote the formation of impurity phases. The substitution of Bi for Co ions may minimize the loss of bismuth owing to volatilization.

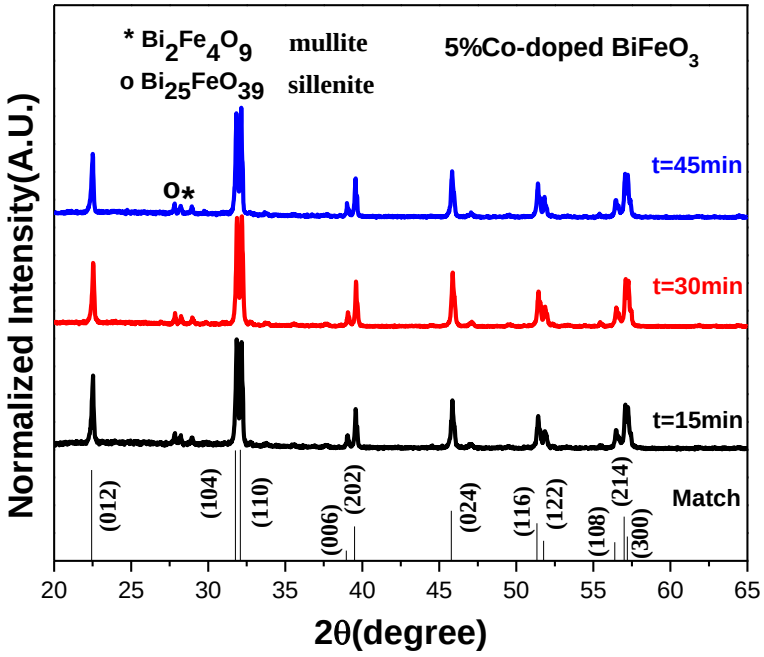

Figure 5.5 XRD patterns for 5% Co-doped BFO annealed at 700°C for 15, 30 and 45 mins.

Figure 5.6 shows XRD patterns of 15% Co-doped $BiFeO_3$ nanocrystalline powders thermal annealed at 700°C for 15, 30 and 45 minutes. XRD analysis revealed that impurity phases were not present in all annealing time conditions. 15% Co-doped $BiFeO_3$ powders annealed at all time conditions exhibited a secondary phase of Cobalt Ferrite (CFO) with a diffraction peak at ~35.4° that belong to cubic spinel structure of Cobalt Ferrite [79].

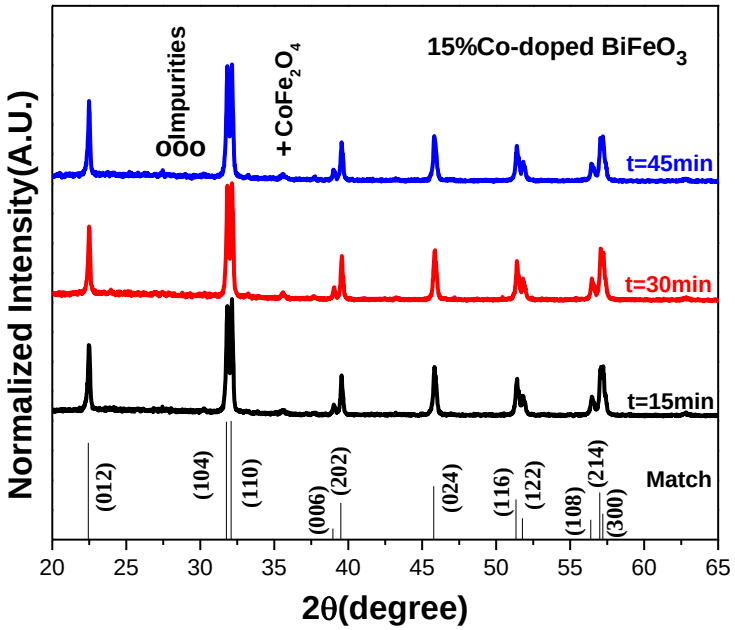

Figure 5.6 XRD patterns for 15% Co-doped BFO annealed at 700°C for 15, 30 and 45mins.

It must be emphasized that the presence of CFO became evident in 15% Co-doped BFO powders. Probably, some of the Co species, which would have replaced totally or partially Bi sites, should have reacted with available Fe(III) species to give the $CoFe_2O_4$ phase and this way inhibited the formation of impurities.

Fourier Transform Infrared Spectroscopy Measurements (FTIR)

FTIR spectra of 15% Co-doped $BiFeO_3$ powders annealed at 700°C for 15, 30 and 45 mins are shown in Figure 5.7. Only one band between 546 and 550cm^{-1} was detected in FTIR measurements for all samples and is attributed to Fe-O bending vibration. The detection of metal-oxygen bands (Fe-O) confirm the formation of perovskite structure and are consistent with other reports for Co-doped $BiFeO_3$ powders [13]. Results showed that annealing time did not have an influence in the frequency of vibration of the bonds.

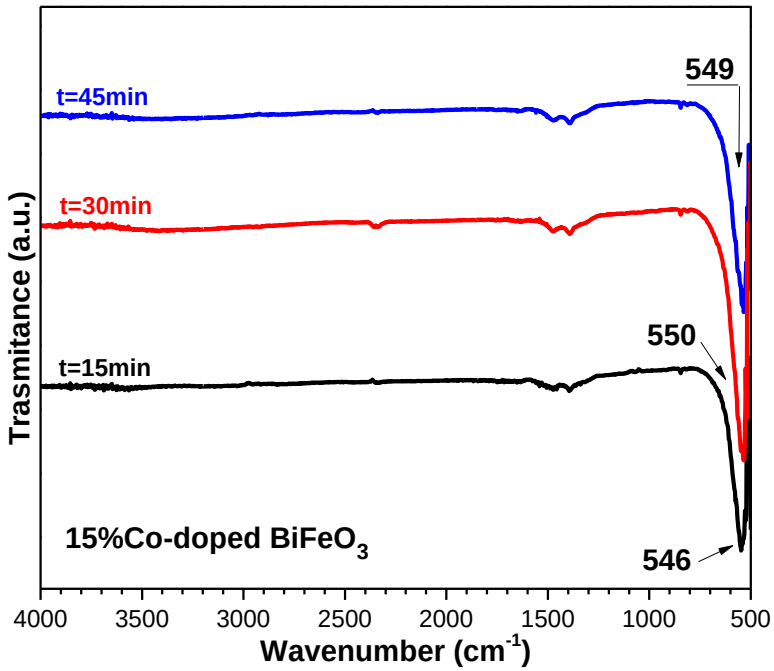

Figure 5.7 FTIR spectra for 15%Co-doped $BiFeO_3$ powders thermal annealed at 700°C for 15, 30 and 45mins.

Scanning Electronic Microscopy Measurements (SEM)

Figure 5.8 shows SEM micrographs of 15% Co-doped $BiFeO_3$ powders prepared by sol-gel method and thermal annealed for 15, 30 and 45 minutes; submicrometric particles with diverse morphologies are shown for all samples. The average particle size for 15% Co-doped $BiFeO_3$ annealed for 15mins was 0.29μm; and decreased to 0.24 and 0.26 μm for 30 and 45 mins of annealing, respectively (Table 5.3). Decrease on the average particle size for 30 and 45 mins of annealing may be due that the thermal energy at such as longer times and temperature accelerated the nucleation rate at prolonged annealing times. But statistically speaking the particles have the same average particle size.

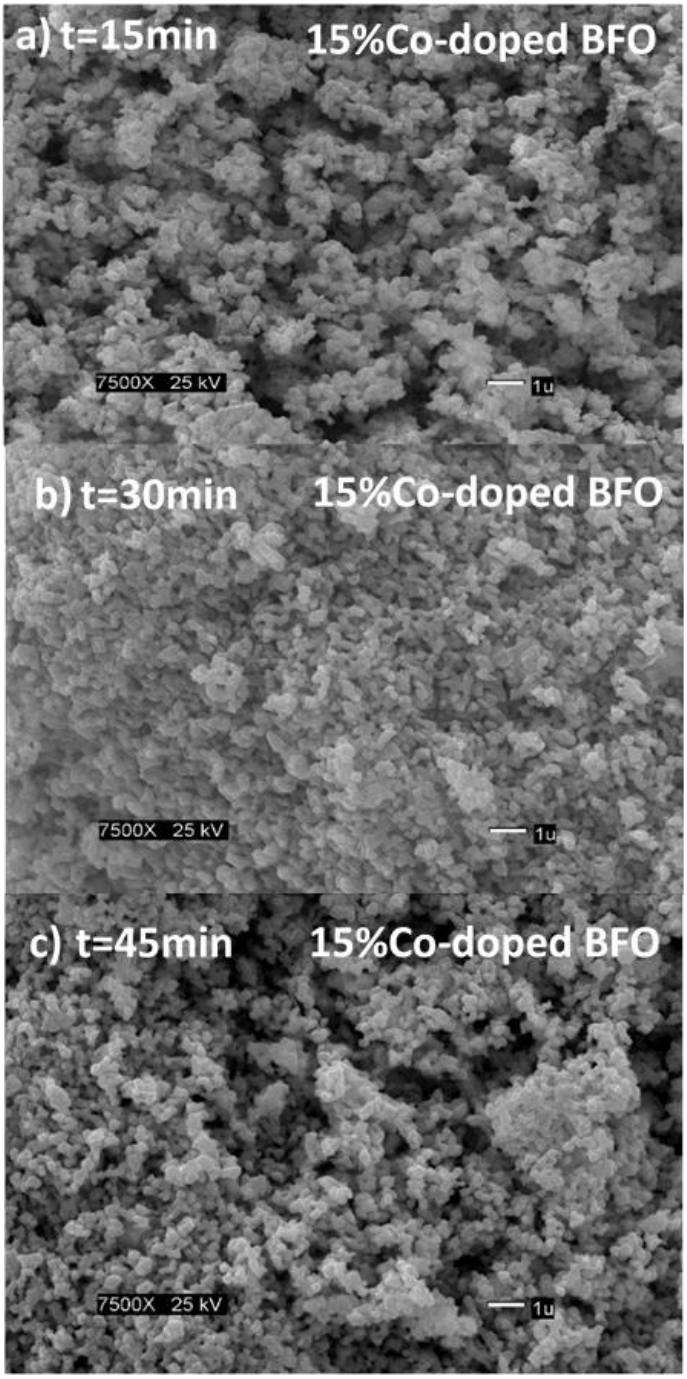

Figure 5.8 SEM micrographs for 15% Co-doped $BiFeO_3$ thermal annealed at 700°C for 15, 30 and 45mins.

Table 5.3 Average particle size for 15% Co-doped $BiFeO_3$ at different annealing times.

Annealing time	**15min**	**30min**	**45min**
Average particle size (nm)	290.4 ± 82.9	242.1 ± 84.1	257.0 ± 57.5

MH Measurements

Figure 5.9 shows the M-H hysteresis loops for 15% Co-doped $BiFeO_3$ powders annealed for 15, 30 and 45 mins. All samples exhibited saturated MH loops with ferromagnetic order. Saturation and remanent magnetization values for the 15 mins-annealed sample was 0.9 and 1.9 emu/g, respectively, when annealing time was increased for 30 and 45mins, these values of magnetization were almost duplicated with respect to the 15mins-annealed sample (Table 5.4). Enhancement in magnetic properties at large annealing times may be due to grain size effects. At large annealing times, the grain must grow, if the grain size increases the coercivity must decrease if the magnetic behavior is in the multidomain range.

On the other hand, SEM measurements showed that 30 and 45 mins-annealed samples have smaller average particle size with respect to the15mins-annealed sample. Reduction in grain size could induce strain in the crystal structure and, as a consequence, changes in the Fe-O-Fe bond angles may occur. These changes could result in an improvement of the ferromagnetic properties according the superexchange interaction effect [80].

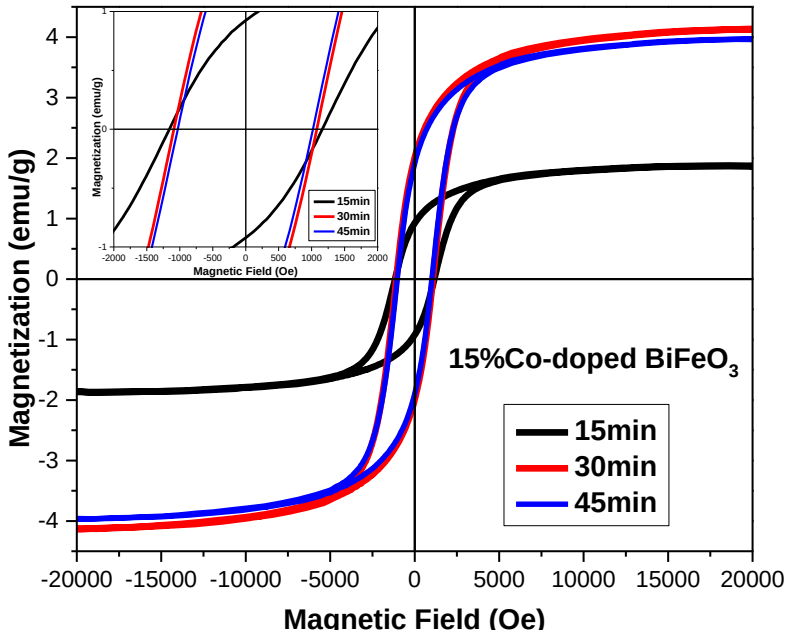

Figure 5.9 Magnetic hysteresis loop and a zoom around small values of magnetic field from -2kOe to 2kOe showed in the upper inset, for 15% Co-doped BFO annealed for 15, 30 and 45 mins.

The 15% Co-doped $BiFeO_3$ powder annealed for 30mins was the best condition due to their remanent and saturation magnetization values being the highest. Also, the smallest value in average particle size was observed for this condition. That may be the principal reason for the enhancement in magnetic properties.

Table 5.4 Magnetic parameters of 15% Co-doped $BiFeO_3$ annealed at different annealing times.

Annealing Time	***Coercivity (Oe)***	***Remanent Magnetization (emu/g)***	***Saturation Magnetization (emu/g)***
15min	1159	0.9	1.9
30min	1083	2	4.1
45min	1025	2	4.0

5.2.2 Effect of composition

X-Ray Diffraction Measurements (XRD)

Figure 5.10, Figure 5.11 and Figure 5.12 shows XRD patterns of $Bi_{(1-x)}Co_xFeO_3$ nanocrystalline powders synthesized in presence of Co(II) species at the following atomic fractions, x= 0, 0.05, 0.06, 0.07, 0.08, 0.09, 0.10 and 0.15, annealed at 700°C for 15, 30 and 45 minutes, respectively. Match software was used to verify that all main peaks belong to the rhombohedral perovskite structure of $BiFeO_3$ for all samples. In the 5% Co-doped $BiFeO_3$ sample annealed for 15mins, the impurity phases increased compared to undoped BFO samples. On the other hand, for Co doping above 5% Co, impurities were removed, and similar behavior was observed at 30 and 45 mins annealed samples. This may suggest that incorporation of Co species in host BFO inhibit the formation of impurity phases.

XRD analysis showed a secondary phase of Cobalt Ferrite (CFO) evidenced by the appearance of a peak at ~35.4° that belong to cubic spinel structure of Cobalt Ferrite [79]. This peak was more visible in 9% , 10% and 15% Co-doped BFO samples for the three annealing conditions. Evidently, in the process of doping a certain amount of Cobalt has synthesized independently as secondary phase of CFO, hence composites of Bismuth Ferrite - Cobalt Ferrite were developed. Previous researchers have detected presence of CFO in high concentrations of Co-doped BFO powders, but elevated levels of impurities like mullite and sillenite were observed is such conditions [51].

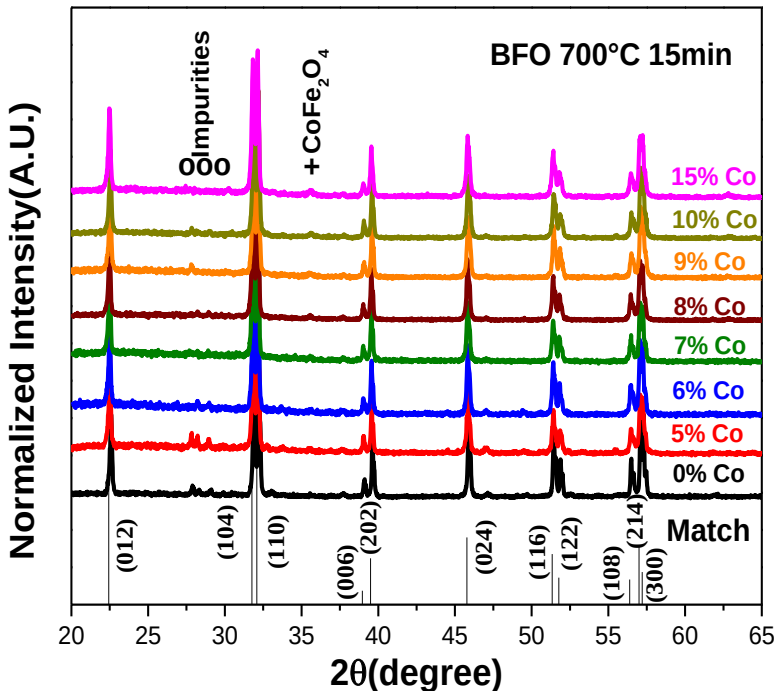

Figure 5.10 XRD patterns for Co-doped BFO thermal annealed at 700°C for 15 mins.

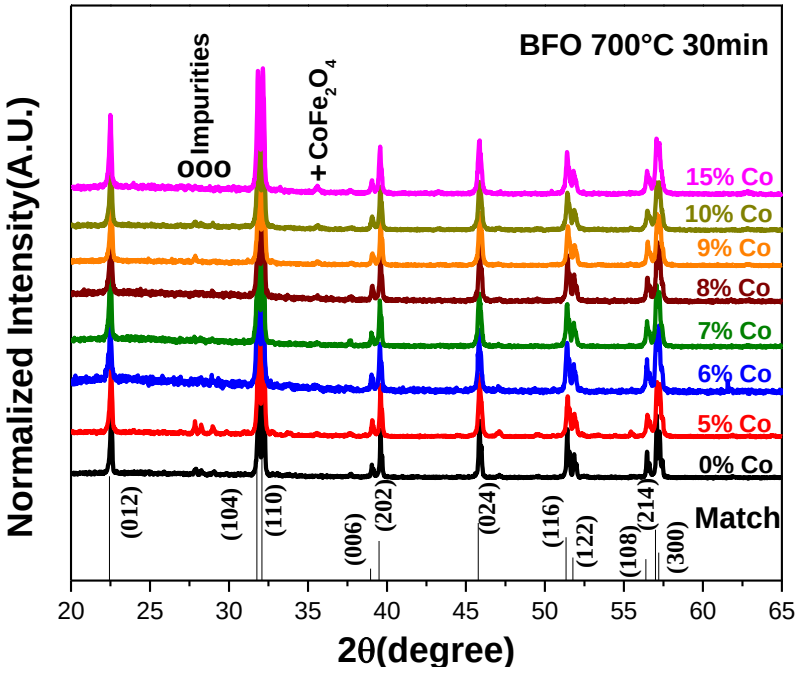

Figure 5.11 XRD patterns for Co-doped BFO thermal annealed at 700°C for 30 mins.

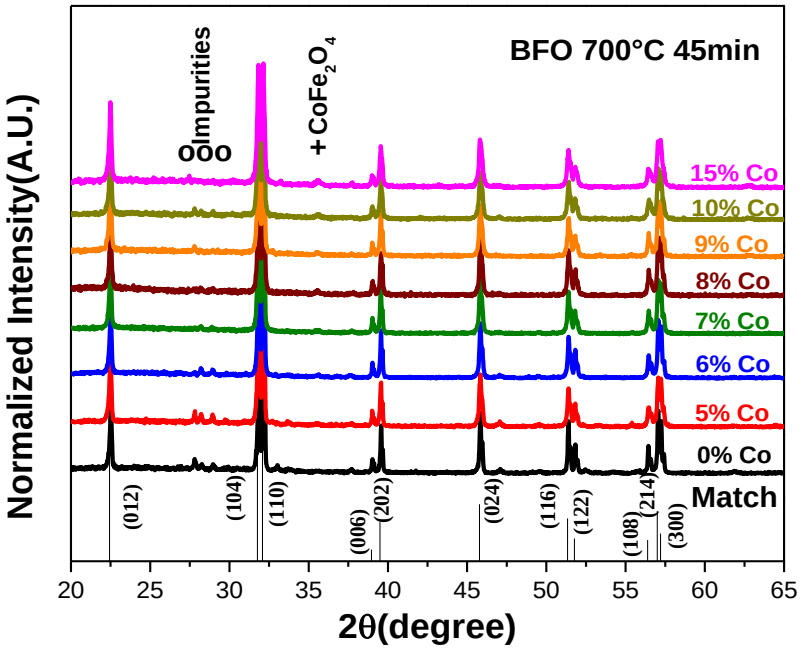

Figure 5.12 XRD patterns for Co-doped BFO thermal annealed at 700°C for 45 mins.

Presence of $CoFe_2O_4$ in some Co-doped $BiFeO_3$ samples suggest an incomplete incorporation of Co^{2+} species in host $BiFeO_3$. As a result, the excess of Co ions reacted with Fe ions in elevated doping concentration of dopants, as in 9%, 10% and 15% Co-doped BFO samples, promoting the isolated formation of Cobalt Ferrite. When the incorporation of Co species is achieved, the unit cell undergoes a shrinking due to the mismatch in ionic radii between Co^{2+} (0.78 Å) and Bi^{3+} (1.20 Å). This should be reflected in a shift peak toward higher diffraction angles in the Co-doped BFO respect to undoped BFO XRD patterns. However, this is not the case for Co-doped BFO samples annealed at 15 mins (Figure 5.13 a)). A shift in the (012) peak is observed towards lower diffraction angles. This suggests an incorporation of Co^{2+} species in the interstitial spaces of the host BFO or in the Fe^{3+} (0.64 Å) sites rather than in Bi^{3+} sites which leads to an expansion of the unit cell. In turn, the shift in the (012) peak was not so obvious in Co-doped BFO samples synthesized at 30 and 45 minutes of annealing. This should imply that in the

incorporation of Co species in BFO did not distort the unit cell, perhaps due to the achievement of an equilibrium conditions that stabilized the unit cell size; however, the variation in the volume of the unit cell at different Co concentrations was analyzed to understand better this effect.

The volume of the unit cell was calculated considering a hexagonal system and random behavior was observed in the variation of volume with the Co content (Figure 5.13 d), e) and f)).

Two mechanisms are proposed for explain the incorporation of Co species in host BFO; samples thermal annealed for 15 mins were analyzed. From 5% up to 8% there is an incorporation of Co in Fe sites and this induces a decrease in the cell volume. On the other hand, for 9% and 10% the Co(II) species react with available Fe(III) to form Cobalt Ferrite, in these cases there is not a great change in the cell volume (Fig. 5.13 d).

According to the proposed mechanisms, at 15% Co-doped BFO the cell volume should not change due the formation of Cobalt Ferrite rather than the incorporation of Co species in the host BFO, but a decrease in the cell volume was observed in this condition, therefore, no valid mechanism has been found to explain this behavior.

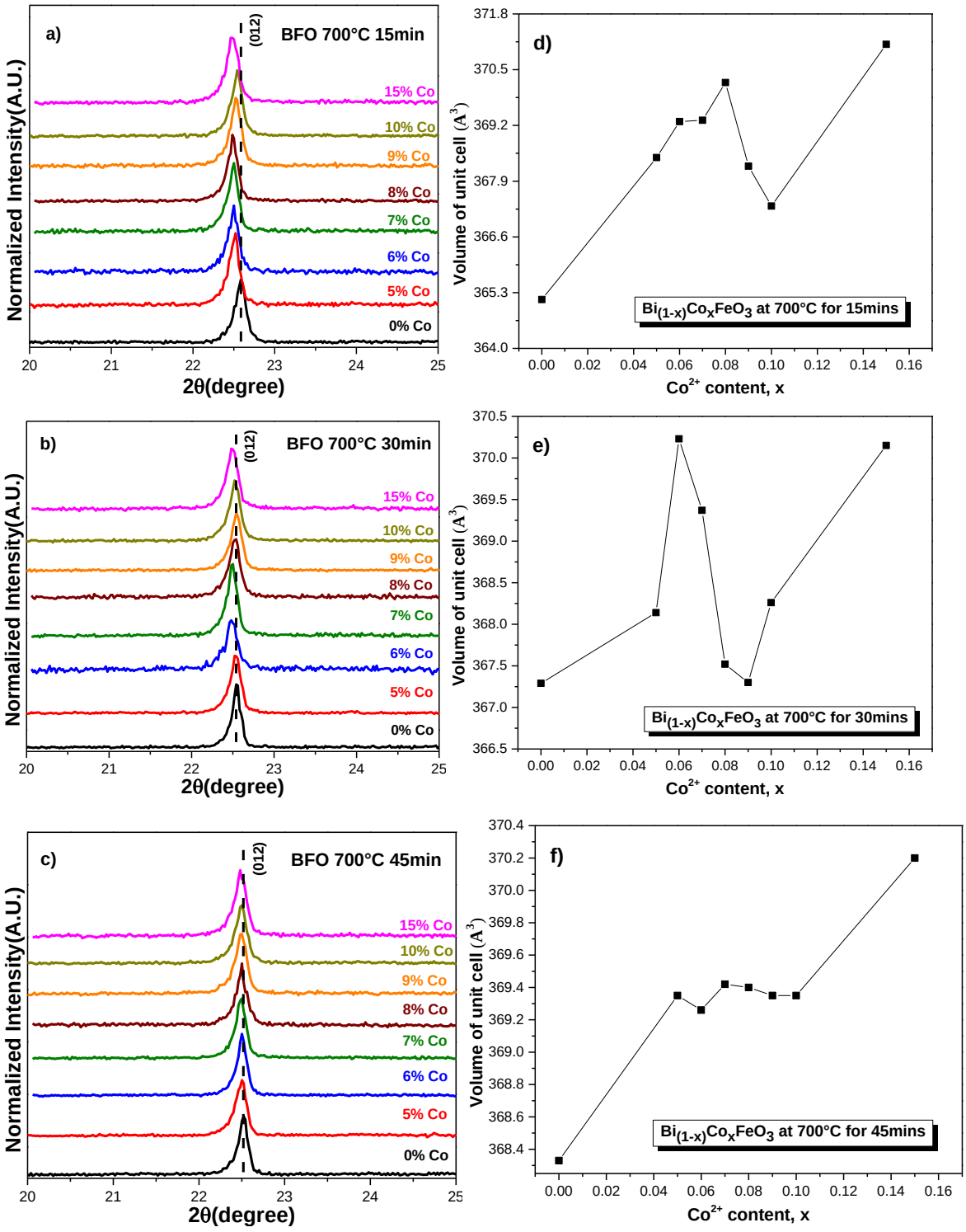

Figure 5.13 Details of the (012) peak shift in Co-doped BFO powders annealed at 700°C for a)15min b) 30min y c) 45min. Variation of Volume of unit cell of BFO with Co^{2+} content, x, for annealing times of d)15min e) 30min y f) 45min.

The volatilization of Bi species is the main reason for the formation of impurity phases in BFO, if Bi ions are replaced for Co ions, the host structure should be stabilized and, hence, minimizing the presence of the impurity phases, but in this case the formation of Cobalt Ferrite (CFO) inhibited the formation of impurity phases, Co (II) reacts with available Fe (III) to form CFO, this way the Fe species are no longer available to the formation of impurities phases.

Based on the above results, the optimal composition conditions were fixed at 9%, 10% and 15% Co-doped BFO samples.

Fourier Transform Infrared Spectroscopy Measurements (FTIR)

Figure 5.14 shows the FTIR spectra of Co-doped BFO powders for different atomic portions of Co, annealed at 700°C for 30 minutes. FTIR spectra of undoped and Co-doped $BiFeO_3$ shows two principal bands, one band around 813 cm^{-1} is attributed to Fe-O stretching vibration and only appears in undoped, 5% and 6% Co-doped BFO samples. Apparently, at higher Co concentrations the Fe-O stretching vibration might be not detected by FTIR spectroscopy. The other main band corresponds to Fe-O bending vibration, which is found at 539 cm^{-1} for undoped BFO, and at higher wavenumber of up to 550 cm^{-1} for 15% Co-doped BFO. The shift in 15% Co-doped samples compared to undoped BFO towards higher wavenumbers may suggest the incorporation of Co^{2+} in Bi^{3+} sites. However, XRD analysis revealed that is not the case because a closer look at the (012) peak shift showed a possible incorporation of Co^{2+} in interstitial sites of host $BiFeO_3$. Therefore, such shift in FTIR bands reveals a distortion in octahedral FeO_6 groups. Principal metal-oxygen (Fe-O) bands in FTIR spectra verified formation of perovskite structure in Bismuth Ferrite for all samples [42], [81].

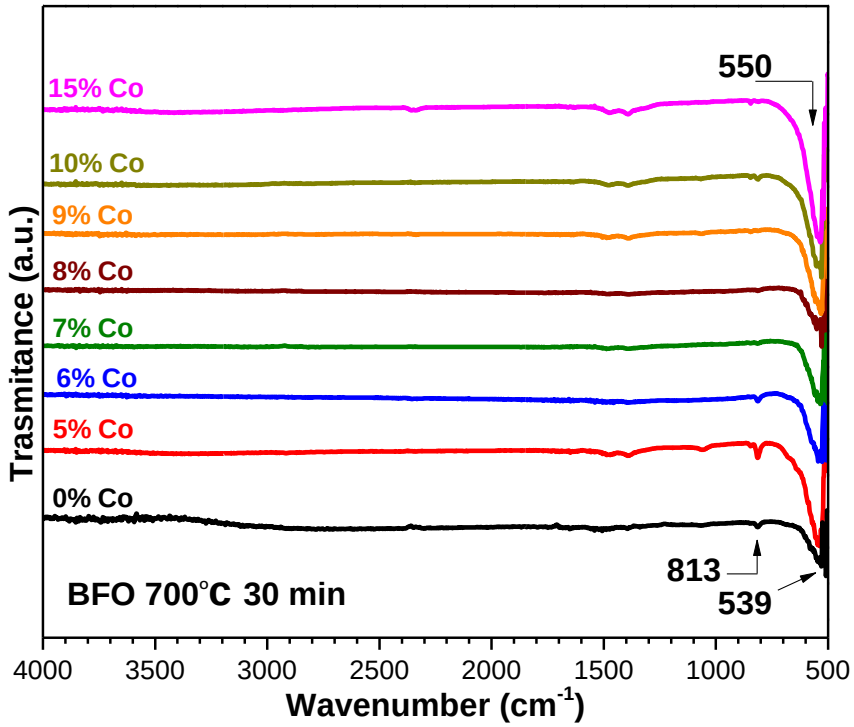

Figure 5.14 FTIR spectra of Co-doped BFO thermal annealed at 700°C for 30 minutes.

Scanning Electronic Microscopy Measurements (SEM)

SEM images of undoped and 15% Co-doped BFO powders annealed at 700°C for 30 minutes are presented in Figure 5.15 which shows that particles are highly agglomerated and oriented randomly. SEM revealed that 15% Co-doping considerably decreased the particle size of $BiFeO_3$ powders. The particle size found for undoped BFO was ~1.20 µm, and it was reduced up to ~0.24 µm for 15%Co-doped BFO. That is approximately five times smaller than undoped samples (Table 5.5).

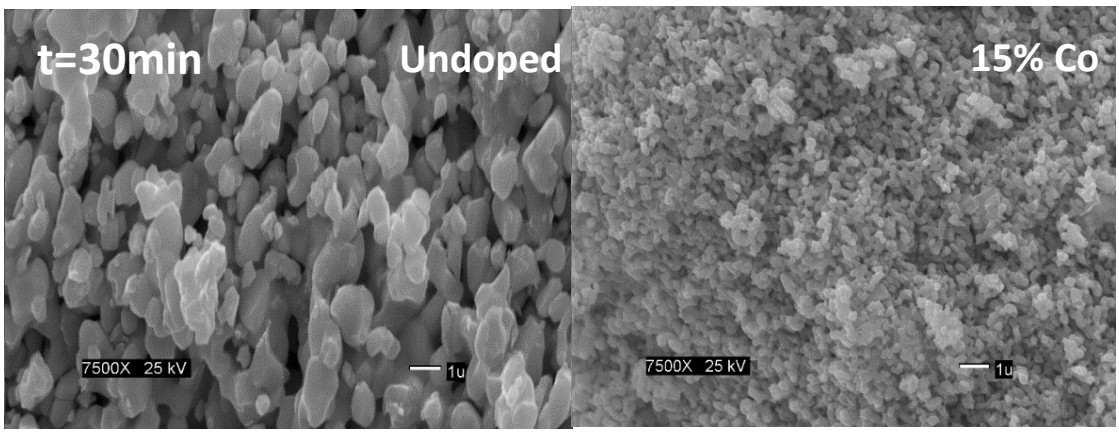

Figure 5.15 SEM micrographs for undoped and 15%Co-doped BFO thermal annealed at 700°C for 30min.

The decrease in particle size for 15% Co-doped BFO powders may be attributed to the change in the nucleation process and growth conditions of the particles due to lattice distortions induced for a possible incorporation of Co species in the host BFO. Other authors also reported a decrease in the average particle size for BFO doped with other elements (Sm, Gd). They suggested that the decrease in particle size may be due to the mismatch between the ionic radius of the dopant and the Bi ion [82], [83].

Table 5.5 Average particle size for undoped and 15% Co-doped BFO thermal annealed at 700°C for 30 minutes.

samples	***Average particle size (nm)***
undoped BFO	1202.9 ± 596.4
15%Co-doped BFO	242.1 ± 84.1

MH Measurements

Figure 5.16 a) shows the M-H hysteresis loop measured with a magnetic field ranging from -20 kOe up to 20 kOe, for undoped and Co-doped BFO powders annealed at 700°C for 30 minutes. Co-doped BFO samples from 5% Co up to 15% Co exhibited saturated ferromagnetic hysteresis unlike undoped BFO that presents antiferromagnetic order. Figure 5.16 b) presents the variation of magnetic properties with the Co^{2+} content, x. A nearly linear trend is observed in saturation and remanent magnetization when Cobalt doping is increased. This corroborate ferromagnetic behavior displayed in M-H hysteresis loop.

Some possible mechanisms are enunciated for explaining the enhancement of magnetic properties in Co-doped BFO compared to undoped BFO samples: Incorporation of Co^{2+} in interstitial or Fe (III) sites of BFO produces a distortion in the crystal structure. As a result, the Fe-O-Fe bond angles may be perturbed, and according to the superexchange interaction effect, a change from antiferromagnetic to ferromagnetic order could be possible. Other reports suggest that the reduction in particle size in doped-samples destroy the spiral spin structure of the undoped BFO and this induces the ferromagnetic behavior. [34], [81], [84], [85]. Neutron Diffraction Measurements are required to corroborate the orientation of the spins in the magnetic structure and decide which mechanism explains the change of antiferromagnetic to ferromagnetic order [86].

According to the proposed mechanisms for the incorporation of Co species in host BFO, the enhancement in the magnetic properties in 5% up 8% Co doping is due to changes in the Fe-O-Fe bond angles induced for the incorporation of Co species in Fe sites.

The presence of $CoFe_2O_4$ (CFO) in 9%, 10% and 15% Co-doped BFO samples corroborated by XRD patterns, promoted the improvement in the magnetic properties in the samples.

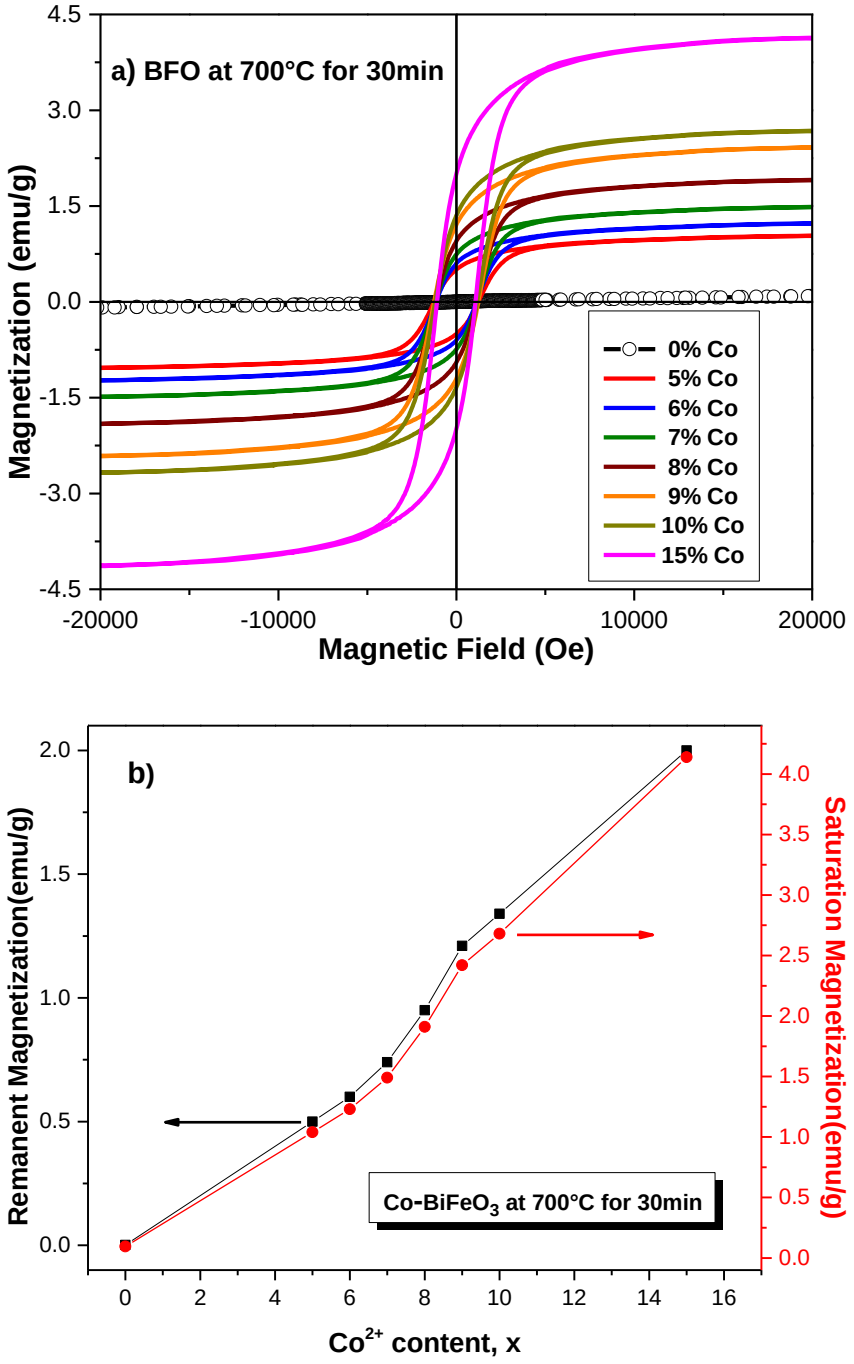

Figure 5.16 a) Magnetic hysteresis loop for Co-doped BFO samples annealed for 30 mins. b) Variation of magnetic parameters with Co^{2+} content x for $Bi_{(1-x)}Co_xFeO_3$ annealed for 30 mins.

It is known that CFO is a hard-magnetic material with modest magnetization and high coercivity [79], [87]. CFO has a large magnetic anisotropy, i.e. their magnetic properties depends of a preferred direction, and hence a high coercive field is necessary for demagnetized the material. This property makes it an excellent candidate for applications permanent magnets and data storage devices. 15% Co-doped BFO exhibited the maximum saturation magnetization (4.1 emu/g) that was 43 times higher than that of undoped BFO (Table 5.6). The improvement in coercivity in the 15% Co-doped BFO sample is attributed to the presence of Cobalt Ferrite which has high coercivity values. Tang et al. [51] reported values of coercivity, remanent and saturation magnetization of 1082.63 Oe, 1.92 and 4.14 emu/g, respectively, for 15% Co-doped $BiFeO_3$ powders. Our results are in excellent agreement with these values. These authors attribute the improvement in the magnetic behavior to the presence of $CoFe_2O_4$ in their samples.

Table 5.6 Magnetic parameters for undoped and 15% Co-doped BFO powders thermal annealed at 700°C for 30 minutes.

samples	***Coercivity (Oe)***	***Saturation Magnetization (emu/g)***
undoped BFO	14.1	0.1
15% Co-doped BFO	1083	4.1

The optimal doping condition was determined to be 15% Co-doped BFO due to the highest values of remanence and saturation magnetization obtained. Materials with large coercivity, remanent and saturation magnetization values are used for permanent magnets and magnetic data storage devices, because they are very difficult to magnetize and demagnetize [62], [13], [88].

5.3 Nanocrystalline Mn-doped $BiFeO_3$ powders

5.3.1 Effect of annealing time

X-Ray Diffraction Measurements (XRD)

Figure 5.17 shows XRD patterns of 3% Mn-doped $BiFeO_3$ nanocrystalline powders annealed at 700°C for 15, 30 and 45 minutes. Rhombohedral perovskite structure (R3c) was confirmed by XRD measurements for all annealing times.

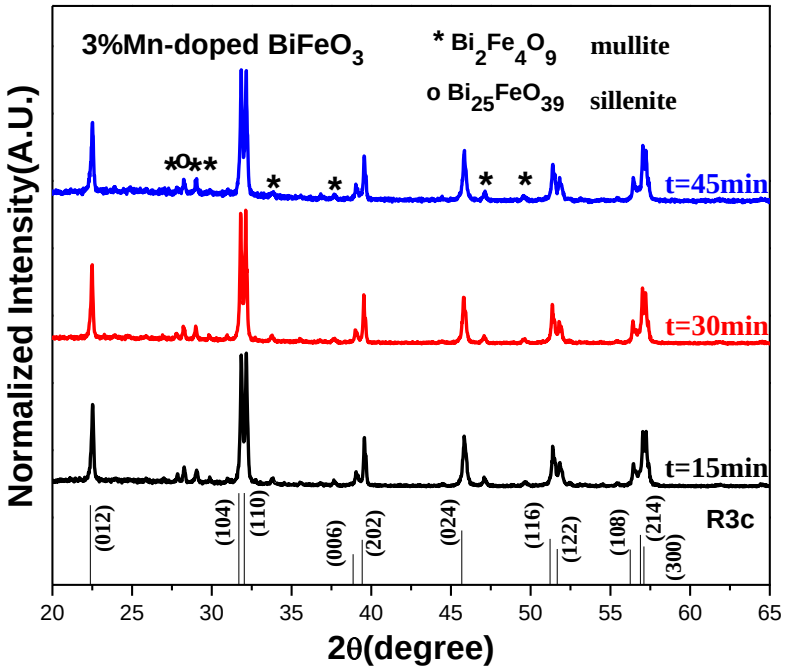

Figure 5.17 XRD patterns for 3% Mn-doped BFO powders annealed at 700°C for 15, 30 and 45 mins.

As the corresponding XRD pattern evidences, the synthesized powders exhibited negligible but evident impurities that could be due to thermal decomposition of the main BFO structure to give parasitic Bi oxides.

Figure 5.18 shows XRD patterns of 7% Mn-doped $BiFeO_3$ nanocrystalline powders annealed at 700°C for 15, 30 and 45 minutes. Tetragonal structure (P4mm) was confirmed by XRD

measurements for all annealing times, due to incorporation of Mn species in Bi sites. For this doping level, the 15 mins-annealed samples showed minimal impurity levels. However, longer annealing times (30 and 45 mins) caused an increase in the relative amount of the impurity phases possibly due to the thermal decomposition of BFO at large annealing times [45], [60].

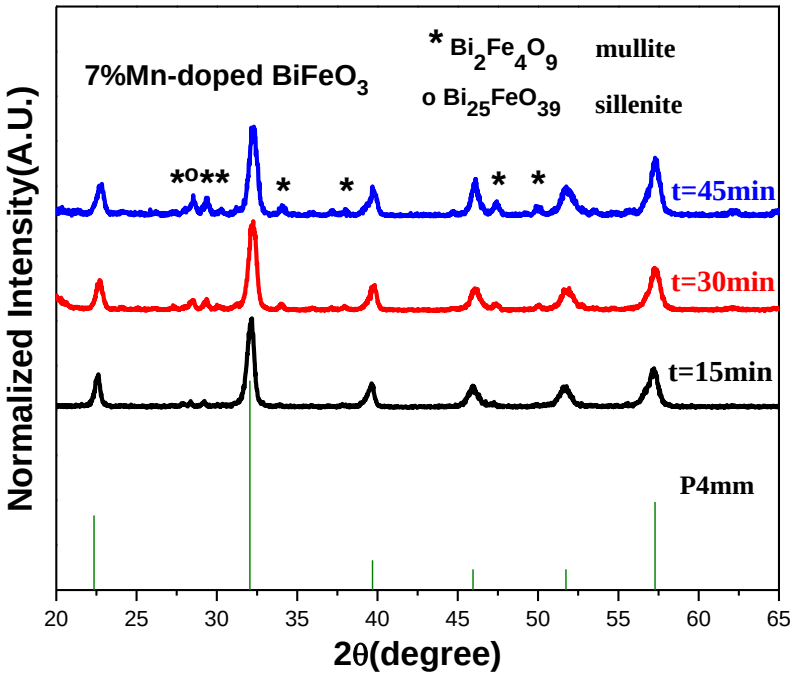

Figure 5.18 XRD patterns for 7% Mn-doped $BiFeO_3$ powders annealed at 700°C for 15, 30 and 45mins.

Table 5.7 shows the average crystallite size determined for 7% Mn-doped BFO using Scherrer's equation. The apparent decrease in the average crystallite size when annealing time is increased may be attributed to enhancement on the concentration of bismuth vacancies due volatilization of bismuth; this distorted unit cell would have inhibited the crystal growth rate. However, this statement needs to be discussed and confirmed in more detail.

Table 5.7 Average crystallite size for 7% Mn-doped BFO samples at different annealing times.

Annealing time	**15min**	**30min**	**45min**
Average crystallite size (nm)	26.4	22.5	21.1

The optimal condition for 7% Mn-doped BFO was attained at 15 mins, where impurities were minimal. The 15 mins annealing time was not enough for promote formation of impurity phases owing decomposition of BFO.

Fourier Transform Infrared Spectroscopy Measurements (FTIR)

FTIR spectra of 7% Mn-doped $BiFeO_3$ powders annealed at 700°C for 15, 30 and 45 mins are shown in Figure 5.19. Two main bands were detected for FTIR measurements. One band around 549, 545 and 545 cm^{-1} in 15, 30 and 45 mins annealed samples, respectively, is attributed to Fe-O bending vibration. The other band observed at 813 cm^{-1} was associated with the Fe-O stretching vibration. This band did not change its wavenumber for all time conditions but increased in intensity with the annealing time. This suggest that at higher annealing times, greater number bonds of Fe-O stretching vibration were detected. Metal-oxygen bands verified the formation of perovskite structure for 7% Mn-doped $BiFeO_3$ samples [73].

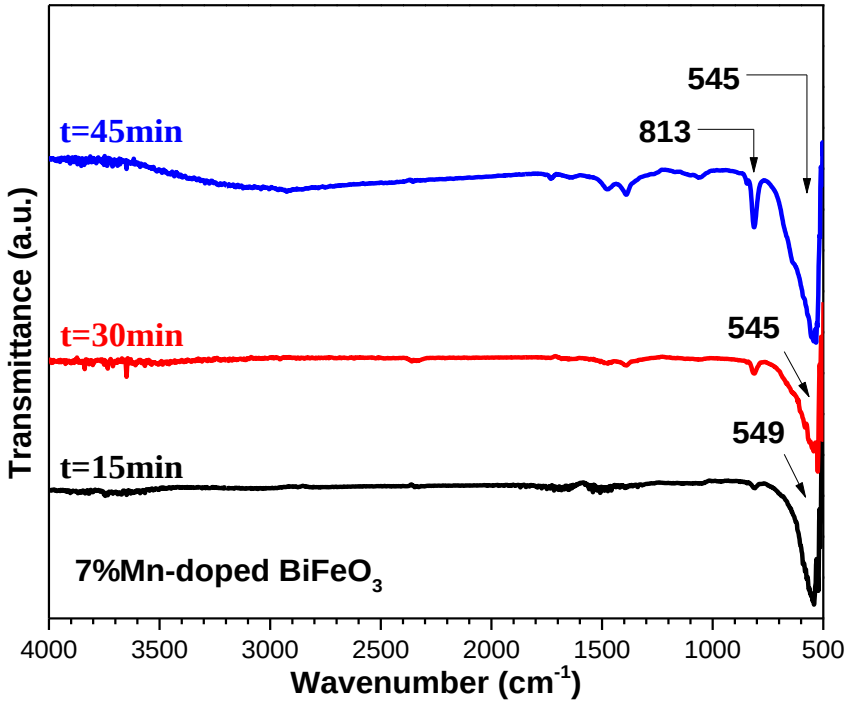

Figure 5.19 FTIR spectra for 7% Mn-doped $BiFeO_3$ powders annealed at 700°C for 15, 30 and 45mins.

Scanning Electronic Microscopy Measurements (SEM)

Figure 5.20 shows SEM micrographs of 7% Mn-doped BFO samples annealed at 700°C for 15, 30 and 45mins. Polydisperse particles with sub-micrometric size were observed for all condition times. Particle size was measured to be ~ 0.39 µm for the 15 mins-annealed sample. When the annealing time was increased up to 30 and 45min, the particle size was reduced to ~ 0.36 µm in both cases (Table 5.8). Prolonged annealing times would have generated stress in the crystal structure, perhaps favored by volatilization of Bi species from the host oxide structure, that may induce distortion and a reduction in the particle size.

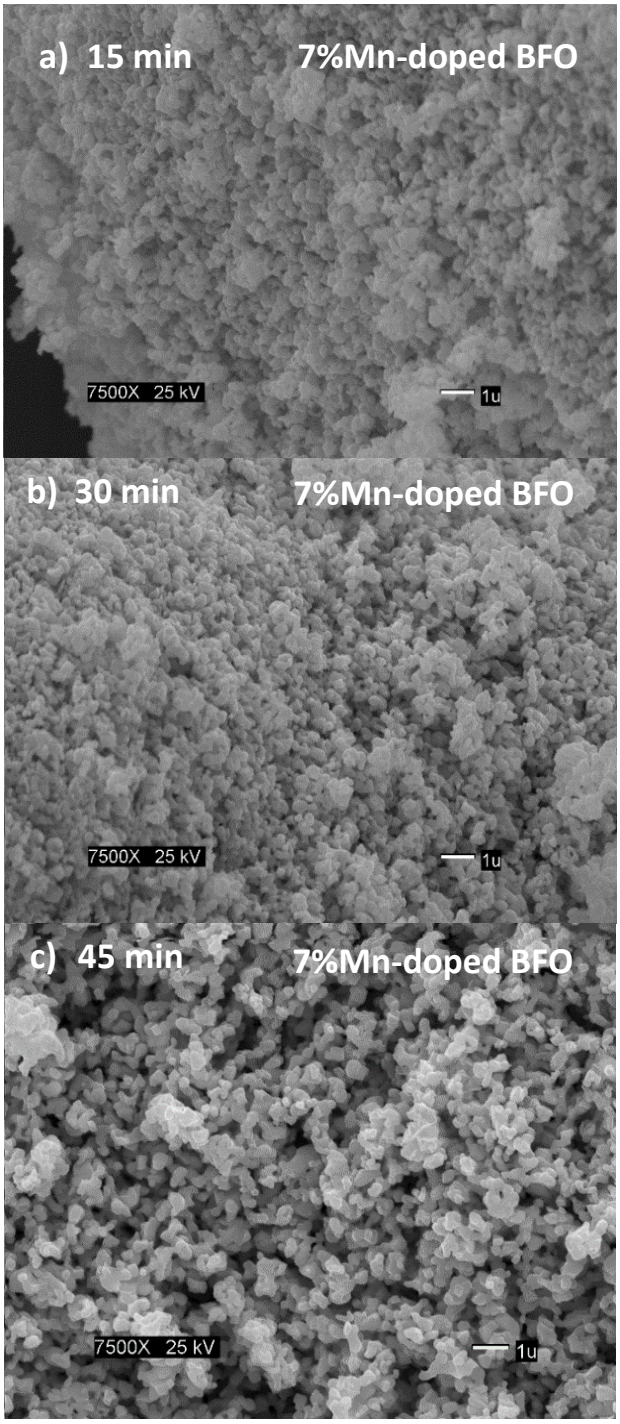

Figure 5.20 SEM micrographs for 7% Mn-doped $BiFeO_3$ thermal annealed at 700°C for 15, 30 and 45mins.

Table 5.8 Average particle size for 7% Co-doped $BiFeO_3$ at different annealing times.

Annealing time	**15min**	**30min**	**45min**
Average particle size (nm)	389.5 ± 90.3	357.3 ± 93.3	364.6 ± 131.3

MH Measurements

Figure 5.21 shows the non-saturated M-H hysteresis loop measured in a magnetic field ranging from -10 kOe up to 10 kOe, for 7% Mn-doped $BiFeO_3$ powders annealed for 15, 30 and 45 minutes. The samples thermal annealed for 15 and 30 mins exhibited a ferromagnetic hysteresis with very low coercivity. Moreover, the 45 mins-annealed sample showed antiferromagnetic behavior. The maximum and remanent magnetization values for the 15 mins-annealed sample were 0.68 and 0.02 emu/g, respectively, and they were reduced when the annealing time was increased (Table 5.9). According to the XRD spectra shown in Figure 5.18 the impurity phases increased with the annealing time, therefore, the presence of these non-magnetic impurities could explain the drop in magnetic properties. Moreover, it has been reported that such impurities have paramagnetic order and they should not contribute to the magnetic properties [16], [51]. The transition of ferromagnetic (15 and 30mins-annealed samples) to antiferromagnetic (45mins-annealed sample) ordering would be induced by the randomizing effects in the spin alignment produced at high thermal energies for prolonged annealing times. It was expected the decrease in coercivity when ferromagnetic behavior switches to antiferromagnetic ordering, however, it was not the case, and coercivity increased in higher annealing times. It is possible that prolonged annealing time induce randomizing effect in the spins due thermal energy, therefore is more difficult demagnetized the material and thus the coercivity increases.

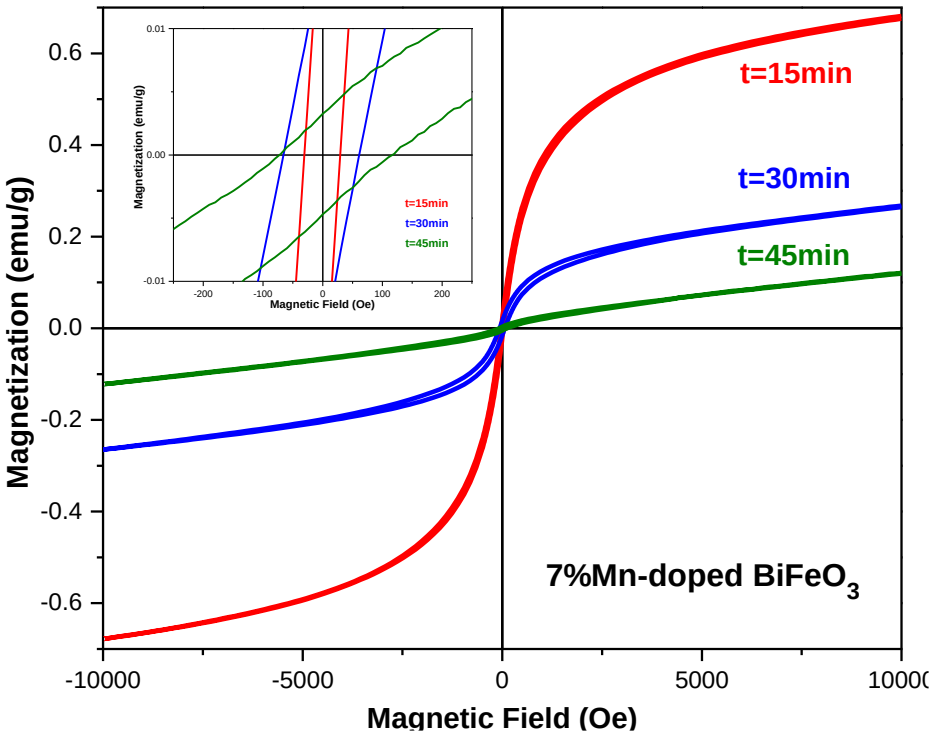

Figure 5.21 Magnetic hysteresis loop for 7% Mn-doped $BiFeO_3$ powders annealed for 15, 30 and 45 mins.

Table 5.9 Magnetic parameters of 7%Mn-doped $BiFeO_3$ powders thermal annealed at different annealing times.

Annealing time	***Coercivity (Oe)***	***Remanent Magnetization (emu/g)***	***Maximum Magnetization (emu/g)***
15min	30	0.02	0.68
30min	63	0.02	0.27
45min	94	~ 0	0.12

5.3.2 Effect of composition

X-Ray Diffraction Measurements (XRD)

The XRD patterns of $Bi_{(1-x)}Mn_xFeO_3$ powders synthesized with Mn atomic fraction values of "x" = 0, 0.03, 0.05, 0.07, 0.13 and 0.15 at 700°C for 15, 30 and 45 minutes are presented in Figure 5.22, Figure 5.23 and Figure 5.24, respectively. The 3% Mn-doped BFO sample annealed for 15 mins (Fig. 5.22) exhibited the rhombohedral perovskite structure, but the 5% Mn-doped BFO and 7% Mn-doped BFO samples showed an evident broadening and overlapping of the doublet principal peaks located at the 31°-33° 2θ range. This change implies a phase transition from rhombohedral to tetragonal structure (P4mm) due the incorporation of Mn species in BFO host. Researchers reported similar results in Mn doped BFO thin films [61]. In 13% Mn-doped and 15% Mn-doped BFO show a different behavior, some peaks from the rhombohedral perovskite structure appear but with poor crystallinity and the structure is not totally defined. An analogous situation of phase changes is observed in XRD patterns at 30 and 45mins time conditions.

Incorporation of Mn species in Bi sites induces a distortion in the crystal structure due the mismatch between the ionic radii of Mn^{2+} (0.80 Å) and Bi^{3+} (1.20 Å). Since ionic radii of Mn^{2+} is smaller than of the Bi^{3+} ion, the unit cell undergoes a shrinking and causes a phase transition from rhombohedral to tetragonal structure that takes place with Mn-doping greater than 3%. XRD revealed presence of impurity phases (mullite and sillenite) located principally at 25°-30° 2θ range. In samples thermal annealed at 700°C for 15 minutes (Fig. 5.22), the impurities increased when Mn concentration increased from 3% up to 5%, but in 7% Mn-doped BFO the impurities were removed. In the 30mins-annealed samples (Fig. 5.23) a similar behavior was observed. For the

45mins-annealed samples (Fig. 5.24), the impurity phases increased proportionally to Mn-doping and thermal decomposition by-products of bismuth ferrite become evident.

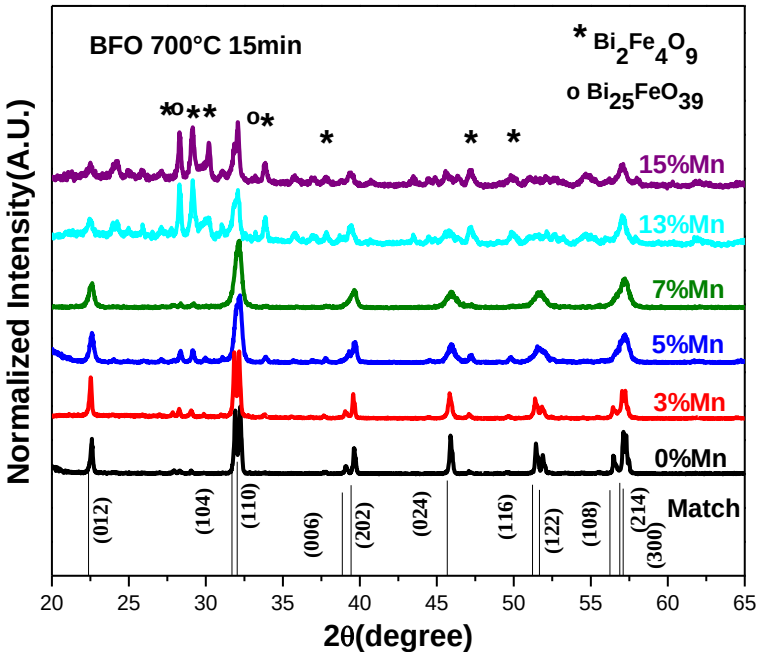

Figure 5.22 XRD patterns for Mn-doped BFO powders thermal annealed at 700°C for 15mins.

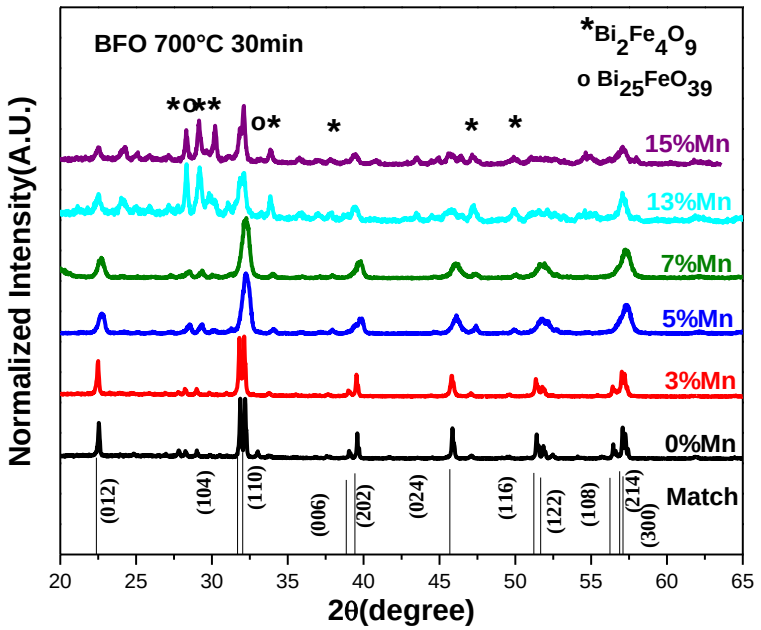

Figure 5.23 XRD patterns for Mn-doped BFO powders thermal annealed at 700°C for 30mins.

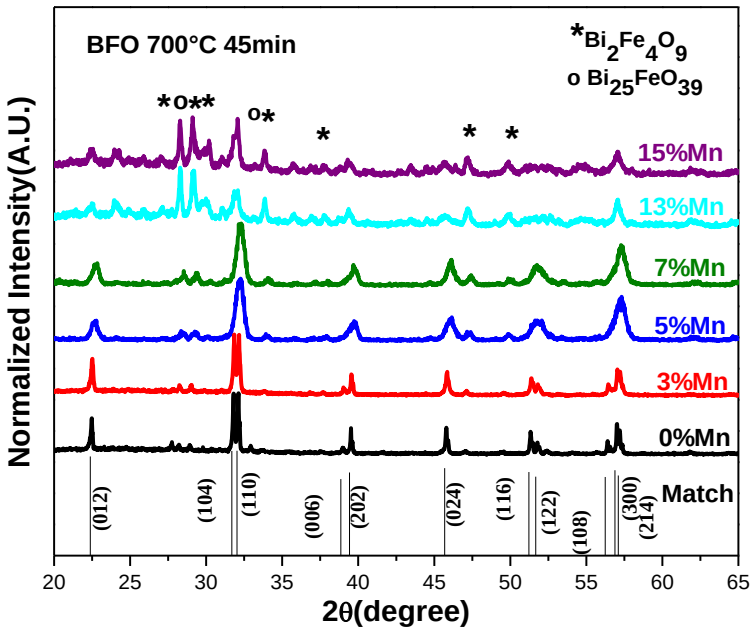

Figure 5.24 XRD patterns for Mn-doped BFO powders thermal annealed at 700°C for 45mins.

Details of the (012) peak for samples produced at different compositions of dopant and annealed for 15 minutes at 700°C are shown in Figure 5.25 (a). A shift of the (012) peak toward lower angles in 3% Mn-doped BFO, compared to undoped BFO, suggests a possible occupation of Mn^{2+} species in Fe sites of $BiFeO_3$ inducing an expansion of the unit cell. This shift was not as evident in 5% Mn-doped and 7% Mn-doped BFO. In samples annealed for 30 minutes (Fig. 5.26 a), 3% Mn-doped BFO exhibited a similar trend and that for shorter annealing time whereas the 5% Mn-doped and 7% Mn-doped BFO showed a shift in the (012) peak toward higher angles that also suggest incorporation of Mn^{2+} species in Bi^{3+} sites. As the ionic radii of Mn^{2+} (0.80Å) is smaller than the Bi^{3+} (1.20Å), the peak shift reflects a shrinking of unit cell. All the Mn-doped $BiFeO_3$ samples annealed for 45 minutes evidenced the XRD peak shift toward higher angles validating the actual incorporation of Mn in $BiFeO_3$ host.

The volume of unit cell was calculated in a hexagonal frame of reference. In the 3%Mn-doped BFO sample annealed for 15 and 30 minutes was observed an expansion of cell volume respect to undoped BFO sample (Fig. 5.25 b and Fig. 5.26 b), however in 5% and 7%Mn-doped BFO annealed for 15 and 30 minutes the cell volume tends to decrease as was suggested for the peak shift analysis. At 45 mins the volume of unit cell decreased with the Mn atomic fraction, "x" (Fig. 5.27 b), suggesting the shrinking of unit cell in agreement with the shift in the diffraction peaks towards higher angles.

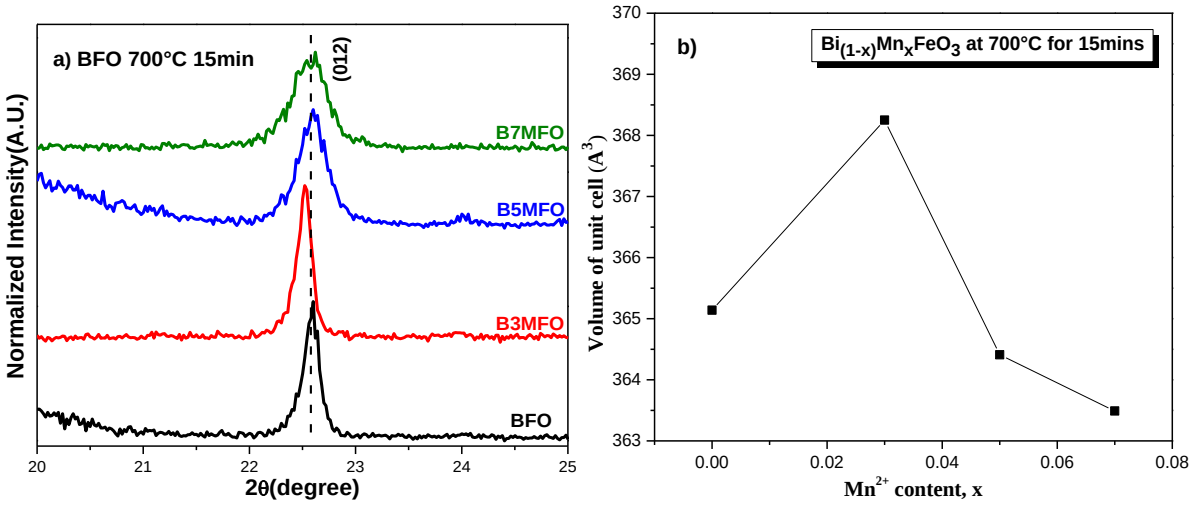

Figure 5.25 a) Details of the (012) peak shift for Mn-doped BFO samples thermal annealed at 700°C for 15 mins. b) Variation of lattice parameters with Mn^{2+} content x, in Mn doped BFO powders thermal annealed at 700°C for 15 mins.

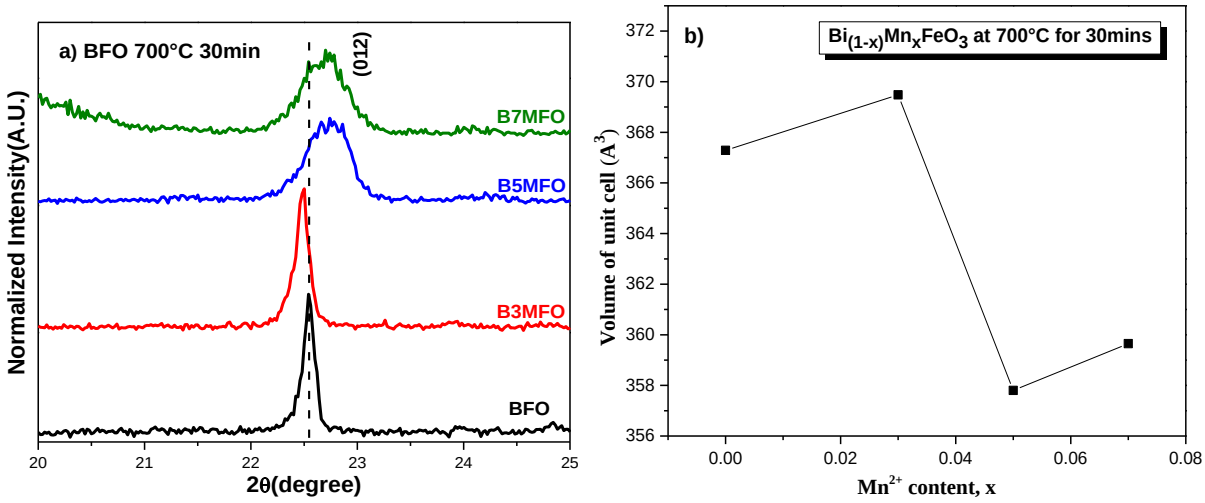

Figure 5.26 a) Details of the (012) peak shift for Mn-doped BFO samples thermal annealed at 700°C for 30 mins. b) Variation of lattice parameters with Mn^{2+} content x, in Mn doped BFO powders thermal annealed at 700°C for 30 mins.

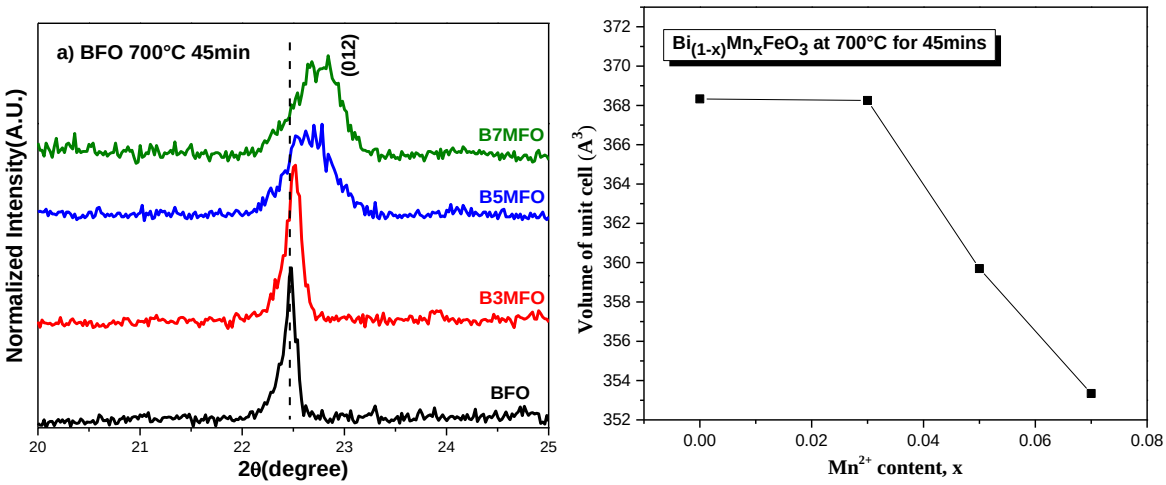

Figure 5.27 a) Details of the (012) peak shift for Mn-doped BFO samples thermal annealed at 700°C for 45 mins. b) Variation of lattice parameters with Mn^{2+} content x, in Mn doped BFO powders thermal annealed at 700°C for 45 mins.

Table 5.10 shows the average crystallite size determined only for 5% Mn-doped and 7% Mn-doped BFO using Scherrer's equation. The estimation of the average crystallite size in other samples do not allow a reliable estimation using the Scherrer's equation. It was observed that when the Mn content increased to 7%, the crystallite size was reduced with respect to the 5%Mn-doping. The

substitution on Mn species in Bi sites produce oxygen vacancies to keep the charge balance. Consequently, for greater Mn-doping, more oxygen vacancies are produced, such vacancies induce stress in the crystal structure, and a decreasing in the crystallite size may take place due these distortions.

Table 5.10 Average crystallite size for 5%Mn-doped and 7%Mn-doped BFO samples thermal annealed for 15 minutes.

samples	***Average crystallite size (nm)***
5%Mn-doped BFO	33.5
7%Mn-doped BFO	26.4

Incorporation of Mn species in Bi sites was corroborated by shrinking of the cell volume. This distortion in the structure induced a phase transition from rhombohedral to tetragonal structure for Mn content higher than 3% Mn. At 7% Mn-doped BFO was produced the optmial condition because impurities were minimized (only for 15 and 30mins-annealed samples).

Fourier Transform Infrared Spectroscopy Measurements (FTIR)

FTIR spectra of undoped and Mn-doped BFO synthesized at 700°C for 15 minutes is shown in Figure 5.28. The broad band at 3000-3600 cm^{-1} present in some samples, belong to antisymmetric and symmetric stretching of H_2O and OH^- bond groups introduced on the samples from the environment where the measurement is performed. Additionally, absorption of CO_2 from the environment occurs and it was evidenced by the appearance of a band at 2350 cm^{-1} in a few of the samples. Bands at 1383-1470 cm^{-1} can be attributed to trapped nitrates obtained from the synthesis process, which are not removed completely after thermal annealing or remained as un-reacted precursors. The FTIR spectra shows two main bands, a peak around 813 cm^{-1} that

correspond to Fe-O stretching vibrations and it keeps in the same position for pure and Mn-doped BFO. There is other main peak at 537 cm^{-1} for undoped BFO, which is attributed to Fe-O bending vibration. In Mn-doped BFO samples there was a shift towards higher wavenumbers from 547 cm^{-1} for 3% Mn-doped BFO up to 549 cm^{-1} for 7% Mn-doped BFO in comparison to undoped BFO [42]. This shift towards higher wavenumber evidences the presence of oxygen vacancies produced to compensate the charge imbalance in the doping process. Substitution of Bi^{3+} species by Mn^{2+} species lead to deficiency of positive charge in the crystal structure which is compensated with oxygen vacancies. Absence of oxygen causes Fe-O bonds to vibrate at higher frequencies [89].

These results confirm inclusion of Mn in host $BiFeO_3$, also supported by the above XRD analysis [90]. According to equation (4.4), shift towards high wavenumbers is also attributed to the substitution of low atomic weight Mn ions instead Bi ions with larger atomic weight [67].

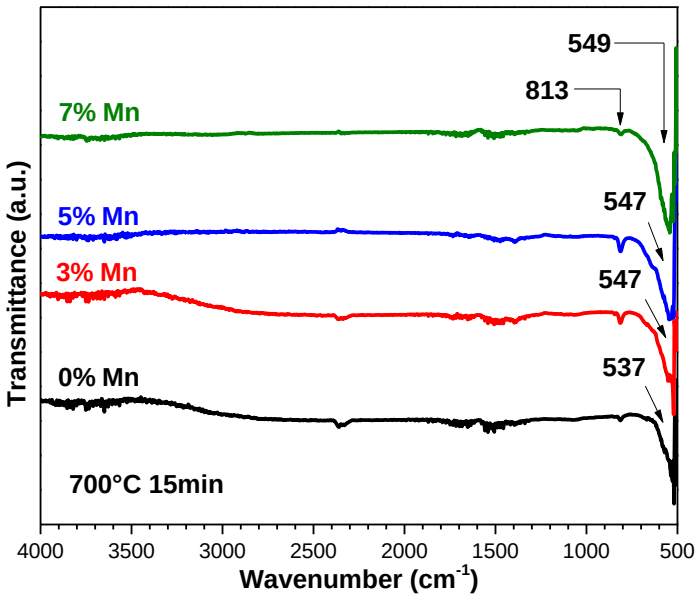

Figure 5.28 FTIR spectra of Mn-doped Bismuth Ferrite powders thermal annealed at 700°C for 15 minutes.

Scanning Electronic Microscopy Measurements (SEM)

Micrographs show agglomerate and polydisperse particles in 7% Mn-doped BFO samples prepared by sol-gel method and annealed for 15 minutes (Figure 5.29). Micrographs verify reduction of the particle size for 7% Mn-doped BFO compared to undoped BFO powders.

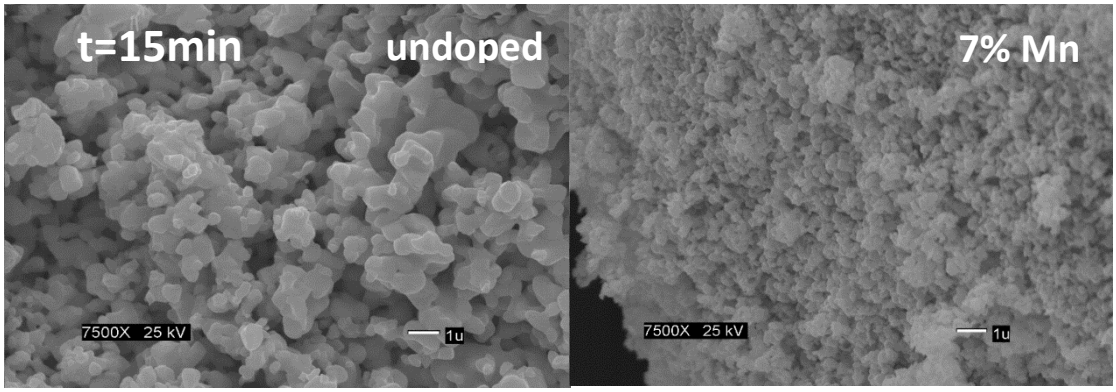

Figure 5.29 SEM micrographs for undoped and 7%Mn-doped $BiFeO_3$ powders thermal annealed at 700°C for 15minutes.

The average particle size for undoped BFO was ~ 0.52 μm and was reduced up to ~ 0.39 μm for 7% Mn-doped BFO (Table 5.11). The incorporation of Mn^{2+} species in Bi^{3+} sites inhibit the particle growth. Inhibition of the grain growth has been reported previously in Sm doped $BiFeO_3$ powders prepared by sol-gel in a study that suggested that the particle size reduction was produced due smaller ionic radii of Sm respect to Bi [91]. In this work, the mismatch between ionic radii of Bi and Mn induce strain in the crystal structure. Consequently, the rate of nucleation may increase, reducing the particle size.

Table 5.11 Average particle size for undoped and 7%Mn-doped BFO thermal annealed for 15 minutes.

samples	***Average grain size (nm)***
undoped BFO	523.3 ± 216.3
7%Mn-doped BFO	389.5 ± 90.3

MH Measurements

Magnetic hysteresis loop measured at room temperature in a magnetic field range from -10 kOe up to 10 kOe of undoped and Mn-doped $BiFeO_3$ powders annealed for 15, 30 and 45 minutes, are presented in Figure 5.30 a), Figure 5.31 a) and Figure 5.32 a) respectively. For the 15 mins-annealed samples, the 3% Mn-doped and 5% Mn-doped BFO showed a weak ferromagnetism with non-saturated magnetic hysteresis loop. On the other hand, when Mn doping was increased up to 7%, the magnetic behavior changed considerably to a ferrimagnetic order. The non-saturated hysteresis loop is attributed to the antiferromagnetic character for undoped BFO and the weak ferromagnetism in the Mn-doped BFO samples. Past reports claimed that non-saturated hysteresis loops are due to the persistence of the uncompensated antiferromagnetism in the Mn-doped BFO samples [56]. The magnetic hysteresis loops for 13% Mn-doped and 15% Mn-doped BFO samples were not measured because for these conditions, the perovskite structure of BFO was not achieved.

Remanent and maximum magnetization values were enhanced as Mn^{2+} content "x" was increased (Fig. 5.30 b). For the 7% Mn-doped BFO the magnetic properties improved notably with respect to the other samples.

The superexchange interaction effect plays a great role as mechanism that explains the enhancement in the magnetic order for the Mn-doped compared to undoped BFO samples. Perturbations in the Fe-O-Fe bond angles may improve the superexchange effect. Incorporation of Mn species in the Fe sites was observed for 3% Mn-doping, which induces a slight distortion in the crystal structure what can be reflected in a transition from antiferromagnetic to weak ferromagnetic order due disturbances in the Fe-O-Fe bond angles. This affects directly the superexchange interaction. For 5% and 7% Mn-doping, the stress in the crystal structure is more obvious, because for these conditions, a phase transition for rhombohedral to tetragonal was observed, hence an enhancement in the superexchange interaction takes place [58]. The spiral spin structure of undoped BFO has a long period of ~ 62 nm. Since the average crystallite size for 5% Mn-doped (33.5 nm) and 7% Mn-doped (26.4 nm) BFO annealed for 15mins, is below 62 nm, the spiral spin could have been suppressed and thus the magnetic order is improved. This statement is in agreement with other reports for Co-doped BFO [51] and Mn-doped BFO [56], [57].

The observed coercivity values reported a random variation; it reached ~77 Oe for undoped BFO, 188 Oe in 3% Mn-doped BFO, 140 Oe in 5% Mn-doped BFO and was reduced up to 30 Oe for 7%Mn-doped BFO. Such variations in coercivity can be explained in terms of magnetic anisotropy according the next relation $\mathbf{K=H_C.M_S / 2}$, where **K** is the anisotropy constant, $\mathbf{H_C}$ is the coercivity and $\mathbf{M_S}$ is the saturation magnetization. From this relation, it can be deduced that for high crystal anisotropy, the coercivity tends to increase [13], [92].

On the other hand, the incorporation of Mn species in Fe sites was suggested for 3% Mn-doping. This induced a strain in the crystal structure that is reflected in an increase in the anisotropy that leads to an increase in the coercivity. A phase transition takes place for 5% and 7% Mn doped BFO samples and this implies a change in the magnetocrystalline anisotropy. First, the magnetization aligns along one of the main crystal directions in rhombohedral structure (undoped BFO). This direction is called the easy direction of magnetization, and when the BFO undergoes a phase transition to tetragonal structure (5% and 7%Mn-doped BFO), the magnetization vector will change its easy direction of magnetization in the new crystal structure. These variations in the magnetocrystalline anisotropy should affect the coercivity values [48], [93].

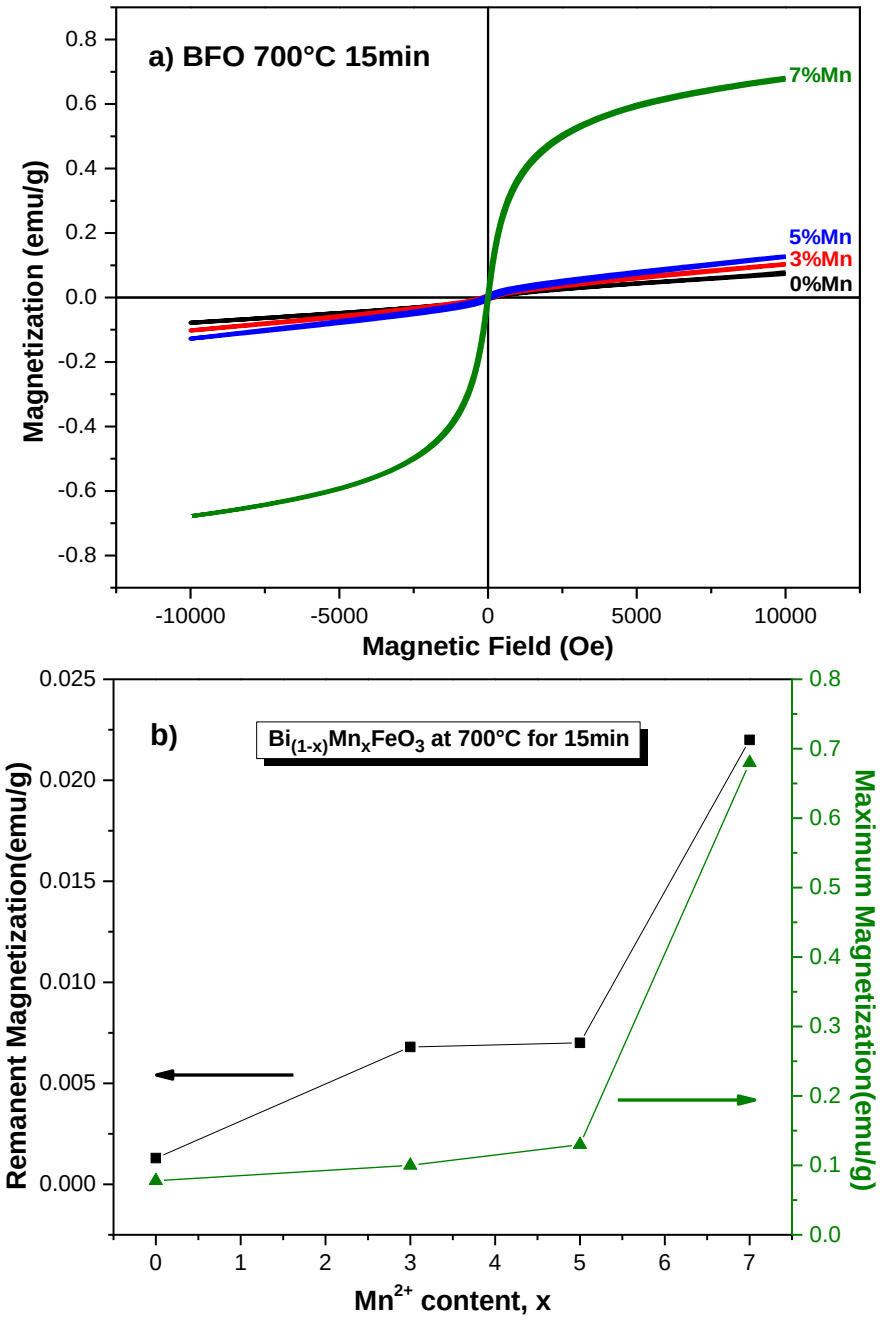

Figure 5.30 a) Magnetic hysteresis loops for Mn-doped BFO samples annealed for 15 mins. b) Variation of magnetic parameters with Mn^{2+} content x for $Bi_{(1-x)}Mn_xFeO_3$ annealed for 15 mins.

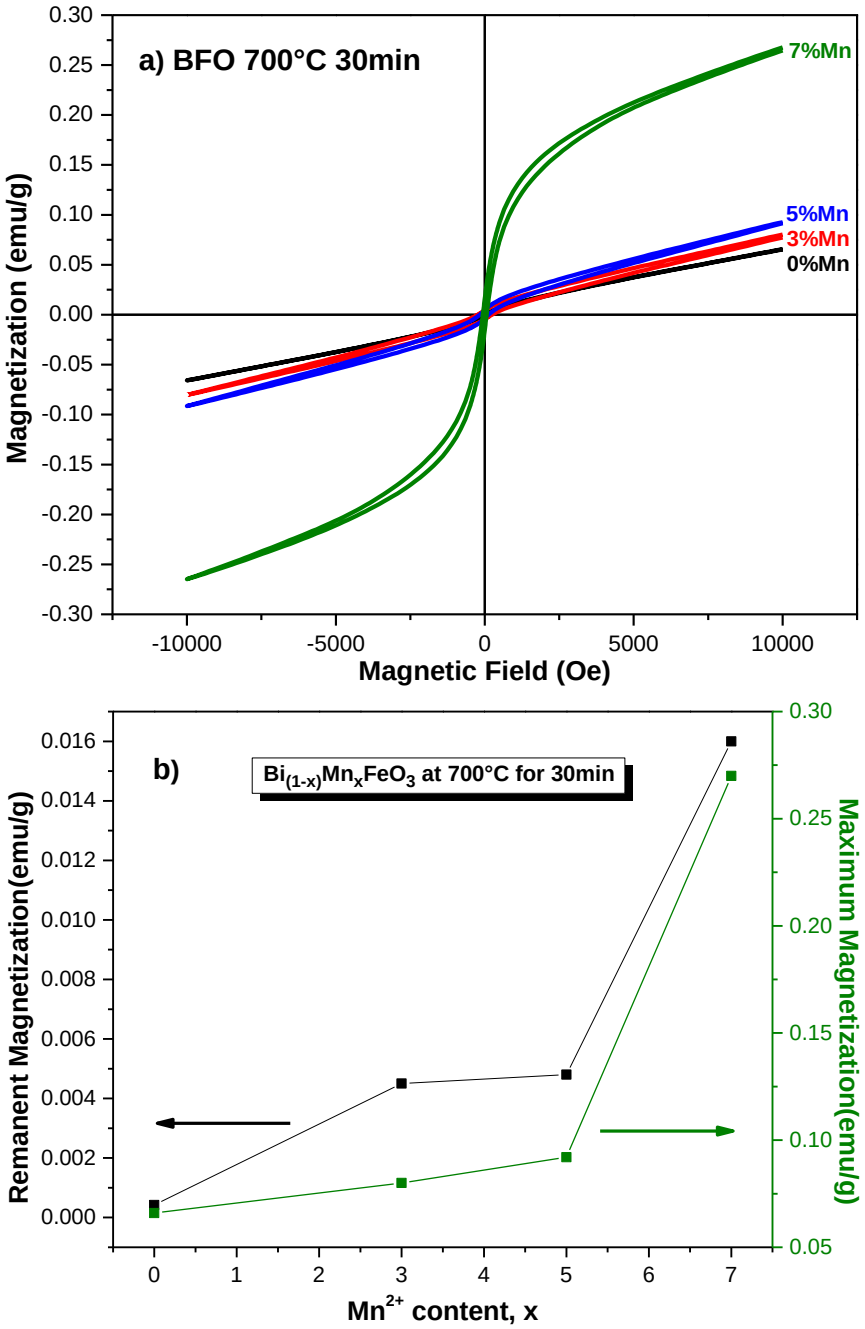

Figure 5.31 a) Magnetic hysteresis loops for Mn-doped BFO samples annealed for 30 mins. b) Variation of magnetic parameters with Mn^{2+} content x for $Bi_{(1-x)}Mn_xFeO_3$ annealed for 30 mins.

Magnetic hysteresis loops for samples annealed for 30 mins (Figure 5.31 a) showed a similar behavior as the samples annealed for 15 mins. Also, the remanent and maximum magnetization values were enhanced as Mn^{2+} content "x" was increased (Fig. 5.31 b). In samples annealed for 45 minutes (Fig. 5.32 a) a different behavior with respect to other annealing time conditions was observed. Undoped BFO presented non-saturated hysteresis loop with a weak ferrimagnetic order, but when Mn doping was increased the magnetic behavior was not enhanced. Additionally, Figure 5.32 b) demonstrates the poor magnetic character of doped samples compared to undoped BFO, reflected in a decrease in the maximum and remanent magnetization values.

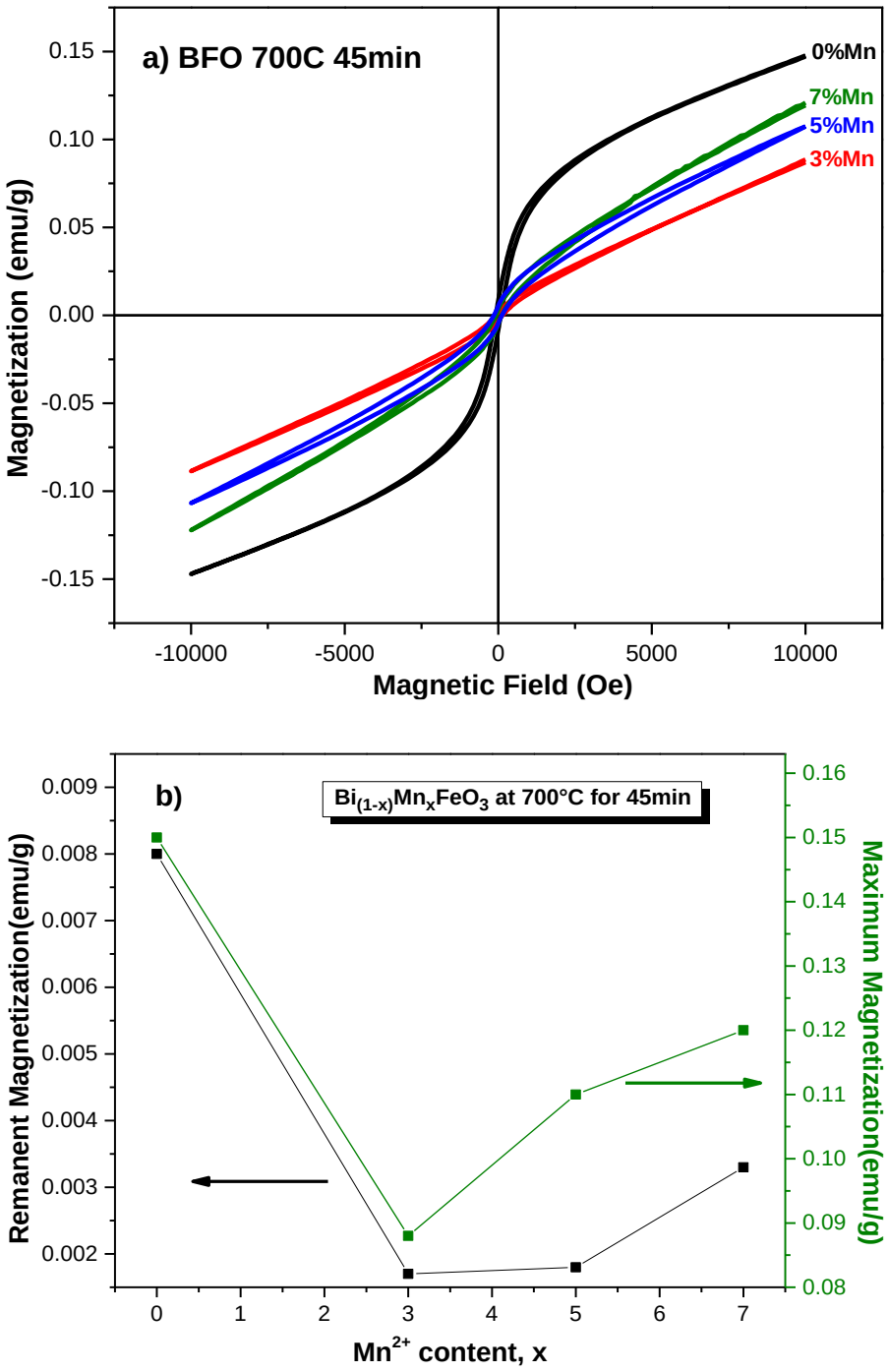

Figure 5.32 a) Magnetic hysteresis loop for Mn-doped BFO samples annealed for 45 mins. b) Variation of magnetic parameters with Mn^{2+} content x for $Bi_{(1-x)}Mn_xFeO_3$ annealed for 45 mins.

A possible interpretation of these results in samples annealed for 45 minutes could be that the prolongated annealing time may lead to an unstable crystal structure and this does not support an improvement in the magnetic properties when Mn doping is increased. The paramagnetic impurities observed in 45mins-annealed samples are paramagnetic and hence they should not contribute to the magnetic properties according with previous reports [40], [51], [94].

The optimal conditions were observed for the 7% Mn-doped BFO annealed for 15 minutes because it reached the highest maximum and remanent magnetization values of ~ 0.68 emu/g and ~ 0.02 emu/g, respectively (Table 5.12). The coercivity obtained from the hysteresis loop was a low value of ~ 30 Oe. This sample can be classified as soft ferromagnet, which are materials with low coercivity, that are easy to magnetize and demagnetize, usually used for magnetic cores in transformers [25].

Table 5.12 Magnetic parameters for undoped and 7% Mn-doped BFO powders thermal annealed at 700°C for 15 minutes.

samples	***Coercivity (Oe)***	***Remanent Magnetization (emu/g)***	***Saturation Magnetization (emu/g)***
undoped BFO	77	0.001	0.08
7%Mn-doped BFO	30	0.02	0.68

5.4 Nanocrystalline Co- and Mn-doped $BiFeO_3$ powders: Comparative Analyses

5.4.1 Effect of dopant type

X-Ray Diffraction Measurements (XRD)

Figure 5.33 shows XRD patterns of undoped, 7%Co and 7%Mn doped BFO nanocrystalline powders synthesized by sol-gel method after an annealing treatment at 700°C for 15 minutes. Match software was used to verify the crystal structure of the samples in the XRD spectra. Undoped and 7% Co-doped BFO showed rhombohedral perovskite structure of $BiFeO_3$, but the 7% Mn-doped BFO sample showed an evident broadening and overlapping of the doublet principal peaks located at the 31°-33° 2θ range. Such variation induces a change in the crystal structure from rhombohedral to tetragonal.

For 7% Co-doped $BiFeO_3$ sample the impurity phases were removed. In turn, at 7% Mn-doped BFO sample impurities did not change respect to the undoped BFO samples. These results suggest that incorporation of Co species in host BFO inhibit the formation of impurity phases and enable a good stability of the crystal structure of BFO. On the other hand, the phase transition from rhombohedral to tetragonal crystal structure disturbed the stability of the BFO, in consequence, impurity phases were maintained. The ionic radii of Bi^{2+} (1.20 Å) is larger than that Co^{2+} (0.78 Å) and Mn^{2+} (0.80 Å), this imply that the incorporation of Co or Mn species in BFO host must induce a shrinking in the unit cell.

The volume of unit cell was calculated to corroborate the incorporation of dopants. In Table 5.13 is showed that the volume of unit cell for 7%Co-doped BFO increase respect to the undoped BFO, that's mean that Co species may have been incorporated in the Fe sites of BFO host. Besides,

the volume of unit cell for 7% Mn-doped BFO has decreased respect to undoped BFO, this evidence the inclusion on Mn species in BFO host.

Table 5.13 Values of the volume of unit cell for undoped, 7% Co- and 7%Mn- doped BFO thermal annealed at 700°C for 15 minutes using a hexagonal representation of the crystal structure.

samples	***Volume of unit cell (A^3)***
undoped BFO	365.14
7% Co-doped BFO	369.32
7% Mn-doped BFO	363.49

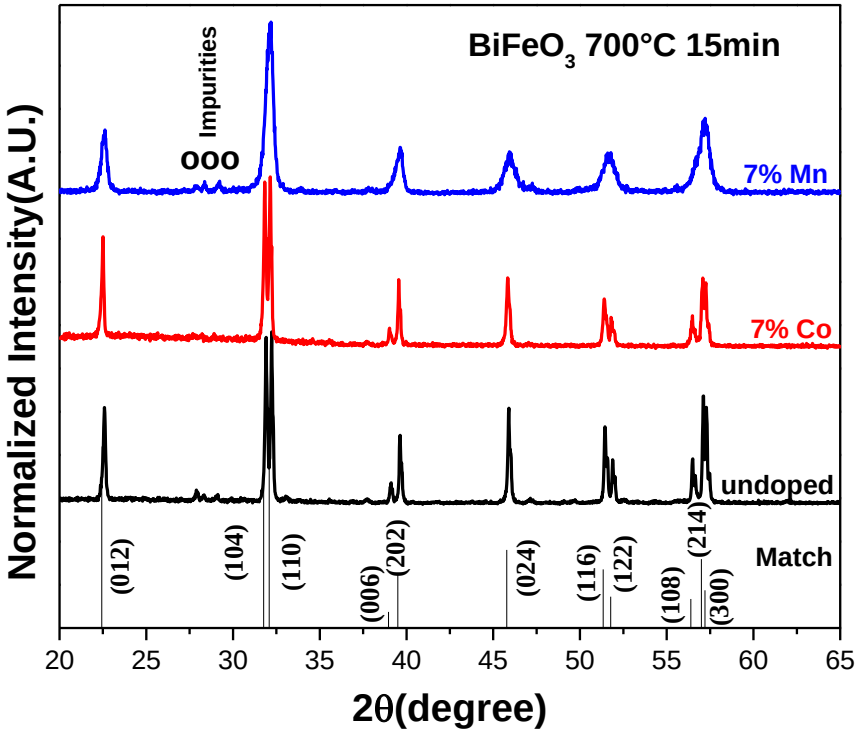

Figure 5.33 XRD patterns for undoped, 7%Co and 7%Mn doped BFO powders thermal annealed at 700°C for 15mins.

Figure 5.34 shows XRD patterns of undoped, 15%Co and 15%Mn doped BFO nanocrystalline powders synthesized by sol-gel method after an annealing treatment at 700°C for 15 minutes. For the 15% Co-doped BFO sample the rhombohedral perovskite structure of $BiFeO_3$ keeps stable without traces of impurities. On the other hand, for 15% Mn-doped BFO the structure turns unstable due that a saturation of substitution sites take place in the BFO host at higher concentration of Mn species. As a consequence, a distortion in the crystal structure is produced and the perovskite structure is not reached. Large number of oxidation states of Mn species could be the reason for make unstable the structure in the synthesis process. In turn, $CoFe_2O_4$ is observed in the XRD patterns (Figure 5.33) as secondary phase in the 15% Co-doped BFO sample; in the 15% Mn-doped BFO sample the final crystal structure was thermally decomposed.

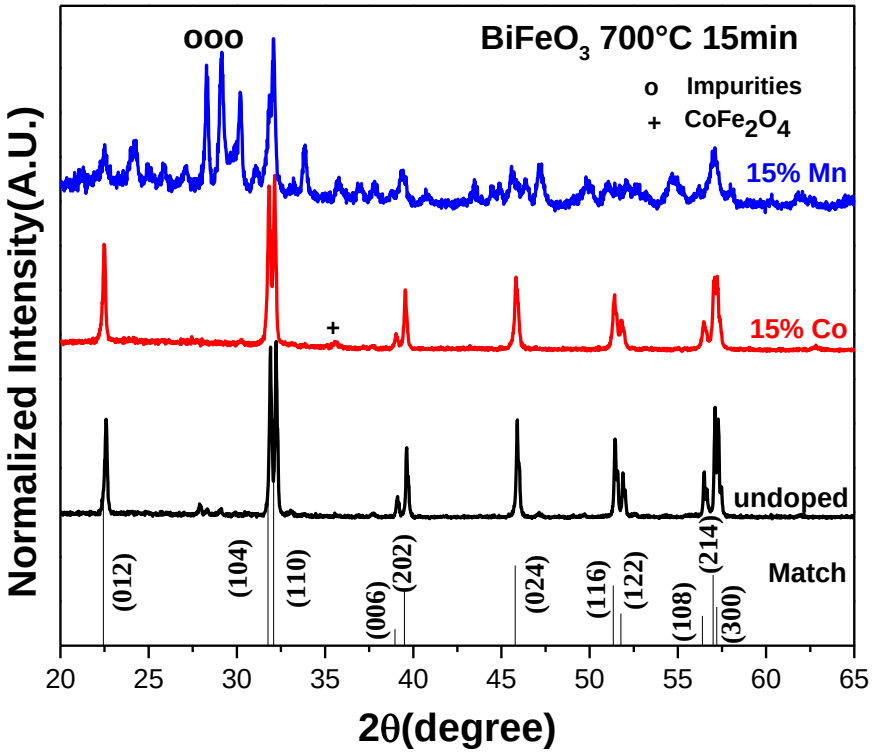

Figure 5.34 XRD patterns for undoped, 15% Co and 15% Mn doped BFO powders annealed at 700°C for 15mins.

Fourier Transform Infrared Spectroscopy Measurements (FTIR)

Figure 5.35 shows the FTIR spectra of undoped, 7% Co and 7% Mn doped BFO powders annealed at 700°C for 15 minutes. FTIR spectra shows two principal bands for all samples, one band around 813 cm^{-1} is attributed to Fe-O stretching vibration, the other band corresponds to Fe-O bending vibration, which is found at 537 cm^{-1} for undoped BFO and it was increased up to 543 and 549 cm^{-1} for 7% Co and 7% Mn doped BFO, respectively. XRD patterns (Figure 5.34) showed that 7% Co and 7% Mn doped BFO have different crystal structures. FTIR spectra was measured for corroborate the perovskite structure, but there was not a significant difference between the FTIR spectra for 7% Co and 7% Mn doped BFO.

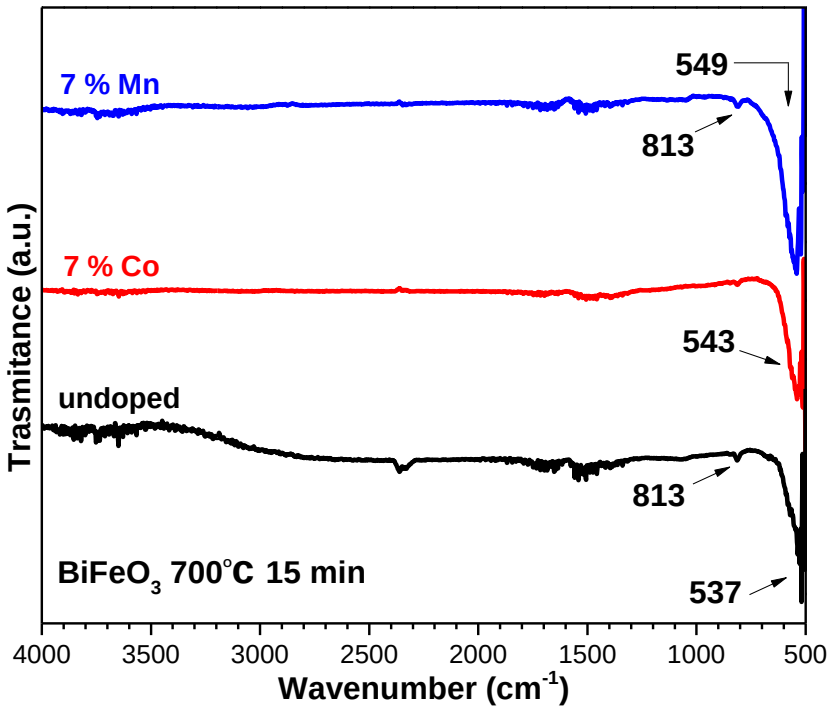

Figure 5.35 FTIR spectra of undoped, 7% Co and 7% Mn doped Bismuth Ferrite powders thermal annealed at 700°C for 15 minutes.

MH Measurements

Figure 5.36 shows the M-H hysteresis loops measured in a magnetic field ranging from -10 kOe up to 10 kOe, for undoped, 7% Co and 7% Mn doped BFO powders annealed at 700°C for 15 minutes. 7% Co-doped BFO exhibited saturated ferromagnetic hysteresis unlike undoped BFO that presents antiferromagnetic order. In turn, 7% Mn doped BFO show a ferrimagnetic ordering but a non-saturated hysteresis loop. Incorporation of Co or Mn species in BFO host induce changes in the Fe-O-Fe bond angles, and according to the superexchange interaction effect, a transition from antiferromagnetic to ferromagnetic order may occur.

Despite that the 7% Mn doped BFO samples presents non-saturated ferrimagnetic hysteresis, the maximum magnetization is higher than the 7% Co-doped BFO sample, the main reason may be the distortion induce in 7% Mn-doped BFO for the transition phase from rhombohedral to tetragonal crystal structure, in consequence, a great perturbation can occur in the Fe-O-Fe bond angle, thus the ferrimagnetic order is reached. On the other hand, values of coercivity for 7% Co-doped BFO is 42 times larger than that of the 7% Mn-doped BFO (Table 5.14), this increase may be attributed to the presence of Cobalt Ferrite in the 7% Co-doped BFO structure. CFO has a high coercivity with a low magnetization [79], [87]. High coercivity, and remanent magnetization values makes 7% Co-doped BFO a good candidate for applications in permanent or hard magnets and data storage devices, due is necessary apply a high magnetic field for demagnetize the material. By contrast, due low values in coercivity for 7% Mn-doped BFO sample, it can classify as soft magnet, and are used for transformers and magnetic cores.

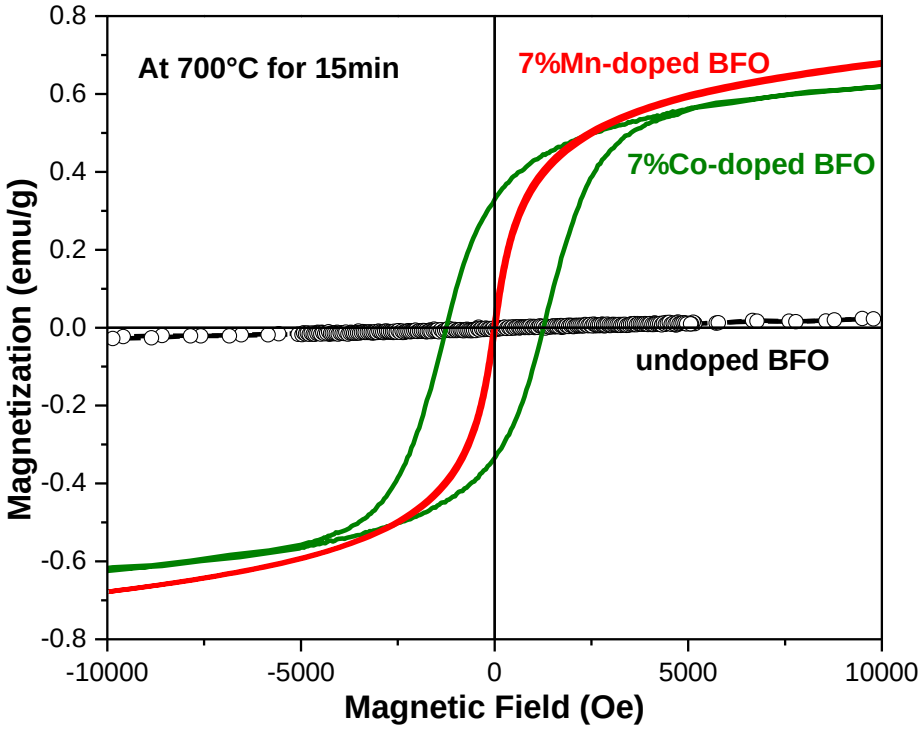

Figure 5.36 Magnetic hysteresis loops measured at room temperature for undoped, 7%Co and 7%Mn doped BFO thermal annealed at 700°C for 15min.

Table 5.14 Magnetic parameters for undoped, 7%Co- and 7%Mn- doped BFO powders thermal annealed at 700°C for 15 minutes.

samples	***Coercivity (Oe)***	***Remanent Magnetization (emu/g)***	***Saturation Magnetization (emu/g)***
undoped BFO	77	~ 0	0.08
7%Co-doped BFO	1254	0.33	0.66
7%Mn-doped BFO	30	0.02	0.68

CHAPTER VI: CONCLUSIONS AND RECOMENDATIONS

Nanocrystalline $BiFeO_3$ powders

- Pure $BiFeO_3$ was successfully synthesized by sol-gel method. XRD diffraction patterns confirmed the rhombohedral perovskite structure of undoped Bismuth Ferrite for all annealing time conditions. The optimum annealing condition was determined at 700°C for 30 mins due to the minimized formation of impurity phases. FTIR spectra corroborated the formation of perovskite structure. SEM micrographs showed a grain size in the submicrometric range.
- Room temperature MH measurements showed a linear relationship between magnetization and applied magnetic field for all undoped BFO samples. This verified the antiferromagnetic order that is characteristic in pure BFO. Increase in the slope in the M-H measurements for prolongated annealing times suggest a preferential alignment of the spins in these conditions, accordingly an increase in maximum magnetization is observed. The optimal maximum magnetization value was of ~0.1 emu/g for undoped BFO obtained at 30 mins because at this time condition, the impurity phases in the material were minimal.

Nanocrystalline Co-doped $BiFeO_3$ powders

- High crystalline Co-doped BFO samples were successfully synthesized via a sol gel method at 700°C. XRD patterns show the rhombohedral perovskite structure in Co-doped BFO samples. Moreover, FTIR measurements corroborated the presence of perovskite structure in Co-doped BFO samples. On the other hand, time annealing did not affect

structural properties in Co-doped BFO samples. The formation of Cobalt Ferrite inhibited the formation of impurity phases from 7%Co doped BFO samples.

- The optimal condition with minimal impurities and a major amount of Cobalt Ferrite was reached at 15%Co doped BFO for all annealing time conditions.
- The average paticle size found for 15%Co-doped BFO sample was ~0.24 μm, which is about five times smaller than that of undoped BFO that was ~1.20 μm.
- Room Temperature MH measurements exhibited saturated ferromagnetic hysteresis for all Co-doped BFO samples. Enhancement in magnetic properties for Co-doped BFO samples was reached due two mechanisms 1° The distortion in the crystalline cell (from 5% up to 7% Co), and 2° The presence of Cobalt Ferrite in (from 8% up to 15% Co).

- The optimal doping condition was determined for 15% Co-doped BFO due to the highest values of coercivity, remanence and saturation magnetization. This material can be classified as a hard magnet.

Nanocrystalline Mn-doped $BiFeO_3$ powders

- Mn-doped BFO samples were successfully synthesized via a sol gel method at 700°C. XRD patterns detected the rhombohedral perovskite structure only in 3%Mn-doped BFO samples, but in 5% Mn and 7% Mn-doped BFO samples showed a phase transition from rhombohedral to tetragonal crystal structure for all annealing time conditions.

- The impurity phases increased with annealing time in Mn-doped BFO samples. For 13% and 15% of Mn doping the perovskite structure was not reached.
- The incorporation of Mn^{2+} species in Bi^{3+} sites inhibited particle growth.
- The annealing time and the presence of paramagnetic impurity phases affect the magnetic properties in Mn-doped BFO samples., the optimal condition was determined to be at 7% Mn doped BFO annealed for 15 minutes because it reached the highest maximum and remanent magnetization values of ~ 0.68 emu/g and ~ 0.02 emu/g, but a low value of coercivity of ~ 30 Oe. Therefore, this material can be classified as soft ferromagnet.

The formation of Bismuth Ferrite-Cobalt Ferrite composites admits high crystalline samples and inhibit the formation of impurity phases for all annealing time conditions. Presence of Cobalt Ferrite enhance magnetic properties in Co-doped BFO samples. Incorporation of Mn species minimized the formation of impurities for optimal time annealing conditions and this favored the enhancement in its magnetic properties.

In this work were synthesized impurities free samples with good magnetic properties at same time, under optimal conditions. This is a difficult challenge in preparation of bismuth ferrite and it had not achieved totally in previous researchs. This approach is the first step in the development of materials with excellent magnetoelectric properties for applications in electronic devices. But, a balance between the already achieve conditions (no impurities and improvement in magnetic properties) and good ferroelectric properties of the bismuth ferrite must be developed too.

On basis to the results of this work, is suggested carry out the following characterizations:

- Transmission Electron Microscopy (TEM) measurements to observe in detail the particle size, morphology and other present phases.
- Raman Spectroscopy measurements for complete the study of the effect of dopant on structure and how this affects magnetic properties.
- Neutron Diffraction for determine the magnetic structure of the samples and corroborate the mechanisms proposed in this work for explain magnetic behavior.

REFERENCES

[1] N. A. Spaldin, S. Cheong, and R. Ramesh, "Multiferroics : Past , present , and future feature," *Phys. Today*, vol. 63, no. 10, p. 38, 2010.

[2] R. Ramesh and N. A. Spaldin, "Multiferroics: progress and prospects in thin films," *Nat. Mater.*, vol. 6, no. 1, pp. 21–29, 2007.

[3] V. V Lazenka, G. Zhang, J. Vanacken, I. I. Makoed, A. F. Ravinski, and V. V Moshchalkov, "Structural transformation and magnetoelectric behaviour in $Bi_{1-x}Gd_xFeO_3$ multiferroics," *J. Phys. D. Appl. Phys.*, vol. 45, no. 12, p. 125002, 2012.

[4] M. S. Bernardo, "Synthesis, microstructure and properties of $BiFeO_3$-based multiferroic materials: A review," *Bol. la Soc. Esp. Ceram. y Vidr.*, vol. 53, no. 1, pp. 1–14, 2014.

[5] J. Wu, Z. Fan, D. Xiao, J. Zhu, and J. Wang, "Multiferroic bismuth ferrite-based materials for multifunctional applications: Ceramic bulks, thin films and nanostructures," *Prog. Mater. Sci.*, vol. 84, pp. 335–402, 2016.

[6] G. Catalan and J. F. Scott, "Physics and applications of bismuth ferrite," *Adv. Mater.*, vol. 21, no. 24, pp. 2463–2485, 2009.

[7] X. Zheng *et al.*, "The magnetic properties of La doped and codoped BiFeO3," *J. Alloys Compd.*, vol. 499, no. 1, pp. 108–112, 2010.

[8] J. T. Han *et al.*, "Tunable synthesis of bismuth ferrites with various morphologies," *Adv. Mater.*, vol. 18, no. 16, pp. 2145–2148, 2006.

[9] S. K. Srivastav and N. S. Gajbhiye, "Low temperature synthesis, structural, optical and magnetic properties of bismuth ferrite nanoparticles," *J. Am. Ceram. Soc.*, vol. 95, no. 11, pp. 3678–3682, 2012.

[10] L. Wang *et al.*, "Synthesis of $BiFeO_3$ nanoparticles by a low-heating temperature solid-state precursor method," *Mater. Res. Bull.*, vol. 48, no. 2, pp. 383–388, 2013.

[11] Y. Yang, Y. B. Yao, Q. Zhang, and X. X. Zhang, "Polarized Raman study on the lattice structure of $BiFeO_3$ films prepared by pulsed laser deposition," *Vib. Spectrosc.*, vol. 75, pp. 101–106, 2014.

[12] A. Lahmar, K. Zhao, S. Habouti, M. Dietze, C. H. Solterbeck, and M. Es-Souni, "Off-stoichiometry effects on BiFeO3 thin films," *Solid State Ionics*, vol. 202, no. 1, pp. 1–5, 2011.

[13] I. K. Batttisha *et al.*, "Dielectric and Magnetic Properties of Nano-Structure $BiFeO_3$ Doped with Different Concentrations of Co Ions Prepared by Sol-Gel Method," vol. 3, no. July, pp. 59–73, 2015.

[14] P. Priyadharsini, A. Pradeep, B. Sathyamoorthy, and G. Chandrasekaran, "Enhanced multiferroic properties in la and Ce co-doped $BiFeO_3$ nanoparticles," *J. Phys. Chem. Solids*, vol. 75, no. 7, pp. 797–802, 2014.

[15] A. Kumar and K. L. Yadav, "Magnetic, magnetocapacitance and dielectric properties of Cr doped bismuth ferrite nanoceramics," *Mater. Sci. Eng. B Solid-State Mater. Adv. Technol.*, vol. 176, no. 3, pp. 227–230, 2011.

[16] Z. X. Cheng *et al.*, "Structure, ferroelectric properties, and magnetic properties of the La-doped bismuth ferrite," *J. Appl. Phys.*, vol. 103, p. 07E507, 2008.

[17] G. M. Montes, O. Perales-Perez, B. Rentería, and M. Gálvez, "Tuning of Magnetic Properties in Cobalt-Doped Nanocrystalline Bismuth Ferrite Gina," *MRS Proc.*, vol. 1368,

2011.
[18] J. Li, K. Liu, J. Xu, L. Wang, L. Bian, and F. Xu, “Structure-Dependent Electrical , Optical and Magnetic Properties of Mn-Doped $BiFeO_3$ Thin Films Prepared by the Sol-Gel Process,” vol. 2, no. 3, pp. 75–81, 2013.
[19] S.-W. Cheong and M. Mostovoy, “Multiferroics: a magnetic twist for ferroelectricity,” *Nat. Mater.*, vol. 6, no. 1, pp. 13–20, 2007.
[20] N. A. Hill, “Why Are There so Few Magnetic Ferroelectrics,” pp. 6694–6709, 2000.
[21] N. A. Spaldin and M. Fiebig, “The Renaissance of Magnetoelectric Multiferroics,” *Science (80-.).*, vol. 309, no. 5733, pp. 391–392, 2005.
[22] W. Ratcliff, J. W. Lynn, V. Kiryukhin, P. Jain, and M. R. Fitzsimmons, “Magnetic structures and dynamics of multiferroic systems obtained with neutron scattering,” *npj Quantum Mater.*, vol. 1, 2016.
[23] C. Lu and J. Liu, “DyMnO 3 : A model system of type-II multiferroics,” vol. 2, pp. 213–224, 2016.
[24] P. T. W. O *et al.*, “Direct observation of magnetodielectric effect in type-I multiferroic,” vol. 15, pp. 1545–1548, 2015.
[25] J. M. D. Coey, *Magnetism and Magnetic Materials*. New York: Cambridge University Press, 2010.
[26] N. A. Spaldin, *Magnetic materials: fundamentals and applications*, Second. New York: Cambridge University Press, 2010.
[27] C. D. G. B. D. Cullity, *Introduction to Magnetic Materials*, Second. Wiley-IEEE Press, 2008.
[28] K. M. Rabe, C. Ahn, and J.-M. Triscone, *Physics of Ferroelectrics*, vol. 105. Springer, 2007.
[29] K. C. Kao, *Dielectric Phenomena in Solids*. Elsevier, 2004.
[30] D. Sando, A. Barthélémy, and M. Bibes, “$BiFeO_3$ epitaxial thin films and devices: past, present and future,” *J. Phys. Condens. Matter*, vol. 26, no. 47, p. 473201, 2014.
[31] A. M. Kadomtseva, A. K. Zvezdin, Y. F. Popov, A. P. Pyatakov, G. P. Vorob’ev, and G. P. Vorob’ev, “Space-time parity violation and magnetoelectric interactions in antiferromagnets,” *J. Exp. Theor. Phys. Lett.*, vol. 79, no. 11, pp. 571–581, 2004.
[32] K. Chakrabarti *et al.*, “Enhanced magnetic and dielectric properties of Eu and Co co-doped $BiFeO_3$ nanoparticles,” *Appl. Phys. Lett.*, vol. 101, no. 4, p. 42401, 2012.
[33] I. Sosnowska, W. Schäfer, W. Kockelmann, K. H. Andersen, and I. O. Troyanchuk, “Crystal structure and spiral magnetic ordering of $BiFeO_3$ doped with,” vol. 1042, pp. 1040–1042, 2002.
[34] K. Chakrabarti, B. Sarkar, V. D. Ashok, S. S. Chaudhuri, and S. K. De, “Enhanced magnetic and dielectric behavior in Co doped $BiFeO_3$ nanoparticles,” *J. Magn. Magn. Mater.*, vol. 381, pp. 271–277, 2015.
[35] L. W. Martin, “Engineering functionality in the multiferroic $BiFeO_3$ – controlling chemistry to enable advanced applications,” vol. 1, pp. 10813–10826, 2010.
[36] L. W. Martin, Y. H. Chu, and R. Ramesh, “Advances in the growth and characterization of magnetic, ferroelectric, and multiferroic oxide thin films,” *Mater. Sci. Eng. R Reports*, vol. 68, no. 4–6, pp. 89–133, 2010.
[37] L. W. Martin, Y. Chu, and R. Ramesh, “Advances in the growth and characterization of magnetic , ferroelectric , and multiferroic oxide thin films,” *Mater. Sci. Eng. R*, vol. 68, no.

4–6, pp. 89–133, 2010.
[38] U. Khan *et al.*, "Influence of cobalt doping on structural and magnetic properties of $BiFeO_3$ nanoparticles," *J. Nanoparticle Res.*, vol. 17, no. 11, pp. 1–9, 2015.
[39] D. Khomskii, "Classifying multiferroics : Mechanisms and effects Introduction . A bit of history How to combine magnetism and ferroelectricity : Different types of multiferroics," vol. 20, 2009.
[40] M. Hasan, M. F. Islam, R. Mahbub, M. S. Hossain, and M. a. Hakim, "A soft chemical route to the synthesis of $BiFeO_3$ nanoparticles with enhanced magnetization," *Mater. Res. Bull.*, vol. 73, pp. 179–186, 2016.
[41] J. Silva, a Reyes, H. Esparza, H. Camacho, and L. Fuentes, "$BiFeO_3$: A Review on Synthesis, Doping and Crystal Structure.," *Integr. Ferroelectr.*, vol. 126, no. 1, pp. 47–59, 2011.
[42] M. Sakar, S. Balakumar, P. Saravanan, and S. N. Jaisankar, "Annealing temperature mediated physical properties of bismuth ferrite ($BiFeO_3$) nanostructures synthesized by a novel wet chemical method," *Mater. Res. Bull.*, vol. 48, no. 8, pp. 2878–2885, 2013.
[43] R. Guo, L. Fang, W. Dong, F. Zheng, and M. Shen, "Magnetically separable $BiFeO_3$ nanoparticles with a γ-Fe_2O_3 parasitic phase: controlled fabrication and enhanced visible-light photocatalytic activity," *J. Mater. Chem.*, vol. 21, no. 46, p. 18645, 2011.
[44] S. Godara, N. Sinha, G. Ray, and B. Kumar, "Combined structural, electrical, magnetic and optical characterization of bismuth ferrite nanoparticles synthesized by auto-combustion route," *J. Asian Ceram. Soc.*, vol. 2, no. 4, pp. 416–421, 2014.
[45] Z. Lin, W. Cai, W. Jiang, C. Fu, C. Li, and Y. Song, "Effects of annealing temperature on the microstructure, optical, ferroelectric and photovoltaic properties of $BiFeO_3$ thin films prepared by sol-gel method," *Ceram. Int.*, vol. 39, no. 8, pp. 8729–8736, 2013.
[46] Y. Wang, Q. H. Jiang, H. C. He, and C. W. Nan, "Multiferroic BiFeO3 thin films prepared via a simple sol-gel method," *Appl. Phys. Lett.*, vol. 88, no. 14, pp. 128–131, 2006.
[47] J. Wang, J. Wang, J. B. Neaton, H. Zheng, V. Nagarajan, and S. B. Ogale, "Epitaxial BiFeO3 Multiferroic Thin Film Heterostructures.pdf," vol. 1719, no. 2003, 2012.
[48] M. Kaur, K. L. Yadav, and P. Uniyal, "Investigations on multiferroic , optical and photocatalytic properties of lanthanum doped bismuth ferrite nanoparticles," *Adv. Mater.*, vol. 6, no. 10, pp. 895–901, 2015.
[49] C.-H. Yang, D. Kan, I. Takeuchi, V. Nagarajan, and J. Seidel, "Doping $BiFeO_3$: approaches and enhanced functionality.," *Phys. Chem. Chem. Phys.*, vol. 14, no. 46, pp. 15953–62, 2012.
[50] G. M. Montes, O. Perales-Perez, B. Rentería, and M. Gálvez, "Synthesis and Magnetic Properties of Pure and Cobalt-Doped Nanocrystalline Bismuth Ferrite," *MRS Proc.*, vol. 1256, no. 111, pp. 1256-N06-14, 2010.
[51] P. Tang, D. Kuang, S. Yang, and Y. Zhang, "Preparation and enhanced ferromagnetic properties in Co doped $BiFeO_3$ nanoparticles prepared by sol–gel method," *Ferroelectrics*, vol. 505, no. 1, pp. 123–129, 2016.
[52] I. K. Batttisha *et al.*, "Dielectric and Magnetic Properties of Nano-Structure BiFeO 3 Doped with Different Concentrations of Co Ions Prepared by Sol-Gel Method," vol. 3, no. July, pp. 59–73, 2015.
[53] L. Peng *et al.*, "Influence of Co doping on structural, optical and magnetic properties of

BiFeO3 films deposited on quartz substrates by sol-gel method," *Appl. Surf. Sci.*, vol. 268, pp. 146–150, 2013.
[54] I. Coondoo *et al.*, "Improved magnetic and piezoresponse behavior of cobalt substituted $BiFeO_3$ thin film," *Thin Solid Films*, vol. 520, no. 21, pp. 6493–6498, 2012.
[55] D. Barrionuevo, S. P. Singh, and M. S. Tomar, "Multiferroic Properties of Co Doped $BiFeO_3$ and Some Composite Films," *Integr. Ferroelectr.*, vol. 124, no. 1, pp. 41–47, 2011.
[56] V. Srinivas, A. T. Raghavender, and K. V. Kumar, "Structural and Magnetic Properties of Mn Doped BiFeO3 Nanomaterials," *Phys. Res. Int.*, vol. 2016, p. 5, 2016.
[57] G. Arya, A. Kumar, M. Ram, and N. S. Negi, "Structural , dielectric , ferroelectric and magnetic properties of Mn -doped $BiFeO_3$ nanoparticles synthesized by ol -gel method," vol. 5, no. 2, pp. 245–252, 2013.
[58] F. Yan, G. Xing, R. Wang, and L. Li, "Tailoring surface phase transition and magnetic behaviors in $BiFeO_3$ via doping engineering," *Sci. Rep.*, vol. 5, p. 9128, 2015.
[59] J. K. Kim, "Enhanced Ferroelectric Properties of Mn-Doped $BiFeO_3$ Thin Films Prepared by Chemical Solution Deposition," vol. 49, no. December, pp. 566–570, 2006.
[60] W. Cai, C. L. Fu, R. L. Gao, W. H. Jiang, X. L. Deng, and G. Chen, "Ferroelectric and Photovoltaic Properties of Mn-Doped Bismuth Ferrite Thin Films," *Mater. Sci. Forum*, vol. 815, pp. 135–140, 2015.
[61] J. Li, K. Liu, J. Xu, L. Wang, L. Bian, and F. Xu, "Structure-Dependent Electrical, Optical and Magnetic Properties of Mn-Doped $BiFeO_3$ Thin Films Prepared by the Sol-Gel Process," *J. Mater. Sci. Res.*, vol. 2, no. 3, pp. 75–81, 2013.
[62] L. Peng, H. Deng, J. Tian, Q. Ren, C. Peng, and Z. Huang, "Influence of Co doping on structural , optical and magnetic properties of $BiFeO_3$ films deposited on quartz substrates by sol – gel method," *Appl. Surf. Sci.*, vol. 268, pp. 146–150, 2013.
[63] J. Li, H. Yuan, G. Li, Y. Liu, and J. Leng, "Cation distribution dependence of magnetic properties of sol – gel prepared $MnFe_2O_4$ spinel ferrite nanoparticles," *J. Magn. Magn. Mater.*, vol. 322, no. 21, pp. 3396–3400, 2010.
[64] H. A. A.-L. K. Kombaiah, J. Judith Vijaya, L. John Kennedy, M. Bououdina, R. Jothi Ramalingam, "Comparative investigation on the structural, morphological, optical, and magnetic properties of $CoFe_2O_4$ nanoparticles," *Ceram. Int.*, vol. 43, no. 10, pp. 7682–7689, 2017.
[65] B. R. and O. P. Gina Montes, Marco Gálvez, "Effect of the Type of Solvent and Bi-Stoichiometric Excess on the Purity of Nanocrystalline Bismuth Ferrite Single Phase," *MRS Proc.*, vol. 1454, 2012.
[66] B. D. Cullity, *Elements of X-ray diffraction*, Third edit. Prentice Hall, New Jersey, 2001.
[67] A. Agarwal, P. Aghamkar, and B. Lal, "Structural and multiferroic properties of barium substituted bismuth ferrite nanocrystallites prepared by sol – gel method," *J. Magn. Magn. Mater.*, vol. 426, no. August 2016, pp. 800–805, 2017.
[68] B. R.-B. and O. P.-P. Gina Montes-Albino, Marco Gálvez-Saldaña, "Effect of the Type of Solvent and Bi-Stoichiometric Excess on the Purity of Nanocrystalline Bismuth Ferrite Single Phase," *MRS Proc.*, vol. 1454, pp. 45–50, 2012.
[69] F. Azough, R. Freer, M. Thrall, R. Cernik, F. Tuna, and D. Collison, "Microstructure and properties of Co-, Ni-, Zn-, Nb- and W-modified multiferroic $BiFeO_3$ ceramics," *J. Eur. Ceram. Soc.*, vol. 30, no. 3, pp. 727–736, 2010.

[70] W. Cai, C. Fu, W. Hu, G. Chen, and X. Deng, “Effects of microwave sintering power on microstructure , dielectric , ferroelectric and magnetic properties of bismuth ferrite ceramics,” *J. Alloys Compd.*, vol. 554, pp. 64–71, 2013.
[71] S. Riaz, F. Majid, S. M. H. Shah, and S. Naseem, “Enhanced magnetic and structural properties of Ca doped BiFeO3 thin films,” *Indian J. Phys.*, vol. 88, no. 10, pp. 1037–1044, 2014.
[72] U. Khan *et al.*, “Influence of cobalt doping on structural and magnetic properties of $BiFeO_3$ nanoparticles,” *J. Nanoparticle Res.*, vol. 17, no. 11, pp. 1–9, 2015.
[73] M. Sakar, S. Balakumar, P. Saravanan, and S. N. Jaisankar, “Annealing temperature mediated physical properties of bismuth ferrite ($BiFeO_3$) nanostructures synthesized by a novel wet chemical method,” *Mater. Res. Bull.*, vol. 48, no. 8, pp. 2878–2885, 2013.
[74] W. Cao *et al.*, “Rapid synthesis of single-phase bismuth ferrite by microwave-assisted hydrothermal method,” *Mater. Chem. Phys.*, pp. 1–5, 2016.
[75] P. He, Z. Hou, C. Wang, Z. Li, J. Jing, and S. Bi, “Mutual promotion effect of Pr and Mg co-substitution on structure and multiferroic properties of BiFeO3 ceramic,” *Ceram. Int.*, vol. 43, pp. 262–267, 2017.
[76] T. Hussain, S. A. Siddiqi, S. Atiq, and M. S. Awan, “Induced modifications in the properties of Sr doped BiFeO 3 multiferroics,” *Prog. Nat. Sci. Mater. Int.*, vol. 23, no. 5, pp. 487–492, 2013.
[77] S. Hussain, S. K. Hasanain, G. H. Jaffari, N. Zafar, M. Siddique, and S. I. Shah, “Correlation between structure , oxygen content and the multiferroic properties of Sr doped $BiFeO_3$,” *J. Alloys Compd.*, vol. 622, pp. 8–16, 2015.
[78] M. A. Garcia *et al.*, “Sources of experimental errors in the observation of nanoscale magnetism (c) (d),” *Appl. Phys. Lett.*, pp. 1–7, 2009.
[79] N. Suresh Kumar, K. Vijaya Kumar, N. Suresh Kumar, and K. Vijaya Kumar, “Synthesis and Structural Properties of Bismuth Doped Cobalt Nano Ferrites Prepared by Sol-Gel Combustion Method,” *World J. Nano Sci. Eng.*, vol. 5, no. 5, pp. 140–151, 2015.
[80] A. Manzoor, A. M. Afzal, M. Umair, A. Ali, M. Rizwan, and M. Z. Yaqoob, “Synthesis and characterization of Bismuth ferrite ($BiFeO_3$) nanoparticles by solution evaporation method,” *J. Magn. Magn. Mater.*, vol. 393, pp. 269–272, 2015.
[81] J. Rout, R. N. P. Choudhary, H. B. Sharma, and S. R. Shannigrahi, “Effect of co-substitutions (Ca-Mn) on structural, electrical and magnetic characteristics of bismuth ferrite,” *Ceram. Int.*, vol. 41, no. 7, pp. 9078–9087, 2015.
[82] G. L. Song, J. Su, G. J. Ma, T. X. Wang, H. G. Yang, and F. G. Chang, “Effects of trivalent gadolinium and cobalt co-substitution on the crystal structure, electronic transport, and ferromagnetic properties of bismuth ferrite,” *Mater. Sci. Semicond. Process.*, vol. 27, pp. 899–908, 2014.
[83] B. K. Vashisth *et al.*, “Modified ferroelectric/magnetic and leakage current density properties of Co and Sm co-doped bismuth ferrites,” *J. Alloys Compd.*, 2017.
[84] A. Mukherjee, S. Basu, L. A. W. Green, N. T. K. Thanh, and M. Pal, “Enhanced multiferroic properties of Y and Mn codoped multiferroic BiFeO3 nanoparticles,” *J. Mater. Sci.*, vol. 50, no. 4, pp. 1891–1900, 2015.
[85] G. S. Lotey and N. K. Verma, “Structural, magnetic, and electrical properties of Gd-doped BiFeO3 nanoparticles with reduced particle size,” *J. Nanoparticle Res.*, vol. 14, no. 3, p.

742, 2012.
[86] J. Ray, A. K. Biswal, P. D. Babu, V. Siruguri, and P. N. Vishwakarma, “Neutron diffraction study of $BiFeO_3$ and $BiFe_{0.98}Co_{0.02}O_3$ nano-particles,” *Solid State Commun.*, vol. 220, pp. 57–60, 2015.
[87] P. Vlazan and M. Vasile, “Synthesis and characterization $CoFe_2O_4$ nanoparticles prepared by the hydrothermal method,” *Optoelectron. Adv. Mater. Comun.*, vol. 4, no. 9, pp. 1307–1309, 2010.
[88] Y. A. Chaudhari, C. M. Mahajan, P. P. Jagtap, and S. T. Bendre, “Structural, magnetic and dielectric properties of nano-crystalline Ni-doped BiFeO3 ceramics formulated by self-propagating high-temperature synthesis,” *J. Adv. Ceram.*, vol. 2, no. 2, pp. 135–140, 2013.
[89] S. Thakur, O. P. Pandey, K. Singh, O. P. Pandey, and K. Singh, “Structural and optical properties of $Bi_{1-x}A_xFeO_3$ (A=Sr, Ca; $0.40 \leq x \leq 0.55$),” *J. Mol. Struct.*, vol. 1074, pp. 186–192, 2014.
[90] R. K. Mishra, D. K. Pradhan, R. N. P. Choudhary, and A. Banerjee, “Effect of yttrium on improvement of dielectric properties and magnetic switching behavior in $BiFeO_3$,” *J. Phys. Condens. Matter*, vol. 29, no. 4, 2008.
[91] V. Verma, “Structural , electrical and magnetic properties of rare-earth and transition element co-doped bismuth ferrites,” *J. Alloys Compd.*, vol. 641, pp. 205–209, 2015.
[92] A. Goldman and A. Goldman, *Modern ferrite technology second edition ^ Springer*. .
[93] P. Suresh and S. Srinath, “Effect of la substitution on structure and magnetic properties of sol-gel prepared $BiFeO_3$,” *J. Appl. Phys.*, vol. 113, no. 17, pp. 17–20, 2013.
[94] N. Shamir, E. Gurewitz, and H. Shaked, “The magnetic structure of $Bi_2Fe_4O_9$: analysis of neutron diffraction measurements,” *Acta Crystallogr. Sect. A*, vol. 34, no. 5, pp. 662–666, 1978.